Paulo Fernando Sá Ribeiro de Faria

Quaternion-based Dynamic Control of a 6-DOF Stewart Platform For Periodic Disturbance Rejection

Porto Alegre - RS, Brazil

2016

Paulo Fernando Sá Ribeiro de Faria

Quaternion-based Dynamic Control of a 6-DOF Stewart Platform For Periodic Disturbance Rejection

Masters dissertation presented to the Graduate Program in Electrical Engineering of the Pontifícia Universidade Católica do Rio Grande do Sul, as requisite to obtain Master's degree in Electrical Engineering.
Focus area: Signals, Systems and Information Technology
Research area: Automation and Systems.

Pontifícia Universidade do Rio Grande do Sul - PUCRS

Engineering Faculty

Graduate Program in Electrical Engineering

Supervisor: Aurélio Tergolina Salton

Porto Alegre - RS, Brazil

2016

Pontifícia Universidade Católica do Rio Grande do Sul
FACULDADE DE ENGENHARIA
PROGRAMA DE PÓS-GRADUAÇÃO EM ENGENHARIA ELÉTRICA

QUATERNION-BASED DYNAMIC CONTROL OF A 6-DOF STEWART PLATFORM FOR PERIODIC DISTURBANCE REJECTION

CANDIDATO: PAULO FERNANDO SÁ RIBEIRO DE FARIA

Esta Dissertação de Mestrado foi julgada para obtenção do título de MESTRE EM ENGENHARIA ELÉTRICA e aprovada em sua forma final pelo Programa de Pós-Graduação em Engenharia Elétrica da Pontifícia Universidade Católica do Rio Grande do Sul.

DR. AURELIO TERGOLINA SALTON - ORIENTADOR

BANCA EXAMINADORA

DR. EDUARDO ANDRÉ PERONDI - DO DEPARTAMENTO DE ENGENHARIA MECÂNICA - UFRGS

DR. JEFERSON VIEIRA FLORES - PÓS-GRADUAÇÃO EM ENGENHARIA ELÉTRICA - PPGEE, DA UFRGS - UFRGS

DRA. LETÍCIA MARIA BOLZANI POEHLS - DO PPGEE - FENG - PUCRS

PUCRS
Campus Central
Av. Ipiranga, 6681 - Prédio 30 - Sala 103 - CEP: 90619-900
Telefone: (51) 3320.3540 - Fax: (51) 3320.3625
E-mail: engenharia.pg.eletrica@pucrs.br
www.pucrs.br/feng

Acknowledgements

I would like to extend my most sincere gratitude to my advisor Prof. Aurélio Tergolina Salton, specially for his ever growing knowledge, patience and availability in the continuous support of writing this work. I would also like to thank Prof. Jeferson Vieira Flores, Prof. Alexandre Rosa Franco, Prof. Guilherme Araujo Pimentel, Prof. Fernando Soares dos Reis and Rafael Castro for the advices and help throughout my research. Last but certainly not least, I would also like to thank my family for all the help, incentive and spiritual support in writing this dissertation.

Abstract

This work proposes a simultaneous decoupled dynamic linear translational and nonlinear rotational quaternion-based control of a Stewart platform. For the dynamic modeling of the manipulator, a Newton-Euler quaternion-based formulation was used for control design simplification. For the platform translation control, a mixed design composed by $\mathcal{H}_\infty$, $\mathcal{D}$-stability framework applied to a dynamic controller is presented along with an augmented representation to allow the use of Linear Matrix Inequalities (LMI). Periodic and constant disturbances are dealt with by the dynamic controller which is based on the Internal Model Principle (IMP). For the end effector orientation control, an approach consisting of a controller that achieves $\mathcal{L}_2$ gain performance and a state-feedback control law based on the IMP is used in order to guarantee stability of the rotation system. The Jacobian of the platform is then used for control signal coupling. Numerical results show that the proposed controller is able to stabilize the system around the desired reference and successfully reject external periodic perturbations. Finally, the suggested control strategy is compared to an inverse dynamics controller and the results of both approaches are compared.

Keywords: Quaternions, Internal Model Principle, Linear Matrix Inequalities, disturbance rejection, Resonant Control, Hamilton-Jacobi Inequality, Stewart Platform, $\mathcal{H}_\infty$ gain, $\mathcal{L}_2$ gain, Newton-Euler dynamics.

Resumo

Este trabalho propõe um controle dinâmico, simultâneo e desacoplado baseado em quaternions para a plataforma de Stewart. Para a modelagem dinâmica do manipulador, uma formulação de Newton-Euler baseada em quaternions foi usada para simplificação do desenvolvimento das estratégias de controle. Para o controle da translação da plataforma, uma arquitetura mista composta por métodos $\mathcal{H}_\infty$ e de $\mathcal{D}$-estabilidade aplicados em um controlador dinâmico é apresentada em conjunto com uma representação aumentada do sistema, permitindo o uso de Desigualdades Matriciais Lineares. Distúrbios periódicos e constantes são tratados pelo controlador dinâmico baseado no Princípio do Modelo Interno. Para o controle da rotação da plataforma, um controlador que obtém desempenho ao ganho $\mathcal{L}_2$, além de uma lei de controle por retro-alimentação de estados baseada em Desigualdades Matriciais Lineares, é usado para garantir a estabilidade do sistema rotacional. A matriz Jacobiana da plataforma é então usada para acoplar os sinais dos dois controladores. Resultados numéricos apresentados mostram que o método de controle usado é capaz de estabilizar o sistema ao redor da referência desejada e de rejeitar perturbações externas periódicas. Ao final, a estratégia de controle sugerida é comparada com um controlador de dinâmica reversa e os resultados de ambas abordagens são apresentados.

Palavras-chaves: Quaternions, Modelo do Princípio Interno, Desigualdades Matriciais Lineares, rejeição a distúrbios, Controle Ressonante, Desigualdade de Hamilton-Jacobi, Plataforma de Stewart, ganho $\mathcal{H}_\infty$, ganho $\mathcal{L}_2$, modelagem dinâmica de Newton-Euler.

List of Figures

List of Tables

List of abbreviations and acronyms

2SPS	Two-sided Power Spectrum
3D	Three dimensional
Att.	Attitude
CKC	Closed Kinematic Chain
DC	Direct Current
DOF	Degree of Freedom
FFT	Fast Fourier Transform
IDC	Inverse Dynamics Controller
IMP	Internal Model Principle
LMI	Linear Matrix Inequality
LSP	Left Semi Plane
LTI	Linear Time Invariant
MSE	Mean Square Error
OKC	Open Kinematic Chain
PC	Performance Criterion
Pos.	Position
RSP	Right Semi Plane
SNR	Signal-to-Noise Ratio
SS	Steady-state
WCS	Worst Case Scenario

List of symbols

$\boldsymbol{q}$	quaternion $\boldsymbol{q}$ in the Hamiltonian domain
q	quaternion $\boldsymbol{q}$ in vector form
x^*	conjugate of vector x
$\dot{x}$	first derivative of x relative to time
$\ddot{x}$	second derivative of x relative to time
$A^\top$	transpose of matrix A
A^{-1}	inverse of matrix A
$A^{-\top}$	inverse of the transpose of matrix A
$\cdot$	vector dot product
$\times$	vector cross product
$\otimes$	Kronecker product
$\star$	transpose of the diagonal block matrix
$\Re(\lambda_a)$	real value of a complex number λ_a
$\|x\|$	modulus of x
$\|\|x\|\|$	euclidean norm of x
$\|\|x\|\|_{\mathcal{L}_2}$	$\mathcal{L}_2$ norm of x
$\|\|x\|\|_{\mathcal{H}_\infty}$	$\mathcal{H}_\infty$ norm of x
$diag(A, B)$	block-diagonal matrix composed of matrices A and B
$rank(A)$	rank of matrix A
$S(x)$	skew-symmetric matrix function
I	3×3 identity matrix
$\boldsymbol{I}$	adequately sized identity matrix
$\mathbf{0}$	adequately sized zero-filled matrix or vector
$\mathcal{H}$	Hamiltonian domain

$\mathbb{C}$	complex plane
$\mathbb{C}^-$	negative complex plane
$\mathbb{N}$	natural number domain
$\mathbb{N}^+$	natural positive number domain
$\mathbb{R}$	real domain
$\mathbb{R}^n$	real euclidean space of order n
$\mathbb{R}^{n\times m}$	real matrix space of dimension $n \times m$
C_θ	cosine of an angle θ
S_θ	sine of an angle θ
■	end of theorem, definition or corollary
□	end of proof
O_I	global inertial frame
O_B	local reference frame, bottom platform
O_T	local reference frame, top platform
b_i	i^{th} joint of the bottom platform
t_i	i^{th} joint of the top platform
r_B	constructive radius of the bottom platform
r_T	constructive radius of the top platform
φ_B	constructive angle between two joints of the same edge, bottom platform
φ_T	constructive angle between two joints of the same edge, top platform
B_i	vector from the local reference frame to the i_{th} joint of the bottom platform
T_i	vector from the local reference frame to the i_{th} joint of the top platform
λ_i	constructive parameters for B_i
υ_i	constructive parameters for T_i
J	Jacobian matrix

$\dot{l}$	linear velocities of the six actuators
$\dot{l}_i$	linear velocity of the i^{th} actuator
p	linear position vector of the platform
v	linear velocity vector of the platform
w	angular velocity vector of the platform
n_i	unit vector with the same direction of the i^{th} leg of the platform (L_i)
L_i	vector that represents the i^{th} leg of the platform (from b_i to t_i)
R_B^I	rotation matrix of the bottom platform regarding the O_I
R_T^I	rotation matrix of the top platform regarding the O_I
f_l	linear forces of the six actuators
F_B	forces applied on the bottom platform
τ_B	torques applied on the bottom platform
F_T	forces applied on the top platform
τ_T	torques applied on the top platform
I_m	inertia tensor of the platform
m	body mass of the platform
η	scalar part of q
ε	vector part of q
p_x, p_y, p_z	positions regarding the x-, y- and z-axis, respectively
u_τ	input torques on the platform
τ_{ext}	perturbation torques on the platform
$\bar{u}_F$	input forces on the platform
u_F	$u_F = \bar{u}_F + g$
g	gravity acceleration
F_{ext}	perturbation forces on the platform
$\bar{S}_1$	linear translational model, original model

S_1	linear translational model, control model
$\bar{S}_2$	non-linear rotational model, original model
S_2	non-linear rotational model, control model
x_1	state vector of $\bar{S}_1$ and S_1
x_2	state vector of $\bar{S}_2$ and S_2
$M(x)$	inertia matrix
$V(x, \dot{x})$	Coriolis matrix
G	gravity matrix
$K_{1...5}$	constants for the Lagrange model of the platform
I_x, I_y, I_z	scalar from the diagonal of I_m
α, β, γ	rotation angles around the x-, y- and z-axis
A_1, A_2	constants used for comparing the Lagrange and quaternion-based Newton-Euler model
σ_c	frequency used for comparing the Lagrange and quaternion-based Newton-Euler model
$r_{ef}(t)$	reference signal for the controller,in Figure 5
$e_{rr}(t)$	error signal for the controller, in Figure 5
z_1	output signal for system S_1
z_2	output signal for system S_2
A	state matrix of system S_1
B_u, B_ϕ	input matrices of system S_1
C	output matrix of system S_1
$C_{x...w_z}$	single state output vector of system S_1
σ_r	fundamental frequency of the perturbation
x_r	resonant states vector
e_r	motion error of the platform (system S_1)
r_x	motion reference of the platform (system S_1)

$\bar{A}_r$	state matrix of the i^{th} harmonic of the resonant controller
B_r	input matrix of the resonant controller
e_1, e_2, e_3	position errors relative to p_x, p_y, p_z respectively
f_s	sampling frequency
A_r	state matrix of a resonant controller on the fundamental frequency σ_r
A_r	state matrix of a resonant controller on the second harmonic of σ_r
S_a	augmented translational model
$\bar{S}_a$	complete augmented translational model, with direct input-to-output matrices
x_a	augmented states vector of system S_a
A_a	augmented state matrix of system S_a
$B_{u,a}, B_{\phi,a}$	augmented input matrices of system S_a
C_a	augmented output matrix of system S_a
$D_{u,a}, D_{\phi,a}$	augmented direct input-to-output matrices of system $\bar{S}_a$
K	static gain of the control law for u_F
$\mathcal{A}$	closed loop state matrix of system S_a
λ_a	closed loop eigenvalues of $\mathcal{A}$]
$\bar{\mu}$	$\mathcal{H}_\infty$ gain of F_{ext} to z_1
μ	optimization variable $\mu > \bar{\mu}$ for the LMI
P, Y, Q	optimization variables for the LMI
L, M	constant matrices for the LMI
g_1, g_2	input functions of system S_2
h	output function of system S_2
ρ	control signal weighting constant of system S_2
ρ_1, ρ_2	attitude control performance tuning constants of system S_2
ζ	non-linear control law for system S_2

a, b_1, b_2, c_1, c_2	positive constants for the controller of system S_2
ν	$\mathcal{L}_2$ gain target for the controller
u_{τ_2}	linear control law for system S_2
$\bar{S}_l$	linearization of system S_2
$\partial\eta$, $\partial\varepsilon$, $\partial\omega$	linearized states of system S_2, state vector of $\bar{S}_l$
$\partial\tau_{ext}$, ∂u_{τ_2}	linearized perturbation and input of system S_2, inputs of $\bar{S}_l$
$\partial\bar{z}_2$	linearized output of system S_2, output of $\bar{S}_l$
S_l	linearized system, from S_2, with the non-controllable state removed
x_l	state vector of system S_l
A_l	state matrix of system S_l
$B_{u,l}$, $B_{\tau_{ext},l}$	input matrices of system S_l
z_2	output of system S_l
$S_{l,a}$	augmented system from S_l
$x_{l,a}$	state vector of system $S_{l,a}$
$A_{l,a}$	state matrix of system $S_{l,a}$
$B_{u,l,a}$, $B_{\tau_{ext},l,a}$	input matrices of system $S_{l,a}$
$C_{l,a}$	output matrix of system $S_{l,a}$
$z_{l,a}$	output of system $S_{l,a}$
K_{rt}	static gain of the control law for u_{τ_2}
$\mathcal{A}_{l,a}$	closed loop state matrix of system $S_{l,a}$
$\lambda_{l,a}$	closed loop eigenvalues of $\mathcal{A}_{l,a}$]
p_d	translational perturbations applied on the simulations
r_d	rotational perturbations applied on the simulations

Contents

1 Introduction

Rigid-body manipulators are widely used mechanical systems capable of positioning its end effector in 3D space with ease, given that enough degrees of freedom are available for the task. The use for such systems ranges from industrial serial manipulators, which may resemble a human arm and are used for welding, part-placement and other uses, to parallel manipulators, such as the Stewart platform.

The Stewart platform manipulator consists in a six degrees of freedom (DOF) parallel kinematic system given by a closed-kinematic chain (CKC) mechanism. Parallel connected mechanisms are constructed in such a way that the links and joints from two or more actuators connect the base of the manipulator to the end effector (FICHTER, 1986). In the case of the Stewart platform, it is composed of a movable platform (end-effector) linked to a static base (bottom platform) by six variable length actuators. While the original intent was to use this platform as an aircraft simulator motion base (STEWART, 1965), CKC mechanisms in general have some inherent benefits that have expanded their applicability. Today, the use of the Stewart platform ranges from industrial-grade manipulators (HUNT, 1978) to offshore cargo transfer mechanisms (GONZALEZ; DUTRA; LENGERKE, 2011).

Open-kinematic chain (OKC) mechanisms, such as a serial linked industrial robot arm, have low stiffness, low strength-to-weight ratio and large position error (NGUYEN et al., 1991). A CKC manipulator such as the Stewart platform has, on the other hand, a higher structural rigidity, noncumulative actuator errors and a payload that is proportionally distributed to the links, granting a higher strength-to-weight ratio (LIU; LEBRET; LEWIS, 1993). Therefore, there is significant interest in this particular configuration of a parallel manipulator, which is, to this date, a highly active research topic (AYAS; SAHIN; ALTAS, 2014; KUMAR; CHALANGA; BANDYOPADHYAY, 2015; MAGED; ABOUEL-SOUD; BAB, 2015).

From a practical perspective, this work considers the scenario where a Stewart platform is used as a stabilization device on the ocean as, for example, an offshore cargo transfer mechanism, as a leveled platform for installation of offshore photovoltaic panels, or even as a reusable rocket landing pad.

In the first scenario, the platform would allow cargo transfer between a large scale vessel and two smaller ships on the ocean, reducing the time and costs attributed to traditional cargo unloading mechanisms (MELLO, 2011). The second scenario envisions a future where photovoltaic (PV) panels are more common and cost-effective than today, whose installation could also be made in offshore PV farms or on the dams of a hydro-

electric plant. The third case may also be used in tandem with a reusable space shuttle, such as the SpaceX orbital launch system, given that the platform would guarantee a horizontal landing pad for the shuttle to descend onto.

In all these cases, it is desired that the end effector (the top platform) remains as steady as possible, negating the effects of waves perturbing the bottom frame. Obviously, the system is subject to external periodic and non-periodic perturbations, whose behavior and mathematical description are only partly known, as well as variable load conditions.

To that extent, suitable control techniques must be developed to achieve the aforementioned desired behavior. As such, consider the objectives from the next section, which will be the main focus area of this work.

1.1 Objectives

The main objective of this work is the development of a dynamic control method for periodic disturbance rejection on a Stewart platform. In order to achieve the proposed goal, the dynamic equations that govern the manipulator must to be described in a formulation that simplifies the design of control strategies capable of attenuating perturbations, namely a quaternion representation of the platform using the Newton-Euler approach. This results in two mathematically decoupled submodels of the linear translational and nonlinear rotational portions of the system. Next, the control method itself is developed to meet the central objective of this work. This includes two dynamic controllers that guarantee asymptotic stability of the unperturbed submodels, $\mathcal{H}_\infty$ and $\mathcal{L}_2$ finite-gain stability of the perturbed translational and rotational subsystems, respectively, and external perturbation attenuation for both submodels, provided its frequency spectrum is known a priori and dominated by resonant peaks. Later, a systematic approach to unify the control signal of both controllers must be defined and the suggested dynamic description must be validated against a more classical formulation.

In addition, the results of this work should then be presented to the reader and the proposed control strategy must be compared to another control proposition which was already implemented in other works, namely the Inverse Dynamics Controller. Finally, future research topics should be outlined to warrant further developments in the same area as this work.

1.2 Structure

This work is organized as follows. Chapter 2 presents the main concepts, theorems and definitions used in the next sections, namely the attitude quaternion and the Hamiltonian algebra, some basic results on linear and nonlinear systems, such as the internal

model principle, linear matrix inequalities, $\mathcal{L}_2$ gain and the classic Lyapunov stability theory. Next, on Chapter 3, the main mathematical descriptions of the Stewart platform are presented, such as its constructive parameters, the inverse kinematics and the dynamic equations of the manipulator. Chapter 4 describes then the proposed control strategy of this work and focuses on the development of the suggested control laws for meeting the aforementioned objectives. Going further, Chapter 5 shows the numerical results obtained from this work and compares the proposed control method to the Inverse Dynamics Controller. Finally, Chapter 6 delineates the final considerations of this work and future research suggestions are given.

2 Preliminaries

In this chapter, the main concepts, theorems and definitions used throughout this work will be presented. This chapter is organized as follows: first, a brief introduction on quaternions is presented, along the essential mathematical operations of the Hamiltonian algebra, the use of quaternions for spatial rotation purposes, and its equivalence to classic Euler angle representation. Next, some basic results on linear systems are brought to attention, namely the internal model principle and its particular use in this work: resonant controllers for periodic perturbation rejection. In this same context of linear systems, the concept of linear matrix inequalities (LMIs) is introduced with a focus on control theory, in order to enable a systematic method of linear control design to be defined later in this work. The $\mathcal{D}$-stability LMI formulation is also featured in this section. Some basic results on nonlinear systems follow on the next section, such as the classic Lyapunov stability theory, the Hamilton-Jacobi inequality and $\mathcal{L}_2$ gain of perturbed systems. Finally, a primer on the nonlinear H_∞ control law used in this work is presented.

2.1 Quaternions and Spatial Rotations

Originally developed by William Rowan Hamilton (HAMILTON, 1844), quaternions can be defined as an extension to complex numbers, described in a hyper-complex domain, also called the Hamiltonian domain. Among other uses, such as electrodynamics (WASER, 2000) and crystallography (MACKAY, 1984), a quaternion $\boldsymbol{q}$ can be seen as a mathematical framework for expressing rotations and attitude (positioning) of an object in a three dimensional space. In an usual comparison to classic Euler angles, quaternions present an easier computation of the kinematics and dynamics of 3D rigid bodies while also avoiding the gimbal lock problem. Such problem arises when a degree of freedom is lost, given that two gimbals are placed in a parallel configuration (KUIPERS et al., 1999).

2.1.1 Definition and Operations

For a formal description of quaternions, consider Definition 2.1.

Definition 2.1. (Quaternion) A quaternion $\boldsymbol{q} \in \mathcal{H}$ is defined as a hyper-complex number with four components that satisfy

$$\boldsymbol{q} = \eta + \varepsilon_1 i + \varepsilon_2 j + \varepsilon_3 k, \tag{2.1}$$

where $\eta \in \mathbb{R}$ is the quaternion real component, i, j and k are imaginary identities that form the basis elements of the Hamiltonian domain and the vector part $\varepsilon = \begin{bmatrix} \varepsilon_1 & \varepsilon_2 & \varepsilon_3 \end{bmatrix}^\top \in \mathbb{R}^3$ is sometimes called the quaternion imaginary component. ■

While the quaternion $\boldsymbol{q} \in \mathcal{H}$ requires an special algebra framework, quaternions can also be represented in a vector form, such as

$$\boldsymbol{q} \;\rightarrow\; q = \begin{bmatrix} \eta \\ \varepsilon \end{bmatrix} \in \mathbb{R}^4. \tag{2.2}$$

In this work, the quaternion vector representation will be used throughout the remaining chapters. As such, consider Definitions 2.2 through 2.5 that will allow a series of manipulations to be computed.

Definition 2.2. (Quaternion sum) The sum of quaternions q_a and q_b can be described as the vector sum

$$\boldsymbol{q_a} + \boldsymbol{q_b} \;\rightarrow\; q_a + q_b \;=\; \begin{bmatrix} \eta_a + \eta_b \\ \varepsilon_a + \varepsilon_b \end{bmatrix}. \tag{2.3}$$

■

Definition 2.3. (Quaternion conjugate) The conjugate quaternion q^* can be defined as the vector

$$\boldsymbol{q^*} \;\rightarrow\; q^* \;=\; \begin{bmatrix} \eta \\ -\varepsilon \end{bmatrix}. \tag{2.4}$$

■

Definition 2.4. (Quaternion product) The product of two quaternions q_a and q_b can be defined as

$$\boldsymbol{q} \;= \boldsymbol{q_a q_b} \;\rightarrow\; q \;= M(q_a)q_b = N(q_b)q_a,$$

where [1,2]

$$M(q) = \begin{bmatrix} \eta & -\varepsilon^\top \\ \varepsilon & \eta I + S(\varepsilon) \end{bmatrix}, N(q) = \begin{bmatrix} \eta & -\varepsilon^\top \\ \varepsilon & \eta I - S(\varepsilon) \end{bmatrix}. \tag{2.7}$$

■

[1] The skew-symmetric matrix function $S : \mathbb{R}^3 \rightarrow \mathbb{R}^{3\times 3}$ defines a square matrix $S(x)^\top = -S(x)$ which represents cross products $\times$ as matrix multiplications, so that

$$x \times y = S(x)y \tag{2.5}$$

and

$$S(x) = \begin{bmatrix} 0 & -x_3 & x_2 \\ x_3 & 0 & -x_1 \\ -x_2 & x_1 & 0 \end{bmatrix}, \forall\, x = \begin{bmatrix} x_1 \\ x_2 \\ x_3 \end{bmatrix} \in \mathbb{R}^3. \tag{2.6}$$

[2] I is the 3×3 identity matrix.

Definition 2.5. (Quaternion length) The length of q is defined as the norm

$$\|\boldsymbol{q}\| \ = \sqrt{\boldsymbol{q}\boldsymbol{q}^*} \ \rightarrow \ \|q\| \ = \sqrt{q^\top q} = \sqrt{\eta^2 + \varepsilon_1^2 + \varepsilon_2^2 + \varepsilon_3^2}. \tag{2.8}$$

■

These definitions form the necessary mathematical basis for the next subsection, attitude quaternions.

2.1.2 Attitude Quaternion and Quaternion Rotations

Attitude or orientation quaternions are a special case of quaternion variables when they are used to represent the rotation of an object relative to a reference coordinate system. While Euler angles α, β and γ can be used to represent rotations of a 3D body in three linearly independent axis as consecutive rotations, attitude quaternions provide a simpler method to represent this rotation, namely by products of quaternions. Consider Definition 2.6 for this case (DIEBEL, 2006).

Definition 2.6. (Attitude quaternion) A quaternion $\boldsymbol{q}$ with length $\|\boldsymbol{q}\| = 1$ of the form

$$\boldsymbol{q} \rightarrow \ q \ = \begin{bmatrix} \cos(\frac{\theta}{2}) \\ r \sin(\frac{\theta}{2}) \end{bmatrix} \tag{2.9}$$

is an attitude quaternion and may be used to represent a rotation of angle θ around the unit vector $r \in \mathbb{R}^3$. ■

Note that the attitude quaternion has unitary norm for a natural rotation without scalings. Consider now that an arbitrary vector $x \in \mathbb{R}^3$ is subject to rotation. If x is represented in augmented quaternion form, i.e.

$$\bar{\boldsymbol{x}} \ = x_1 i + x_2 j + x_3 k \ \rightarrow \ \bar{x} \ = \begin{bmatrix} 0 \\ x \end{bmatrix}, \tag{2.10}$$

then its rotation by angle θ around the unit vector r can be represented as proposed by the following definition.

Definition 2.7. (Quaternion rotation) The rotation of vector x by angle θ around the unit vector r is defined by

$$\bar{\boldsymbol{y}} \ = \boldsymbol{q}\bar{\boldsymbol{x}}\boldsymbol{q}^* \ \rightarrow \ y \ = R(q)x, \tag{2.11}$$

where $\bar{\boldsymbol{x}}$ is the augmented quaternion of vector x, $\bar{\boldsymbol{y}}$ is the augmented quaternion of the resulting rotated vector y, $\boldsymbol{q}$ is the attitude quaternion defined from (θ, r) and $R(q) \in \mathbb{R}^{3\times3}$ is the equivalent rotation matrix defined by

$$R(q) \ = I + 2\eta S(\varepsilon) + 2S^2(\varepsilon). \tag{2.12}$$

■

Furthermore, a given representation of an attitude quaternion $\boldsymbol{q}$ may also be represented in equivalent Euler angles, and vice-versa, as the next section shows.

2.1.3 Equivalent Euler Angles

Given that Euler angles are more natural and easier to understand than the same attitude in quaternion representation, equivalent Euler angles can be described as a function of an orientation quaternion $\boldsymbol{q}$. As such, consider Definition 2.8.

Definition 2.8. (Equivalent Euler angles) Let $\boldsymbol{q}$ be an orientation quaternion. The equivalent Euler angles α, β and γ of $\boldsymbol{q}$ can be obtained by computing

$$\begin{bmatrix}\alpha\\ \beta\\ \gamma\end{bmatrix} = \begin{bmatrix}\arctan\left(\dfrac{2(\eta\varepsilon_1+\varepsilon_2\varepsilon_3)}{1-2(\varepsilon_1^2+\varepsilon_2^2)}\right)\\ \\ \arcsin(2(\eta\varepsilon_2-\varepsilon_3\varepsilon_1))\\ \\ \arctan\left(\dfrac{2(\eta\varepsilon_3+\varepsilon_1\varepsilon_2)}{1-2(\varepsilon_2^2+\varepsilon_3^2)}\right)\end{bmatrix} \tag{2.13}$$

and q can be derived from α, β and γ by computing

$$\boldsymbol{q} = \begin{bmatrix}\cos\left(\frac{\alpha}{2}\right)\cos\left(\frac{\beta}{2}\right)\cos\left(\frac{\gamma}{2}\right)-\sin\left(\frac{\alpha}{2}\right)\sin\left(\frac{\beta}{2}\right)\sin\left(\frac{\gamma}{2}\right)\\ \sin\left(\frac{\alpha}{2}\right)\cos\left(\frac{\beta}{2}\right)\cos\left(\frac{\gamma}{2}\right)-\cos\left(\frac{\alpha}{2}\right)\sin\left(\frac{\beta}{2}\right)\sin\left(\frac{\gamma}{2}\right)\\ \cos\left(\frac{\alpha}{2}\right)\sin\left(\frac{\beta}{2}\right)\cos\left(\frac{\gamma}{2}\right)-\sin\left(\frac{\alpha}{2}\right)\cos\left(\frac{\beta}{2}\right)\sin\left(\frac{\gamma}{2}\right)\\ \cos\left(\frac{\alpha}{2}\right)\cos\left(\frac{\beta}{2}\right)\sin\left(\frac{\gamma}{2}\right)-\sin\left(\frac{\alpha}{2}\right)\sin\left(\frac{\beta}{2}\right)\cos\left(\frac{\gamma}{2}\right)\end{bmatrix}. \tag{2.14}$$

■

2.1.4 Error Quaternion

Even though this work will not make use of trajectory tracking, that is, the reference will always be that of an horizontal platform, it was developed in such way that reference tracking is easily added. For that, consider that an error quaternion describes the attitude error to a reference quaternion q_{ref} and is computed as shown on Definition 2.9.

Definition 2.9. (Error Quaternion) The error quaternion q_e is defined as

$$q_e = \begin{bmatrix}\eta_e\\ \varepsilon_e\end{bmatrix} = \begin{bmatrix}\eta_{ref}\eta+\varepsilon_{ref}^\top\varepsilon\\ \eta_{ref}\varepsilon-\varepsilon_{ref}\eta+S(-\varepsilon_{ref})\varepsilon\end{bmatrix}, \tag{2.15}$$

where $q_{ref} = \begin{bmatrix}\eta_{ref} & \varepsilon_{ref}^\top\end{bmatrix}^\top \in \mathbb{R}^4$ is the reference attitude. ■

Since both q_{ref} and q represent rotations and are unitary quaternions, $\|q_e\| = 1$ and the null error quaternion is $q_e^0 = \begin{bmatrix} \pm 1 & 0 & 0 & 0 \end{bmatrix}^\top$. Furthermore, every orientation unit quaternion is considered a redundant representation of attitude, since it has two equilibria ($\varepsilon = \mathbf{0}, \eta = \pm 1$) that describe the same pose of the system.

2.2 Basic Results on Linear Systems

This section aims at presenting the reader to the main results on linear systems used throughout this work, namely the Internal Model Principle, Linear Matrix Inequalities and the $\mathcal{D}$-stability LMI formulation.

2.2.1 Internal Model Principle

The internal model principle (IMP) (FRANCIS; WONHAM, 1975), also called internal-model-based tracking, is a concept applied in asymptotic tracking of prescribed trajectories or, more specifically in this work, asymptotic rejection of disturbances. In contrast to other methods used for this purpose, such as dynamic inversion or adaptive tracking, the IMP handles both uncertainties in the model of a given system, as well as in the trajectory which is to be tracked (ISIDORI; MARCONI; SERRANI, 2012). It is well known from the IMP that a perturbation signal can be asymptotically rejected if its dynamics are reproduced by the states of the controller. In other words, if the trajectory to be rejected belongs to the set of all trajectories of a given perturbed system, a dynamic controller that incorporates an internal model of such perturbation guarantees robust (regarding parameter uncertainties) asymptotic rejection of this disturbia for every trajectory in this set (ISIDORI; MARCONI; SERRANI, 2012).

Figure 1 – Block diagram of a linear control system.

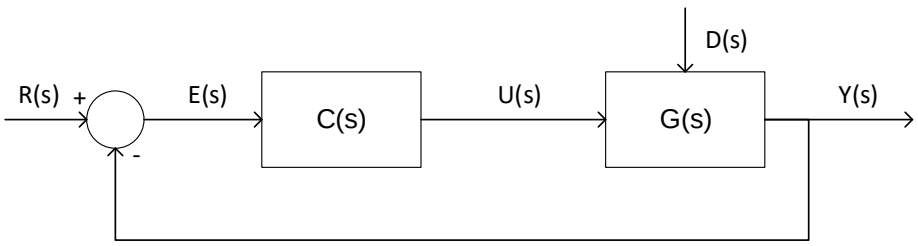

Source: the author (2016).

Consider the closed-loop block diagram from Figure 1. In this diagram, $R(s)$ is the reference input signal, $E(s)$ is the error signal, $U(s)$ is the control signal, $D(s)$ is the exogenous perturbation and $Y(s)$ is the output signal of the given system. In addition

to the signals that are included in the diagram, the transfer functions $C(s) = \frac{U(s)}{E(s)}$ and $G(s) = \begin{bmatrix} G_1(s) & G_2(s) \end{bmatrix}$ are defined for the controller and the linear system, respectively. Furthermore, define $G_1(s) = \frac{Y(s)}{U(s)}$ as the input-to-output transfer function and $G_2(s) = \frac{Y(s)}{D(s)}$ as the perturbation-to-output transfer function and assume that the poles from G_2 belong to the same set of the poles from G_1, that is, the system is controllable regarding $U(s)$.

It is desirable to partition the reference and perturbation signals in such form that the poles in the left and right semi-plane (LSP and RSP, respectively) may be independently evaluated. Therefore, consider the polynomial partition of $R(s)$ and $D(s)$ as

$$R(s) = \frac{Z_R(s)}{P_R^{lsp}(s)P_R^{rsp}(s)}, D(s) = \frac{Z_D(s)}{P_D^{lsp}(s)P_D^{rsp}(s)}, \tag{2.16}$$

so that for every $i = (R, D)$

1. No common roots exist in $Z_i(s)$, $P_i^{lsp}(s)$ and $P_i^{rsp}(s)$;
2. Polynomials $P_i^{lsp}(s)$ contain only stable poles, i.e. poles in the LSP;
3. Polynomials $P_i^{rsp}(s)$ contain only unstable or marginally stable poles, i.e. poles on the RSP or on the imaginary axis.

Similarly, partition the controller and system transfer functions as

$$C(s) = \frac{Z_c(s)}{P_c(s)}, G(s) = \begin{bmatrix} \frac{Z_{G_1}(s)}{P_{G_1}(s)} & \frac{Z_{G_2}(s)}{P_{G_2}(s)} \end{bmatrix}, \tag{2.17}$$

so that for every $i = (C, G_1, G_2)$ no common roots exist in $Z_i(s)$ and $P_i(s)$.

Considering the provisions above, the internal model principle regarding linear systems is presented on Theorem 2.1 and its corresponding proof is found in (CASTRO, 2015).

Theorem 2.1. *(Internal Model Principle) Consider the linear time-invariant closed-loop system presented on Figure 1 and assume that it is stabilizable and detectable. Assume also that the perturbation is neutrally stable, i.e forward and backward in time stable in the sense of Lyapunov (Definition 2.12), and that the error signal $E(s)$ is readable from the output $Y(s)$. Then, for every initial condition of $x(t)$, $c(t)$ and $d(t)$,*

$$\lim_{t\to\infty} e(t) = 0$$

where $c(t)$ is the states vector of the controller, if the following conditions hold true:

1. *The unperturbed system with characteristic polynomial*

$$\xi(s) = Z_C(s)Z_{G_1}(s) + P_C(s)P_{G_1}(s)$$

contain roots in the LSP only, that is, the closed-loop system is stable;
2. *Polynomial $P_C(s)$ contains all poles from $P_R^{rsp}(s)$ and $P_D^{rsp}(s)$, that is, the controller must replicate the unstable or marginally stable dynamics of the system;*
3. *Polynomial $Z_{G_1}(s)$ contains no common roots from $P_R^{rsp}(s)$ and $P_D^{rsp}(s)$, that is, the zeros of the system do not cancel the added controller poles.* ■

One such use of Theorem 2.1 is for the rejection of periodic signals, in the form of a resonant controller later used in this work. As such, the rejection of perturbations with marginally stable poles implies in singularities on the same frequencies that are present in this perturbation, i.e. with $|C(jw)| \to \infty$ on such frequencies, so that in closed-loop $e(t) \to 0$.

Going further, linear matrix inequalities will be presented on the next section, which may be used for systematically computing a control law that stabilizes the system from Figure 1.

2.2.2 Linear Matrix Inequalities in Control Theory

Linear matrix inequalities (LMIs) are widely utilized in dynamic systems analysis, with uses ranging from stability and performance evaluations, control law synthesis, optimal system realization and for many optimization problems in control theory that are constrained by LMIs (BOYD et al., 1994). Even though its use got widened in the late 1980's with the development of computational algorithms, the first LMI used to evaluate the stability of a system was the Lyapunov inequality on P. Mathematically, a linear matrix inequality takes the form of

$$F(x) = F_0 + \sum_{i=1}^{m} x_i F_i > 0, \tag{2.18}$$

where $x \in \mathbb{R}^n$ is the decision variable vector and matrices $F_i = F_i^\top \in \mathbb{R}^{m\times m}, i = 0, \ldots, n$ are given[3]. This defines $F(x)$ as positive definite and that its leading principal minors are positive (BOYD et al., 1994). Furthermore, multiple LMIs $F_1(x) > 0, \ldots, F_p(x) > 0$, $p \in \mathbb{N}^+$ can be expressed as a single LMI when disposed diagonally, i.e., $diag(F_1(x), \ldots, F_p(x)) > 0$.

[3] Note that variables that are function of time have this notation omitted, i.e. $x(t) \to x$, unless when necessary or for better comprehension, e.g., when representing limits and integrals.

Aside from the characteristics already presented, (2.18) is also convex on x, that is, it belongs on a convex set $\mathcal{X}$ so that for points $(g, h) \in \mathcal{X} \subseteq \mathbb{R}$ and scalar $\alpha \in [0, 1]$,

$$\begin{cases} F(g) > 0, \\ F(h) > 0 \end{cases} \implies F(x) > 0, \forall\ x = \alpha g + (1 - \alpha)h \in \mathcal{X} \subseteq \mathbb{R}, \tag{2.19}$$

which means that the line segment that unites the points (g, h) also belongs to set $\mathcal{X}$ and if $F(g) > 0$ and $F(h) > 0$, then $F(x) > 0$ for any x along this line segment.

While LMIs have plenty of uses, most pertinent cases naturally present themselves in nonlinear forms, specially in control systems design. In this regard, the following mathematical manipulations were used in this work (BOYD et al., 1994).

Lemma 2.2. *(Matrix congruence, congruence transformation) Consider an invertible symmetric matrix $P \in \mathbb{R}^{n\times n}$. Then*

$$P > 0 \implies Q^\top P Q > 0\ \forall\ Q \in \mathbb{R}^{n\times n}, \tag{2.20}$$

where Q has full rank. ■

Lemma 2.3. *(Schur complement) Consider matrix $S \in \mathbb{R}^{n\times m}$ and symmetric matrices $R \in \mathbb{R}^{n\times n}, T \in \mathbb{R}^{m\times m}$, with $T > 0$. Then*[4]

$$R - ST^{-1}S^\top > 0 \implies \begin{bmatrix} R & S \\ \star & T \end{bmatrix} > 0. \tag{2.21}$$

■

One of the uses of linear matrix inequalities in this work is regarding the $\mathcal{D}$-stability concept, as further explained in the next subsection.

2.2.2.1 $\mathcal{D}$-stability LMI Formulation

The $\mathcal{D}$-stability concept lets one create LMI-based constraints for an optimization problem that places the eigenvalues of a given system on a region $\mathcal{D}$. The definition to $\mathcal{D}$-stability is given below.

Definition 2.10. (D-stability) A generic LTI system $\dot{x} = Ax$ is $\mathcal{D}$-stable if, and only if, all the eigenvalues λ_i of the matrix A belong to the sub-region $\mathcal{D}$ of the negative complex plane $\mathbb{C}^-$, namely:

$$\lambda_i(A) \in \mathcal{D} \subset \mathbb{C}^-,\ \forall\ i \leq n \in \mathbb{N}^+, \tag{2.22}$$

where n is the number of eigenvalues of the system. ■

[4] The symbol $\star$ denotes the transpose of the diagonal block matrix.

This defines a sub-region of the complex plane that, when all the eigenvalues of a given closed-loop system reside within it, guarantees asymptotic stability and defines the dynamic behavior of the process. To allow the use of $\mathcal{D}$-stability in an LMI optimization problem, the sub-region $\mathcal{D}$ must also be an LMI region as follows on Definition 2.11. Such region is described by constant matrices L and M, which denote the format that the desired region will take. For instance, the region can be circular, planar, conical, intersections between these regions or even take other formats.

Definition 2.11. (LMI Regions) A subset $\mathcal{D}$ of the negative complex semi-plan is denoted an LMI region if constant matrices $L = L^T$ and M exist, such that

$$\mathcal{D} = \{s \in \mathbb{C} | L + sM + s^* M^\top < 0\}, \tag{2.23}$$

where $s = \sigma + j\omega$ and $s^* = \sigma - j\omega$. ■

The complete LMI formulation of the $\mathcal{D}$-stability theorem was originally developed by (CHILALI; GAHINET; APKARIAN, 1999), and given by

Theorem 2.4. *($\mathcal{D}$-stability LMI Formulation) The system S is $\mathcal{D}$-stable if, and only if, a matrix $P = P^\top > 0$ with appropriate dimensions exists so that*

$$L \otimes P + M \otimes (PA) + M^\top \otimes (A^\top P) < 0, \tag{2.24}$$

where $\otimes$ is the Kronecker product [5]. ■

2.3 Basic Results on Nonlinear Systems

Similarly to Section 2.2, results on nonlinear systems are presented to the reader, namely the Lyapunov stability theory, the $\mathcal{L}_2$ gain concept and the nonlinear $\mathcal{H}_\infty$ control law that will be later used in this work. The Sylvester's criterion is also introduced in this segment, mainly for its use for determining the definiteness of Lyapunov candidate functions.

2.3.1 Lyapunov Stability Theory

The Lyapunov stability theory is a classic result used in nonlinear systems control design. By using the concept of a generalized energy function, this theorem enables one to

[5] Given matrices $A \in \mathbb{R}^{m \times n}$ and $B \in \mathbb{R}^{p \times q}$, the Kronecker product is defined by

$$A \otimes B = \begin{bmatrix} a_{11}B & \dots & a_{1n}B \\ \vdots & \ddots & \vdots \\ a_{m1}B & \dots & a_{mn}B \end{bmatrix} \in \mathbb{R}^{mp \times nq}.$$

draw conclusions about the trajectories of a given system without solving the differential equations that govern it.

The main goal of a stability proof in typical Lyapunov form is to find a scalar Lyapunov candidate function $V(x)$ and $\dot{V}(x)$ that satisfies some conditions regarding its definiteness. For instance, consider a nonlinear time-invariant system in the form of

$$\dot{x} = f(x), \tag{2.25}$$

where $x \in \mathcal{B} \subseteq \mathbb{R}^n$ is the state vector, the function $f : \mathbb{R}^n \to \mathbb{R}^n$ is locally Lipschitz on x and $\mathcal{B}$ is an open set containing the origin $x = 0$. Consider also that this system has an equilibrium point $x_{eq} \in \mathcal{B}$, such that $f(x_{eq}) = 0$.

In this regard, a set of stability classes can be established as presented on Definition 2.12 and the definiteness of a function as shown on Definition 2.13. Furthermore, the Lyapunov stability concept is presented on Theorem 2.5 (KHALIL; GRIZZLE, 1996).

Definition 2.12. (System stability) Consider the equilibrium point x_{eq}. This equilibrium point, and, thus system (2.25), is:

1. **Stable in the sense of Lyapunov** if all solutions that start near x_{eq} remain near x_{eq}, that is, if for every $\epsilon > 0$ there exists $\delta > 0$ such that

$$\|x(0) - x_{eq}\| < \delta \implies \|x(t) - x_{eq}\| < \epsilon, \forall t \geq 0. \tag{2.26}$$

2. **Asymptotically stable** if x_{eq} is stable in the sense of Lyapunov and locally attractive, i.e. all solutions that start near x_{eq} tend to x_{eq} with $t \to \infty$, that is,

$$\|x(0) - x_{eq}\| < \delta \implies \lim_{t\to\infty} \|x(t) - x_{eq}\| = 0, \forall t \geq 0. \tag{2.27}$$

3. **Globally asymptotically stable** if x_{eq} is asymptotically stable for all initial conditions $x_0 \in \mathbb{R}^n$. ■

Definition 2.13. (Definiteness of a function) Consider a continuously differentiable function $V(x(t)), V : \mathbb{R}^n \to \mathbb{R}$. This function is:

1. **Positive definite** if $V(0) = 0$ and $V(x) > 0 \ \forall x \neq 0 \in \mathcal{B}$.
2. **Positive semi-definite** if $V(0) = 0$ and $V(x) \geq 0 \ \forall x \neq 0 \in \mathcal{B}$.
3. **Negative definite** if $V(0) = 0$ and $V(x) < 0 \ \forall x \neq 0 \in \mathcal{B}$.
4. **Negative semi-definite** if $V(0) = 0$ and $V(x) \leq 0 \ \forall x \neq 0 \in \mathcal{B}$. ■

Theorem 2.5. *Consider the equilibrium point x_{eq} for system (2.25) and the continuously differentiable positive definite function $V : \mathbb{R}^n \to \mathbb{R}^n$, with $x \in \mathcal{B} \subseteq \mathbb{R}^n$ and $\mathcal{B}$ an open set containing the origin $x = 0$. The system is*

1. ***Stable in the sense of Lyapunov*** *if* $\dot{V}(x)$ *is negative semi-definite.*
2. ***Asymptotically stable*** *if* $\dot{V}(x)$ *is negative definite.*
3. ***Globally asymptotically stable*** *if* $\dot{V}(x)$ *is negative definite and* $V(x)$ *is radially unbounded, i.e.* $\|x\| \to \infty \implies V(x) \to \infty$. ■

2.3.2 Sylvester's Criterion

The Sylvester's Criterion is a necessary and sufficient condition to evaluate if a given real symmetric matrix is positive-definite and may, thus, be used to determine the definiteness of a Lyapunov candidate function. For that, consider Definition 2.14 and Theorem 2.6 (GILBERT, 1991).

Definition 2.14. (Principal minors) A leading principal minor D_k of order k of matrix M is defined as the determinant of the sub-matrix obtained by deleting the last $n-k$ rows and columns of M. ■

Theorem 2.6. *(Sylvester's criterion) A real symmetric matrix* $M(x) = M(x)^\top \in \mathbb{R}^{n\times n}$ *is positive-definite if and only if all leading principal minors of* M *are positive, i.e.* $D_k > 0$*, with* $k \leq n \in \mathbb{N}^+$. ■

2.3.3 $\mathcal{L}_2$ Gain

The $\mathcal{L}_2$ gain describes how the energy of an external perturbation relates to the output energy of a given system and can be defined as a positive scalar ν. For example, a system that has $\mathcal{L}_2$ gain less than or equal ν from a perturbation $d(t) \in \mathcal{L}_2[0,\infty)$ [6] to an output $z(t) \in \mathcal{L}_2[0,\infty)$ is represented by

$$\|z(t)\|_{\mathcal{L}_2} \leq \nu \|d(t)\|_{\mathcal{L}_2} + \Upsilon, \tag{2.28}$$

where Υ is a positive scalar and the $\mathcal{L}_2$ norm of $z(t)$ is given by

$$\|z(t)\|_{\mathcal{L}_2} = \int_0^t \|z(t)\|^2 \,\mathrm{d}t. \tag{2.29}$$

Systems that have small ν have perturbation attenuation characteristics. In order to test for inequality (2.28), consider Theorem 2.7 and the corresponding proof (KHALIL; GRIZZLE, 1996).

Theorem 2.7. *Consider system*

$$S := \begin{cases} \dot{x} = f(x) + G(x)u, \\ z = h(x), \end{cases} \tag{2.30}$$

[6] The $\mathcal{L}_2$-space is formed by a set of square integrable $\mathcal{L}_2$ functions that form a Hilbert space.

where $f(x)$ is locally Lipschitz and $G(x)$ and $h(x)$ are continuous over $\mathbb{R}^n$. Let ν be a positive scalar and u the input of the system, which may contain exogenous perturbations. If there exists a continuously differentiable positive semidefinite function $V(x)$ that satisfies the inequality

$$\bar{H}_v = \left(\frac{\partial V(x)}{\partial x}\right) f(x) + \frac{1}{2\nu^2}\left(\frac{\partial V(x)}{\partial x}\right) g(x)g(x)^\top \left(\frac{\partial V(x)}{\partial x}\right)^\top + \frac{1}{2}h(x)^\top h(x) \leq 0, \tag{2.31}$$

then the system is finite-gain $\mathcal{L}_2$ stable and its $\mathcal{L}_2$ gain is less than or equal to ν. ■

Proof. Complete the squares, such that

$$\begin{aligned}\frac{\partial V}{\partial x}f(x) + \frac{\partial V}{\partial x}G(x)u = -\frac{1}{2}\nu^2\left\|u - \frac{1}{\nu^2}G^\top(x)\left(\frac{\partial V}{\partial x}\right)^\top\right\|^2 + \frac{\partial V}{\partial x}f(x) \\ + \frac{1}{2\nu^2}\frac{\partial V}{\partial x}G(x)G(x)^\top\left(\frac{\partial V}{\partial x}\right)^\top + \frac{1}{2}\nu^2\|u\|^2.\end{aligned} \tag{2.32}$$

Use (2.31) to obtain

$$\frac{\partial V}{\partial x}f(x) + \frac{\partial V}{\partial x}G(x)u \leq \frac{1}{2}\nu^2\|u\|^2 - \frac{1}{2}\|z\|^2 - \frac{1}{2}\nu^2\left\|u - \frac{1}{\nu^2}G^\top(x)\left(\frac{\partial V}{\partial x}\right)^\top\right\|^2 \tag{2.33}$$

and thus

$$\frac{\partial V}{\partial x}f(x) + \frac{\partial V}{\partial x}G(x)u \leq \frac{1}{2}\nu^2\|u\|^2 - \frac{1}{2}\|z\|^2. \tag{2.34}$$

Notice that

$$\dot{V}(x) = \frac{\partial V}{\partial x}\dot{x} = \frac{\partial V}{\partial x}f(x) + \frac{\partial V}{\partial x}G(x)u \tag{2.35}$$

and integrate both sides from $t = 0$ to $t = T \geq 0$, with initial conditions $x(0) = x_0$ to achieve

$$\int_0^T \|z(t)\|^2\,\mathrm{d}t \leq \nu^2\int_0^T \|u(t)\|^2\,\mathrm{d}t + 2(V(x_0) - V(x(T))). \tag{2.36}$$

Given that $V(x) \geq 0$,

$$\int_0^T \|z(t)\|^2\,\mathrm{d}t \leq \nu^2\int_0^T \|u(t)\|^2\,\mathrm{d}t + 2(V(x_0)). \tag{2.37}$$

Take the square roots from both sides and use the inequality $\sqrt{a^2+b^2} \leq a + b,\ \forall\ (a,b) \geq 0 \in \mathbb{R}$ to yield

$$\|z(T)\|_{\mathcal{L}_2} \leq \nu \|u(T)\|_{\mathcal{L}_2} + \sqrt{2V(x_0)}, \tag{2.38}$$

and, thus, the proof to Theorem 2.7 is complete. □

In the next section, an expanded Hamilton-Jacobi inequality will be presented, as well as a control law that guarantees $\mathcal{L}_2$ gain performance for a given system.

2.3.4 Nonlinear $\mathcal{H}_\infty$ Control Law

The state-feedback control law that is used in later sections of this work, namely as the controller for the rotation submodel of the platform, leverages the Hamilton-Jacobi inequality in order to prove closed-loop $\mathcal{L}_2$ finite-gain stability of a given system S, as described by Theorem 2.8 and the proof that follows (SCHAFT, 1992).

Theorem 2.8. *Consider an expanded system derived from (2.30)*

$$S := \begin{cases} \dot{x} = f(x) + g_1(x)d + g_2(x)u, \\ z = \begin{bmatrix} h(x) \\ \rho u \end{bmatrix}, \end{cases}$$

where $f(x)$ is locally Lipschitz, $g_1(x)$, $g_2(x)$ and $h(x)$ are continuous over $\mathbb{R}^n$, u is the input and d is a perturbation that affects the system, ρ is a positive weighting scalar for the control signal and $h(x)$ is an output function.

If there exists a positive semidefinite function $V(x)$ that satisfies Theorem 2.7 with generalized Hamilton-Jacobi inequality

$$H_v = \left(\frac{\partial V(x)}{\partial x}\right) f(x) + \frac{1}{2}\left(\frac{\partial V(x)}{\partial x}\right)\left(\frac{1}{\nu^2} g_1(x) g_1(x)^\top - \frac{1}{\rho^2} g_2(x) g_2(x)^\top\right)\left(\frac{\partial V(x)}{\partial x}\right)^\top + \frac{1}{2} h(x)^\top h(x) \leq 0, \tag{2.39}$$

then the control law

$$u = -\frac{1}{\rho^2} g_2^\top \frac{\partial^\top V}{\partial x}, \tag{2.40}$$

with $g_2 \in \mathbb{R}^n$ and scalar $\rho > 0$, stabilizes system S with $\mathcal{L}_2$ gain from d to $z = \begin{bmatrix} h^\top(x) & \rho u^\top \end{bmatrix}^\top$ less than or equal a positive scalar ν. ■

Proof. Consider the first derivative of $V(x)$ and complete the squares, i.e.

$$\begin{aligned}
\frac{dV}{dt} &= \frac{\partial V}{\partial x} f(x) + \frac{\partial V}{\partial x} g_1(x) d + \frac{\partial V}{\partial x} g_2(x) u \\
&\leq \frac{1}{2}\rho^2 \left\| u + \frac{1}{\rho^2} g_2^\top \frac{\partial^\top V}{\partial x} \right\|^2 - \frac{1}{2}\nu^2 \left\| d - \frac{1}{\nu^2} g_1^\top \frac{\partial^\top V}{\partial x} \right\|^2 \\
&- \frac{1}{2}\rho^2 \|u\|^2 + \frac{1}{2}\nu^2 \|d\|^2 + \frac{\partial V}{\partial x} f(x) - \frac{1}{2}\frac{1}{\rho^2}\frac{\partial V}{\partial x} g_2 g_2^\top \frac{\partial^\top V}{\partial x} \\
&+ \frac{1}{2}\frac{1}{\nu^2}\frac{\partial V}{\partial x} g_1 g_1^\top \frac{\partial^\top V}{\partial x},
\end{aligned} \tag{2.41}$$

and use (2.39) to obtain

$$\begin{aligned}
\frac{dV}{dt} &\leq \frac{1}{2}\rho^2 \left\| u + \frac{1}{\rho^2} g_2^\top \frac{\partial^\top V}{\partial x} \right\|^2 - \frac{1}{2}\nu^2 \left\| d - \frac{1}{\nu^2} g_1^\top \frac{\partial^\top V}{\partial x} \right\|^2 \\
&- \frac{1}{2}\rho^2 \|u\|^2 + \frac{1}{2}\nu^2 \|d\|^2 - \frac{1}{2}\|h\|^2.
\end{aligned} \tag{2.42}$$

Now substitute the control law (2.40)

$$-2\frac{dV}{dt} - \nu^2 \left\| d - \frac{1}{\nu^2} g_1^\top \frac{\partial^\top V}{\partial x} \right\|^2 \leq \|h\|^2 + \rho^2 \|u\|^2 - \nu^2 \|d\|^2, \tag{2.43}$$

and integrate both sides from $t = 0$ to $t = T \geq 0$, with initial conditions $x(0) = x_0$ to achieve

$$\int_0^T \left(\|h(t)\|^2 + \|\rho u(t)\|^2 \right) \mathrm{d}t \leq \nu^2 \int_0^T \|d(t)\|^2 \,\mathrm{d}t + 2(V(x_0) - V(x(T))). \tag{2.44}$$

Given that $V(x) \geq 0$,

$$\int_0^T \|z(t)\|^2 \,\mathrm{d}t \leq \nu^2 \int_0^T \|d(t)\|^2 \,\mathrm{d}t + 2(V(x_0)), \tag{2.45}$$

and, thus, the proof to Theorem 2.8 is complete. □

3 Stewart Platform

This chapter approaches the main mathematical descriptions of the Stewart platform that are necessary in order to develop the control methods that will later be proposed on Chapter 4. This chapter is organized as follows: first, a geometric description of the platform used throughout this work will be presented, along with the main constructive parameters of the manipulator. Next, the inverse kinematics of the system is addressed in order to present the Jacobian matrix as defined in terms of a quaternion description. In this same context, the Jacobian singularities are presented to the reader. The dynamics of the end effector is then described in quaternion terms using the Newton-Euler formulation and mathematically expressed in two decoupled submodels. Finally, the quaternion-based Newton-Euler model is validated against the more classical Euler-angle Lagrange model.

3.1 Geometric Description of the Stewart Platform

Consider the Stewart platform from Figure 2. Define three reference systems, a global inertial frame O_I, a local reference frame for the bottom platform O_B and for the end effector O_T[1]. For both local reference frames, the coordinate origins coincide with the center of mass of the respective bodies.

Figure 2 – The Stewart platform and its reference systems.

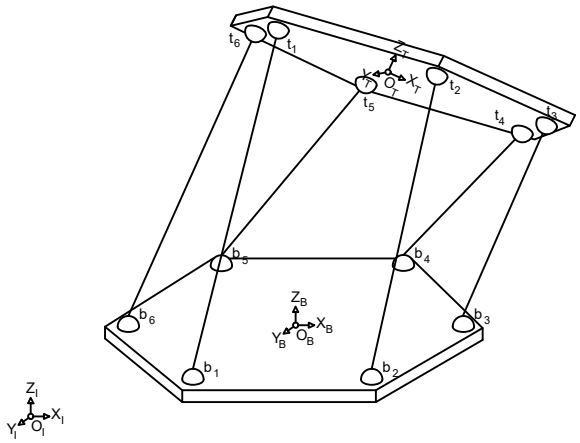

Source: the author (2016).

This manipulator has $i = (1, \ldots, 6)$ linear actuators, also called legs of the system, which concede to the platform its six degrees of freedom (DOF). Each joint b_i and t_i is a vertex of an hexagon inscribed in a circle with radius r_B and r_T. Furthermore, let angles

[1] The subscripts B and T will be used from now on to denote reference to the bottom and top platforms, respectively, when regarding the geometric definition of the manipulator.

φ_B and φ_T define the length of each edge of the platform, as Figure 3 shows. Given that the joints are arranged in pairs, spaced 120° apart from each other (MELLO, 2011), φ_B and φ_T also define the spacing between each joint in a pair.

Figure 3 – Geometric parameters of joint placement, with $\varphi \rightarrow \varphi_j$, with $j = (T, B)$.

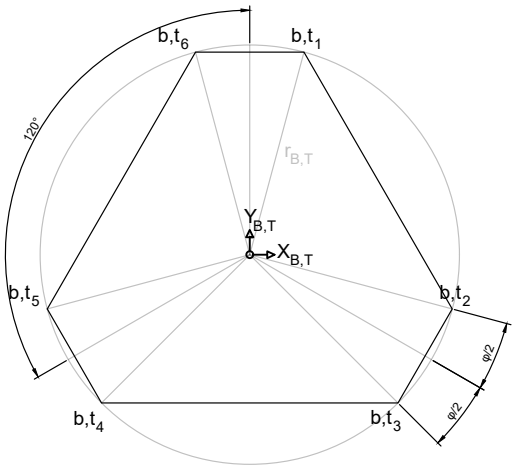

Source: the author (2016).

Furthermore, the joints b_i and t_i are geometrically defined by vectors $B_i \in \mathbb{R}^3$ and $T_i \in \mathbb{R}^3$ for the bottom and top platforms, respectively, regarding each local reference frame, such as

$$B_i = \begin{bmatrix} r_B \cos(\lambda_i) \\ r_B \sin(\lambda_i) \\ 0 \end{bmatrix}, T_i = \begin{bmatrix} r_T \cos(\upsilon_i) \\ r_T \sin(\upsilon_i) \\ 0 \end{bmatrix}, \tag{3.1}$$

where,

$$\lambda_i = \begin{cases} \dfrac{i\pi}{3} - \dfrac{\varphi_B}{2}, & i = (1, 3, 5) \\ \lambda_{i-1} - \varphi_B, & i = (2, 4, 6) \end{cases}$$

$$\upsilon_i = \begin{cases} \dfrac{i\pi}{3} - \dfrac{\varphi_T}{2}, & i = (1, 3, 5) \\ \upsilon_{i-1} - \varphi_T & i = (2, 4, 6). \end{cases} \tag{3.2}$$

Therefore, parameters r_B, r_T, φ_B and φ_T define the geometric structure of a given Stewart platform.

Now that the platform is geometrically described, the next section will approach the inverse kinematics of the system to define a Jacobian matrix, which will allow the outputs of the later proposed controllers to drive the linear actuators of the manipulator.

3.2 Quaternion-based Jacobian and Inverse Kinematics

As a standard definition, the Jacobian matrix J transforms the linear velocities of the six actuators $\dot{l} \in \mathbb{R}^6$ to the linear and angular velocities of the platform, $\dot{p}_j \in \mathbb{R}^3$ and $\omega_j \in \mathbb{R}^3$, respectively, with $j = (T,\ B)$. That is,

$$\dot{l} = J \begin{bmatrix} \dot{p}_T \\ \omega_T \\ \dot{p}_B \\ \omega_B \end{bmatrix}, \tag{3.3}$$

with angular velocities ω_T and ω_B referenced in each local body frame.

Going further, from Figure 4, the vectors T_i and B_i are defined from the center of the top and bottom platforms, to the i^{th} top and bottom links, relative to the top and bottom platforms, respectively, and p_T and p_B are the position vectors of the platforms. This allows, thus, Theorem 3.1 to be presented.

Figure 4 – Main vectors of the platform.

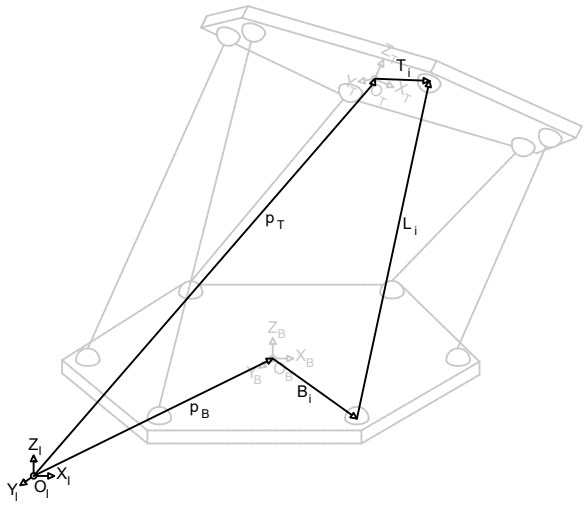

Source: the author (2016).

Theorem 3.1. *(Jacobian matrix) Consider the Stewart platform and vectors shown on Figure 4. There exists a Jacobian matrix $J \in \mathbb{R}^{6\times 12}$ given by*

$$J = \begin{bmatrix} n_1^\top & (S(R_T^I T_1)n_1)^\top & -n_1^\top & -(S(R_B^I B_1)n_1)^\top \\ \vdots & \vdots & \vdots & \vdots \\ n_6^\top & (S(R_T^I T_6)n_6)^\top & -n_6^\top & -(S(R_B^I B_6)n_6)^\top \end{bmatrix}, \tag{3.4}$$

if the relation (3.3) holds true, where

$$n_i = \frac{L_i}{\|L_i\|} \tag{3.5}$$

is an unit vector with the same direction of the i^{th} *leg* L_i *(*$i = 1 \dots 6$*) such as*

$$L_i = R_T^I T_i + p_T - (R_B^I B_i + p_B), \tag{3.6}$$

and R_T^I *and* R_B^I *are the rotation matrices regarding the global inertial frame of the platforms, given by*

$$R_j(\eta_j, \varepsilon_j) = I + 2\eta_j S(\varepsilon_j) + 2S^2(\varepsilon_j), \tag{3.7}$$

where η_j *and* ε_j *are the real and imaginary values of* $\mathbf{q}_j$*,* $j = T,\ B$*.* ■

Proof. Differentiate both sides of (3.6) relative to time to obtain

$$\dot{L}_i = \dot{p_T} + S(\omega_T)(R_T^I T_i) - \dot{p_B} - S(\omega_B)(R_B^I B_i), \tag{3.8}$$

and define the velocity vector with the same direction of the i^{th} leg:

$$\dot{l}_i = \dot{L}_i \cdot n_i. \tag{3.9}$$

Substitute (3.9) in (3.8) to achieve

$$\dot{l}_i = \dot{p_T} \cdot n_i + (S(\omega_T)(R_T^I T_i)) \cdot n_i - \dot{p_B} \cdot n_i - (S(\omega_B)(R_B^I B_i)) \cdot n_i. \tag{3.10}$$

Using the property that the vector dot product is the same as the product of a transposed vector, that is,

$$a \cdot b = b^\top a,$$

and the cross product property given by

$$u \cdot (S(v)w) = (S(u)v) \cdot w,$$

yields

$$\dot{l}_i = n_i^\top \dot{p_T} - n_i^\top \dot{p_B} + (S(R_T^I T_i)n_i)^\top \omega_T - (S(R_B^I B_i)n_i)^\top \omega_B. \tag{3.11}$$

Finally, (3.11) may be rewritten into

$$\dot{l} = J \begin{bmatrix} \dot{p}_T \\ \omega_T \\ \dot{p}_B \\ \omega_B \end{bmatrix}, \tag{3.12}$$

where J is the Jacobian matrix from (3.4). □

Corollary. *If the global inertial frame coincides with the local reference frame of the bottom platform of the manipulator, (3.6) is simplified to*

$$L_i = R_T^I T_i + p_T, \tag{3.13}$$

and the Jacobian matrix (3.4) is given by

$$J = \begin{bmatrix} n_1^\top & (S(R_T^I T_1)n_1)^\top \\ \vdots & \vdots \\ n_6^\top & (S(R_T^I T_6)n_6)^\top \end{bmatrix}. \tag{3.14}$$

■

Another important result used in this work is that of Theorem 3.2, which allows the use of the Jacobian matrix to relate the forces and torques of the platform to the forces of the six actuators that power the manipulator.

Theorem 3.2. *(Actuator linear forces to platform forces and torques relation) If J is a Jacobian matrix, its transpose $J^\top$ may also be used to relate the linear forces of the six actuators $f_l = [f_{l_1} \dots f_{l_6}]^\top$ to the forces and torques applied on the top (F_T and τ_T) and bottom platforms (F_B and τ_B), that is*

$$F = \begin{bmatrix} F_T \\ \tau_T \\ F_B \\ \tau_B \end{bmatrix} = J^\top f_l. \tag{3.15}$$

■

Proof. From the definition of work and power

$$W = \int F^\top \, \mathrm{d}t,$$

$$P = \frac{dW}{dt} \therefore P = F^\top v,$$

where W is the work, P is the power and v is the velocity, consider the following relations:

$$\begin{aligned} P &= F^\top v, \\ P_l &= f_l^\top \dot{l}, \end{aligned} \tag{3.16}$$

where $\dot{l}$ is the linear velocities of the six actuators and

$$v = \begin{bmatrix} \dot{p}_T \\ \omega_T \\ \dot{p}_B \\ \omega_B \end{bmatrix} \in \mathbb{R}^{12}.$$

From the energy conservation principle, it follows that the resulting power P produced by the forces and torques applied to the platform must equal that of the resulting power produced by f_l, that is

$$P = P_l.$$

Going further, expand the equations and continue the computation such as

$$\begin{aligned} F^\top v &= f_l^\top \dot{l} \quad \therefore \\ F^\top v &= f_l^\top J v \quad \therefore \\ F^\top &= f_l^\top J \quad \therefore \\ F &= J^\top f_l, \end{aligned} \tag{3.17}$$

which results in (3.15), and, thus, the proof to Theorem 3.2 is complete. □

From the theorems presented in this section, more specifically Theorem 3.2, if matrix $J^{-\top} := (J^\top)^{-1}$ is locally pseudo invertible, the output signals of the controllers presented on Chapter 4 may be successfully transformed in the inputs of the linear actuators that effectively control the platform. In this sense, the attitude of the platform must be analyzed for singularities, given that in some stances of the manipulator $rank(J^\top) < 6$, where six is the number of actuators.

3.2.1 Jacobian Singularities

As briefly introduced in the last section, the Jacobian matrix transpose $J^\top$ must be pseudo[2] invertible in order to allow the coupling of the controller signals later presented in this work. More specifically, $rank(J^\top)$ must be equal to the number of actuators of the platform and the actuators must not be saturated, else (3.15) does not have a solution. Physically, the platform loses one or more degrees of freedom when the length of the actuators reach their maximum or minimum values or when J loses rank. There exist two cases where $rank(J^\top)$ is less than the number of actuators[3], namely (GOSSELIN; ANGELES, 1990):

[2] Since $J^\top \in \mathbb{R}^{12\times 6}$, a pseudo inverse algorithm must be used to obtain $J^{-\top}$, such as the Moore-Penrose pseudoinverse computed via singular value decomposition (BARATA; HUSSEIN, 2012).

[3] Since $J^\top$ is not a square matrix, $rank(J^\top)$ is computed via QR decomposition with column pivoting (HIGHAM, 2000).

1. When two or more actuators belong to the same plane or when two or more links are parallel;

2. When all actuators are parallel to each other, i.e., the platform is non-controllable given ill-defined structural parameters $r_T = r_B$ and $\varphi_T = \varphi_B$.

In those cases or when the actuators are saturated, the platform assumes a so-called singular configuration where the manipulator becomes uncontrollable, and, thus, must be avoided.

Singular attitude determination of closed-kinematics mechanisms are a research field on their own. For detection of singularities of the Stewart platform modeled in quaternion terms, refer to (CHARTERS; ENGUIÇA; FREITAS, 2009).

3.3 Quaternion-based Dynamic Model

This section aims to provide the necessary mathematical description of the dynamics of the Stewart platform, which will then later be used on Chapter 4. While many works (GARCÍA, 2015) (MELLO, 2011) use the Lagrange formulation for modeling the dynamics of this system, it is inherently complex to compute the matrices that describe such dynamics. Some other works use the Newton-Euler formulation, which is easier to compute in itself, but using regular Euler angles (LEE et al., 2003).

This work uses, thus, a different approach, namely a Newton-Euler formulation in quaternion form. Such use of quaternions simplify the controller design for this system, mainly when describing Lyapunov candidate functions, given the properties of an attitude quaternion as presented on Section 2.1.2. This enables one to design different simple controllers for each submodel, one for the translational dynamics and another for the rotational dynamics, which may later be combined in a single control signal using the Jacobian matrix.

3.3.1 Quaternion-based Newton-Euler Model

The Stewart platform, when its corresponding description is mathematically coupled, is a nonlinear system that is usually modeled using the Lagrange or Newton-Euler formulation, being the latter used in this work. The main goal of this section is to present a decoupled mathematical model for the Stewart platform using quaternions, in such form that the translational dynamics of the manipulator are represented by a linear system and the rotational dynamics by a nonlinear system.

For this purpose, the classic description of a generic 3D rigid body with respect to a coordinate frame whose origin coincides with the center of mass of the body will be

used. Consider, thus, the Newton-Euler equations that represent the upper platform (end effector) given by

$$\begin{aligned} \tau &= I_m\dot{\omega} + S(\omega)I_m\omega, \\ F &= m\dot{v}, \end{aligned} \tag{3.18}$$

where $\tau \in \mathbb{R}^3$ is the torque vector, $I_m \in \mathbb{R}^{3\times3}$ is the inertia tensor and $\omega \in \mathbb{R}^3$ is the angular velocity vector, all represented in the local body frame of the upper platform. In addition, $F \in \mathbb{R}^3$ is the force vector and $v \in \mathbb{R}^3$ is the linear velocity vector, where these last two are represented in the global inertial frame, and m is the body mass of the end effector, whose center of mass is described by point O_T in Figure 2. The term $S(\omega)I_m\omega$ represents the gyroscopic effect on the platform.

In order to relate the dynamics of the velocities, position and orientation of the upper platform, the mapping

$$\begin{aligned} \dot{q} &= \tfrac{1}{2}\begin{bmatrix} -\varepsilon^\top \\ \eta I + S(\varepsilon) \end{bmatrix}\omega, \\ \dot{p} &= v, \end{aligned} \tag{3.19}$$

may be used (XU; MANDIC, 2014), where $q = \begin{bmatrix} \eta & \varepsilon^\top \end{bmatrix}^\top \in \mathbb{R}^4$ is the body orientation unit quaternion (with scalar and vector parts $\eta \in \mathbb{R}$, $\varepsilon \in \mathbb{R}^3$) and $p = \begin{bmatrix} p_x & p_y & p_z \end{bmatrix}^\top \in \mathbb{R}^3$ is the position vector of the end effector regarding the global inertial frame, with p_x, p_y and p_z related to the x-, y- and z-axis respectively.

Add the gravity force on the system and the complete dynamics of the upper platform can then be expressed by

$$\dot{x} = \begin{bmatrix} \dot{q} \\ \dot{w} \\ \dot{p} \\ \dot{v} \end{bmatrix} = \begin{bmatrix} \tfrac{1}{2}\begin{bmatrix} -\varepsilon^\top \\ \eta I + S(\varepsilon) \end{bmatrix}\omega \\ {I_m}^{-1}(u_\tau + \tau_{ext} - S(\omega)I_m\omega) \\ v \\ m^{-1}(\bar{u}_F + F_{ext}) + g \end{bmatrix}, \tag{3.20}$$

where $u_\tau \in \mathbb{R}^3$ and $\tau_{ext} \in \mathbb{R}^3$ are the input and perturbation torques referenced on the local body frame, $\bar{u}_F \in \mathbb{R}^3$ and $F_{ext} \in \mathbb{R}^3$ are the input and perturbation forces referenced on the global inertial frame and g is the gravity vector.

In this work, I_m and m are assumed constant in the dynamic models so that variations on their values are treated as perturbations. Actuator dynamics are also con-

sidered[4] as perturbations. Therefore, external perturbations represent some important disturbances that the platform is subject to, such as: mass increase and center of mass shift in load conditions, external forces and torques applied directly on the base and top platforms, unmodelled elements and uncertain parameters. In addition, it is assumed that the actuators do not saturate.

From (3.20), two systems may defined: a linear translational model $\bar{S}_1$ and a non-linear rotational model $\bar{S}_2$ as follows:

$$\bar{S}_1 := \begin{cases} \begin{bmatrix} \dot{p} \\ \dot{v} \end{bmatrix} = \begin{bmatrix} \mathbf{0} & I \\ \mathbf{0} & \mathbf{0} \end{bmatrix} \begin{bmatrix} p \\ v \end{bmatrix} + \begin{bmatrix} \mathbf{0} \\ m^{-1}I \end{bmatrix} u_F + \begin{bmatrix} \mathbf{0} \\ m^{-1}I \end{bmatrix} F_{ext} \\ \\ x_1 = \begin{bmatrix} p \\ v \end{bmatrix} \end{cases}, \tag{3.21}$$

where $u_F = \bar{u}_F - g$ and

$$\bar{S}_2 := \begin{cases} \begin{bmatrix} \dot{q} \\ \dot{\omega} \end{bmatrix} = \begin{bmatrix} \frac{1}{2} \begin{bmatrix} -\varepsilon^\top \\ \eta I + S(\varepsilon) \end{bmatrix} \omega \\ -{I_m}^{-1} S(\omega) I_m \omega \end{bmatrix} + \begin{bmatrix} 0 \\ 0 \\ I_m^{-1} \end{bmatrix} \tau_{ext} + \begin{bmatrix} 0 \\ 0 \\ I_m^{-1} \end{bmatrix} u_\tau, \\ \\ x_2 = \begin{bmatrix} q \\ \omega \end{bmatrix} \end{cases}. \tag{3.22}$$

The choices made in this work, namely the reference frames for each parameter, the decoupled equations presented on (3.21) – (3.22) and the use of quaternions are key to obtaining a simple control solution for the platform, later presented on Chapter 4.

3.3.2 Validating the Quaternion-based Dynamic Model

For comparison purposes, the quaternion-based dynamic model presented on Section 3.3.1 will be validated against the more common Lagrange formulation, as to confirm that it is a valid description of the platform. In order to do that, consider the Lagrange dynamic equation of the platform described in Euler angles (KIM; KANG; LEE, 2000):

$$M(x)\ddot{x} + V(x, \dot{x})\dot{x} + G = \begin{bmatrix} F_j \\ \tau_j \end{bmatrix}, \tag{3.23}$$

[4] This assumption was made given that the bandwidth of the closed-loop system is generally significantly smaller than that of the actuators. Furthermore, this work provides a general control solution for the Stewart platform, regardless of the chosen actuator solution.

with $j = (T, B)$, where $M(x) \in \mathbb{R}^{6\times6}$ is the inertia matrix, $V(x, \dot{x}) \in \mathbb{R}^{6\times6}$ is the Coriolis matrix and $G \in \mathbb{R}^{6\times1}$ is the gravity matrix, with

$$M(x) = \begin{bmatrix} m & 0 & 0 & 0 & 0 & 0 \\ 0 & m & 0 & 0 & 0 & 0 \\ 0 & 0 & m & 0 & 0 & 0 \\ 0 & 0 & 0 & I_x C_\beta^2 C_\gamma^2 + I_y C_\beta^2 S_\gamma^2 + I_z S_\beta^2 & (I_x - I_y) C_\beta C_\gamma S_\gamma & I_z S_\beta \\ 0 & 0 & 0 & (I_x - I_y) C_\beta C_\gamma S_\gamma & I_x S_\gamma^2 + I_y C_\gamma^2 & 0 \\ 0 & 0 & 0 & I_z S_\beta & 0 & I_z \end{bmatrix}, \tag{3.24}$$

$$V(x, \dot{x}) = \begin{bmatrix} 0 & 0 & 0 & 0 & 0 & 0 \\ 0 & 0 & 0 & 0 & 0 & 0 \\ 0 & 0 & 0 & 0 & 0 & 0 \\ 0 & 0 & 0 & K_1\dot{\beta} + K_2\dot{\gamma} & K_1\dot{\alpha} + K_5\dot{\beta} + K_3\dot{\gamma} & K_2\dot{\alpha} + K_3\dot{\beta} \\ 0 & 0 & 0 & -K_1\dot{\alpha} + K_3\dot{\gamma} & K_4\dot{\gamma} & K_3\dot{\alpha} + K_4\dot{\beta} \\ 0 & 0 & 0 & -K_2\dot{\alpha} - K_3\dot{\beta} & -K_3\dot{\alpha} - K_4\dot{\beta} & 0 \end{bmatrix}, \tag{3.25}$$

$$G = \begin{bmatrix} 0 & 0 & mg & 0 & 0 & 0 \end{bmatrix}^\top. \tag{3.26}$$

In addition, the operators C and S denote the cosine and sine functions of the variable subscripted, the variables K_i (i = 1, ..., 5) are defined by

$$\begin{aligned} K_1 &= -C_\beta S_\beta (C_\gamma^2 I_x + S_\gamma^2 I_y - I_z), \\ K_2 &= -C_\beta^2 C_\gamma S_\gamma (I_x - I_y), \\ K_3 &= \frac{1}{2} C_\beta (C_\gamma - S_\gamma)(C_\gamma + S_\gamma)(I_x - I_y), \\ K_4 &= C_\gamma S_\gamma (I_x - I_y), \\ K_5 &= -C_\gamma S_\gamma S_\beta (I_x - I_y), \end{aligned} \tag{3.27}$$

and the scalars I_x, I_y, I_z are obtained from the inertia matrix I_m as follows

$$I_m = \begin{bmatrix} I_x & 0 & 0 \\ 0 & I_y & 0 \\ 0 & 0 & I_z \end{bmatrix}. \tag{3.28}$$

Both mathematical models were simulated with the scenario as follows. A sinusoidal torque of the form $A_1 \sin(\sigma_c t)$ was applied on every axis, i.e. α, β and γ, and a sinusoidal force of the form $A_2 \sin(\sigma_c t)$ on the z-axis of the bottom platform, A_1 and $A_2 \in \mathbb{R}$. For reference, the default values were $A_1 = \frac{1}{3}$, $A_2 = 5$ and $\sigma_c = 0.2$Hz.

For a more objective approach, the mean square error (MSE) was calculated on both the motion and attitude errors as simulated, such as

$$\text{MSE} = \frac{1}{n}\sum_{i=1}^{n}\left(\|v_{Q_i}\| - \|v_{L_i}\|\right)^2,$$

where $i = size(v_Q) = size(v_L)$ is the number of samples considered and v_Q, v_L are the considered vectors for the quaternion-based and Lagrange-based models, respectively, e.g. the motion and attitude errors to the reference stance.

The resulting MSE was numerically null for sample values truncated after the seventh decimal point, which validates the quaternion-based Newton-Euler model as a valid alternative for describing the Stewart platform.

4 Proposed Control Methods

In this chapter, the proposed control methods are presented to the reader. The first topic is the suggested controller for the translational submodel, which starts by augmenting such model with resonant and integral action states. Next, a state-feedback law is designed to control this augmented translational system via an optimization problem subject to LMIs and performance criteria, namely $\mathcal{H}_\infty$ gain minimization and $\mathcal{D}$-stability concepts. Going further, a nonlinear state-feedback control law for the rotational submodel is designed to achieve $\mathcal{L}_2$ gain performance. The resulting closed-loop system is then linearized and augmented with resonant and integral states. It is subsequently subject to another control law defined via an optimization problem subject to LMIs and $\mathcal{D}$-stability criteria.

Next, instead of using the Jacobian matrix inside the computation of the control law that will be applied on the platform, the proposed approach effectively defers the use of such matrix to the very last computational step, while also leveraging the signal coupling characteristic that is inherent to it. The coupling of the control signals of both controllers is, thus, addressed via the Jacobian presented earlier on Chapter 3. For reference, consider Figure 5, which illustrates the control loop.

Figure 5 – Proposed control loop.

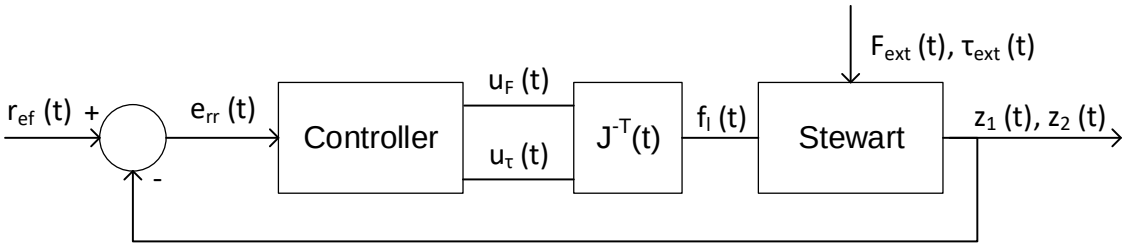

Source: the author (2016).

Finally, an inverse dynamics controller is described in order to allow comparisons of the controller suggested in this work to be drawn against control methods proposed in other works.

4.1 Translational Control

This section aims to provide a clear understanding on the developed dynamic translation controller applied on the Stewart platform.

As the reader can notice from the submodels that arose from decoupling the system, the translational portion of the model is linear. Therefore, all the classic theories of linear control design can be applied on this submodel of the platform, namely, in this particular work, a mixed dynamic controller with resonant states based on the IMP with integral action, $\mathcal{H}_\infty$ gain minimization and region-based eigenvalue placement with $\mathcal{D}$-stability. To allow for a systematic method for designing the control parameters, an optimization problem subject to Linear Matrix Inequalities is defined.

The first step to achieve this design is to describe an augmented model which encompasses the desired resonant and integral-action states to be added on the original system. These additions will guarantee both rejection to sinusoidal perturbations and DC component removal of the motion error, respectively. The next step is to define a set of constraints for an LMI-based optimization problem that minimizes the $\mathcal{H}_\infty$ gain to the external perturbation and places the closed-loop eigenvalues of the system inside a subregion $\mathcal{D}$ of the negative complex plane.

4.1.1 Augmented Model

The main goal of the translation control, beyond the necessary condition of closed-loop stability, is to reject external sinusoidal perturbations included in the external disturbance F_{ext}. This perturbation can have known frequencies, e.g. from ocean waves, which are no higher than 0.2Hz on oceans near Brazil (MELLO, 2011), known dynamics, e.g. gravity, or unknown dynamics, such as model uncertainties, wind, load conditions on the platform, and so forth. So as to tackle the first case presented, the use of a resonant controller, which is based on the IMP, is the starting point of the proposed design.

4.1.1.1 Resonant Controller

Recall the translation submodel $\bar{S}_1$, which represents the dynamics around the equilibrium point $(p = \mathbf{0}, v = \mathbf{0})$[1] regarding only the cartesian position p and linear velocities v of the platform, but with an output function z_1, such as

$$S_1 := \begin{cases} \dot{x}_1(t) = Ax_1(t) + B_u u_F(t) + B_\phi F_{ext}(t) \\ z_1(t) = Cx_1(t) \end{cases}, \tag{4.1}$$

[1] $\mathbf{0}$ is the appropriately sized zero-filled matrix or vector.

where $x_1(t) = \begin{bmatrix} p(t)^\top & v(t)^\top \end{bmatrix}^\top \in \mathbb{R}^6$ is the state vector for the translation of the platform and the matrices

$$A = \begin{bmatrix} \mathbf{0} & I \\ \mathbf{0} & \mathbf{0} \end{bmatrix} \in \mathbb{R}^{6\times 6}, B_u = B_\phi = \begin{bmatrix} \mathbf{0} \\ m^{-1}I \end{bmatrix} \in \mathbb{R}^{6\times 3} \tag{4.2}$$

represent the state (or system) matrix and the input matrices, respectively. The state vector x_1 represents the deviation from the equilibrium point, with $u_F = \bar{u}_F - g$.

Assume that all states are available to the controller, with $C = \mathbf{I} \in \mathbb{R}^{6\times 6}$ and that S_1 is also controllable under sustained perturbation F_{ext}. The state output vector C is of the form

$$C = \begin{bmatrix} C_x \\ C_y \\ C_z \\ C_{w_x} \\ C_{w_y} \\ C_{w_z} \end{bmatrix} \in \mathbb{R}^{6\times 6}, C_x = \begin{bmatrix} 1 \\ 0 \\ 0 \\ 0 \\ 0 \\ 0 \end{bmatrix}^\top, C_y = \begin{bmatrix} 0 \\ 1 \\ 0 \\ 0 \\ 0 \\ 0 \end{bmatrix}^\top, \ldots, C_{w_z} = \begin{bmatrix} 0 \\ 0 \\ 0 \\ 0 \\ 0 \\ 1 \end{bmatrix}^\top, \tag{4.3}$$

where C_x to C_{w_z} represent the single state output vectors for each state.

It is well known from the IMP, presented on Section 2.2.1, that a perturbation signal can be asymptotically rejected if its dynamics are reproduced by the states of the controller. If the periodic perturbation applied to the system is a sinusoidal signal of fundamental frequency σ_r, the control loop must include additional resonant states $x_r \in \mathbb{R}^2$ in the form of

$$\begin{aligned} \dot{x}_r(t) &= \bar{A}_r x_r(t) + B_r e_r(t), \\ y_r(t) &= x_r(t), \end{aligned} \tag{4.4}$$

where $e_r(t) \in \mathbb{R}$ is the motion error, i.e., $r_x - p_x$ for the state regarding the x axis, $r_x(t) \in \mathbb{R}$ being the reference,

$$\bar{A}_r = \begin{bmatrix} 0 & 1 \\ -(h\sigma_r)^2 & 0 \end{bmatrix}, B_r = \begin{bmatrix} 0 \\ 1 \end{bmatrix}, \tag{4.5}$$

and h representing the h_{th} harmonic, with $h = 1$ for the fundamental frequency and $h > 1 \in \mathbb{N}$ for the harmonics.

4.1.1.2 FFT Analysis

Even though the translational submodel S_1 of the top platform is by itself linear, the perturbations applied on the bottom platform in the form of prescribed movements

are defined on the global inertial frame, i.e. instead of the reference frames used on the translational model, and must propagate through the entire nonlinear structure of the complete coupled system consisting of the bottom and top platforms. This process is done by applying rotations and translations on the end effector, so as to correctly represent the movement of the bottom platform onto the upper one, as seen on Figure 6.

Figure 6 – The Stewart platform simulated with the necessary rotations applied.

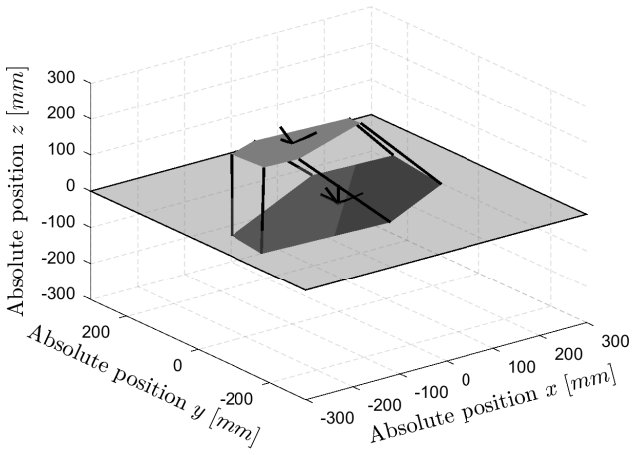

Source: the author (2016).

Given that it is nonlinear, this process of applying transformations on the various reference frames can, thus, generate harmonics on the translation of the top platform. A Fourier analysis of the system output should be performed, as this will enable the appropriate tuning of the right harmonics to include on the resonant controller.

To illustrate the phenomenon, consider the scenario used on Section 3.3.2. Let e_1, e_2 and e_3 be the position errors relative to $p = \begin{bmatrix} p_x & p_y & p_z \end{bmatrix}^\top$ and the reference stance. The resulting movement of the upper platform is presented on Figure 7.

While the motion errors of the x and y-axis visually maintain the same frequency of the torques applied on the bottom frame, the z-axis error presents a higher order harmonic on its output, along with a DC signal. The resulting two-sided power spectrum (2SPS) of a Discrete Fast Fourier Transform, with sampling frequency of $f_s = 100$Hz, of the motion error on the top platform is obtained as presented of Figure 8. The remaining harmonics of the open loop system are negligible when compared to the first and second harmonics, and, thus not shown.

As it is clear to see, both the fundamental frequency and the second harmonic of the z-axis motion error possess a high amplitude and should be attenuated. The remaining errors from axis x and y concentrate themselves on the fundamental frequency. Higher harmonics are found to not significantly impact the performance of the system so

Figure 7 – Motion error of the top platform when subject to torques and forces applied on the bottom frame.

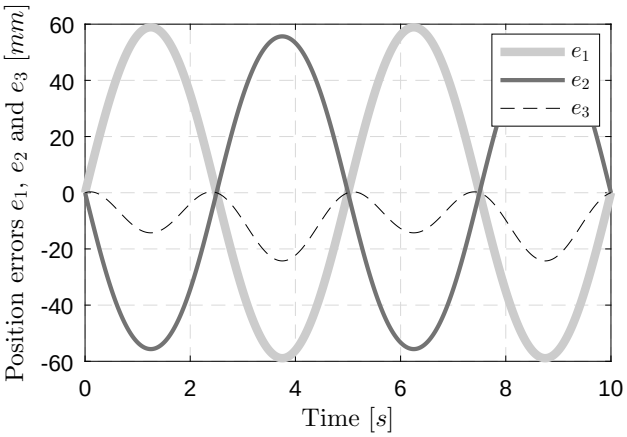

Source: the author (2016).

Figure 8 – 2SPS of the motion error shown on Figure 7.

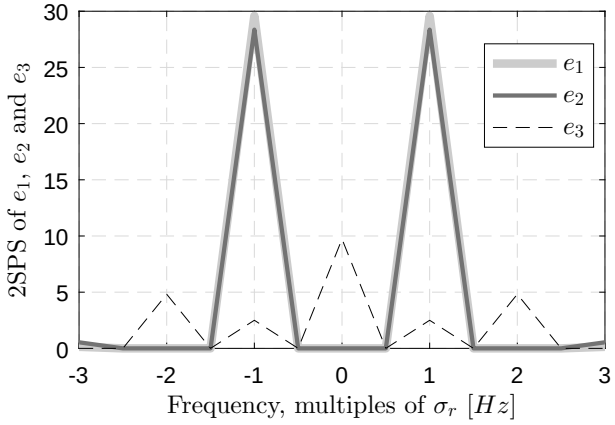

Source: the author (2016).

as to require adding additional states to the controller. Nevertheless, such higher-order harmonics will be attenuated by the $\mathcal{H}_\infty$ controller.

For the purposes of this work, both the fundamental frequency and the second harmonic of all three axis will be attenuated. Define, thus, matrices A_r and A_h with $h = 1$ and $h = 2$ respectively

$$A_r = \begin{bmatrix} 0 & 1 \\ -(\sigma_r)^2 & 0 \end{bmatrix}, A_h = \begin{bmatrix} 0 & 1 \\ -(2\sigma_r)^2 & 0 \end{bmatrix}, \tag{4.6}$$

which represent the fundamental frequency and its second harmonic to be attenuated. Since the platform has 3 axis of linear movement and the resonant controller has 2 states for each frequency to be rejected, i.e. σ_r and $2\sigma_r$, at each axis, twelve states have to be introduced in the control loop, or rather, in the augmented model of the system.

4.1.1.3 Complete Augmented Model

In order to deal with unknown load conditions, e.g. increment of mass on top of the platform, model uncertainties, e.g. mass variations between the mathematical and physical systems, and to remove DC components of the motion error as seen on Figure 8, three extra states are introduced in the controller. Namely, integrator states in the form $\dot{x}_I(t) = e(t)$, $y_I(t) = x_I(t)$, one for each linear axis.

To better define the proposed control loop, consider an augmented system S_a in the form of (4.1), where the matrices and vectors denoted with subscript a are the equivalent augmented counterparts of (4.2) given by

$$A_a = \begin{bmatrix} A & \mathbf{0} & \mathbf{0} & \mathbf{0} & \mathbf{0} & \mathbf{0} & \mathbf{0} & \mathbf{0} \\ -B_r C_x & A_r & \mathbf{0} & \mathbf{0} & \mathbf{0} & \mathbf{0} & \mathbf{0} & \mathbf{0} \\ -B_r C_x & \mathbf{0} & A_h & \mathbf{0} & \mathbf{0} & \mathbf{0} & \mathbf{0} & \mathbf{0} \\ -B_r C_y & \mathbf{0} & \mathbf{0} & A_r & \mathbf{0} & \mathbf{0} & \mathbf{0} & \mathbf{0} \\ -B_r C_y & \mathbf{0} & \mathbf{0} & \mathbf{0} & A_h & \mathbf{0} & \mathbf{0} & \mathbf{0} \\ -B_r C_z & \mathbf{0} & \mathbf{0} & \mathbf{0} & \mathbf{0} & A_r & \mathbf{0} & \mathbf{0} \\ -B_r C_z & \mathbf{0} & \mathbf{0} & \mathbf{0} & \mathbf{0} & \mathbf{0} & A_h & \mathbf{0} \\ -C_x & \mathbf{0} & \mathbf{0} & \mathbf{0} & \mathbf{0} & \mathbf{0} & \mathbf{0} & \mathbf{0} \\ -C_y & \mathbf{0} & \mathbf{0} & \mathbf{0} & \mathbf{0} & \mathbf{0} & \mathbf{0} & \mathbf{0} \\ -C_z & \mathbf{0} & \mathbf{0} & \mathbf{0} & \mathbf{0} & \mathbf{0} & \mathbf{0} & \mathbf{0} \end{bmatrix}, \tag{4.7}$$

$$B_{u,a} = \begin{bmatrix} B_u^\top & \mathbf{0} \end{bmatrix}^\top, B_{\phi,a} = \begin{bmatrix} B_\phi^\top & \mathbf{0} \end{bmatrix}^\top,$$

such that $x_a(t) \in \mathbb{R}^{21}$ encompasses the plant and controller states, $A_a \in \mathbb{R}^{21\times 21}$, $B_{u,a} \in \mathbb{R}^{21\times 3}$, $B_{\phi,a} \in \mathbb{R}^{21\times 3}$. That is,

$$S_a := \begin{cases} \dot{x}_a(t) = A_a x_a(t) + B_{u,a} u_F(t) + B_{\phi,a} F_{ext}(t), \\ z_1(t) = C_a x_a(t), \end{cases} \tag{4.8}$$

with $C_a = \mathbf{I} \in \mathbb{R}^{21\times 21}$.

4.1.2 Optimization Subject to LMI constraints

The proposed augmented model has notable sinusoidal perturbation rejection characteristics, but it does not stabilize the system nor rejects unknown disturbia, since the augmented model is still open-loop. To that extent, a state feedback in the form of $u_F = K x_a$ is proposed in order to guarantee closed-loop stability of S_a, while also meeting additional performance criteria such as region-based eigenvalue placement and $\mathcal{H}_\infty$ gain minimization.

The main goal of this section is to present an optimization problem subject to constraints in the form of LMIs to systematically design the proposed controller for the translational augmented submodel of the Stewart platform presented on (4.8). In this sense, consider the stabilization task as defined in Problem 4.1, together with additional performance criteria.

Problem 4.1. *Design a feedback gain K such that*

$$\dot{x}_a = \mathbb{A}x_a, \tag{4.9}$$

for $\mathbb{A} = (A_a + B_{u,a}K)$, is asymptotically stable and satisfy the following performance criteria:

PC1. *Place the closed loop eigenvalues λ_a of $\mathbb{A}$ inside a stable subregion of the complex plane*

$$\mathcal{D} = \mathcal{D}_c \cap \mathcal{D}_p \tag{4.10}$$

composed by the intersection of a circular region $\mathcal{D}_c$ centered at $-c < 0$ with radius r and the plane $\mathcal{D}_p := \{\lambda_a \in \mathbb{C} \mid \Re(\lambda_a) < -\xi < 0\}$.

PC2. *Minimize the $\mathcal{H}_\infty$ gain of the unknown perturbation F_{ext} to the output z_1, i.e., minimize*

$$\bar{\mu} = \sup_{\|F_{ext}\|_{\mathcal{H}_\infty} \neq 0} \frac{\|z_1(t)\|_{\mathcal{H}_\infty}}{\|F_{ext}(t)\|_{\mathcal{H}_\infty}} = \sqrt{\frac{\int_0^\infty z_1^\top(t) z_1(t) dt}{\int_0^\infty F_{ext}(t)^\top F_{ext}(t) dt}}. \tag{4.11}$$

The solution of Problem 4.1 subject to the performance criteria **PC1** and **PC2** is presented in Theorem 4.1.

Theorem 4.1. *Consider the linear augmented system S_a and given constant matrices L and M. If there are matrices $P = P^\top = Q^{-1} > 0$ and Y with appropriate dimensions and a positive scalar $\mu > 0$ subject to the following constraints*[2]

$$\begin{cases} L \otimes Q + M \otimes \Gamma(Q,Y) + M^\top \otimes \Gamma(Q,Y)^\top < 0, \\ \\ \begin{bmatrix} \Gamma(Q,Y) + \Gamma(Q,Y)^\top & \star & \star \\ B_{\phi,a}^\top & -\mu^2 I & \star \\ C_a Q & \mathbf{0} & -\mathbf{I} \end{bmatrix} < 0, \end{cases} \tag{4.12}$$

[2] $\mathbf{I}$ denotes the appropriately sized identity matrix.

with $\Gamma(Q, Y) = (A_a Q + B_{u,a} Y)$*, then the control law*

$$u_F = K x_a \tag{4.13}$$

with $K = YQ^{-1}$ *solves Problem 4.1 and satisfies* ***PC1****. Furthermore, if the above inequalities are satisfied while minimizing* μ*,* ***PC2*** *is also satisfied.* ■

Proof. The first step in this particular design makes use of the $\mathcal{D}$-stability concept, which seeks to guarantee asymptotic stability of the unperturbed system and to place the eigenvalues within a desired region $\mathcal{D}$, all with respect to the closed-loop system.

To establish the desired boundaries within which the eigenvalues λ_a will be placed, let matrices L and M (from Definition 2.11) be described in terms of the intersection of regions $\mathcal{D}_c$ and $\mathcal{D}_p$ so that $\mathcal{D} = \mathcal{D}_c \cap \mathcal{D}_p$, with

$$L = \begin{bmatrix} L_c & 0 \\ 0 & L_p \end{bmatrix} \quad \text{and} \quad M = \begin{bmatrix} M_c & 0 \\ 0 & M_p \end{bmatrix}, \tag{4.14}$$

where $\mathcal{D}_c$ is a circular region in the complex plane with radius r centered at $-c < 0$, described by

$$L_c = \begin{bmatrix} -r & c \\ c & -r \end{bmatrix} \quad \text{and} \quad M_c = \begin{bmatrix} 0 & 1 \\ 0 & 0 \end{bmatrix}, \tag{4.15}$$

and $\mathcal{D}_p := \{\lambda_a \in \mathbb{C} \mid \Re(\lambda_a) < -\xi < 0\}$ is a plane described by

$$L_p = 2\xi \quad \text{and} \quad M_p = 1. \tag{4.16}$$

Consider the D-stability equation from Theorem 2.4 in a closed-loop scenario, with control law $u_F = K x_a$ and $K = YQ^{-1}$ so that

$$L \otimes Q + M \otimes \Gamma(Q, Y) + M^\top \otimes \Gamma(Q, Y)^\top < 0, \tag{4.17}$$

with $\Gamma(Q, Y) = (A_a Q + B_{u,a} Y)$. The state-feedback control gain $K = YQ^{-1}$ is obtained by solving for Q and Y, given the constraints presented.

While the $\mathcal{D}$-stability criterion is capable of stabilizing the system, further unknown perturbations may still affect negatively the motion error. The second step is to design a controller that aims at minimizing the $\mathcal{H}_\infty$ gain of the unknown perturbation F_{ext} to the output z_1. To that extent, assume the Lyapunov candidate function

$$V(x_a) = x_a^\top P x_a. \tag{4.18}$$

From the standard Lyapunov theory, the system is globally asymptotically stable if

$$\begin{cases} V(x_a) > 0 & \text{(a)} \\ \dot{V}(x_a) + z_1^\top z_1 - \mu^2 F_{ext}^\top F_{ext} < 0 & \text{(b)} \end{cases} \tag{4.19}$$

holds true. From (4.18) and (4.19.a), the Lyapunov candidate function is positive definite if the optimization variable $P > 0$.

Rearrange (4.19.b) to

$$\dot{V}(x_a) < -z_1^\top z_1 + \mu^2 F_{ext}^\top F_{ext} \tag{4.20}$$

and integrate both sides of the equation on the temporal variable t with limits $[0, \infty)$:

$$\lim_{t\to\infty} V(x_a(t)) - V(x_a(0)) < -\int_0^\infty z_1^\top(t) z_1(t)\,\mathrm{d}t + \mu^2 \int_0^\infty F_{ext}^\top(t) F_{ext}(t)\,\mathrm{d}t. \tag{4.21}$$

Given that the system is stabilized via $\mathcal{D}$-stability, i.e.

$$\lim_{t\to\infty} V(x_a(t)) = 0. \tag{4.22}$$

and that $V(x_a(0)) > 0$ by definition, (4.21) becomes

$$0 < -\int_0^\infty z_1^\top(t) z_1(t)\,\mathrm{d}t + \mu^2 \int_0^\infty F_{ext}^\top(t) F_{ext}(t)\,\mathrm{d}t. \tag{4.23}$$

Let the $\mathcal{H}_\infty$ gain be as defined by

$$\|\mathcal{H}(s)\|_\infty = \sup_{\|F_{ext}(t)\|_{\mathcal{H}_\infty} \neq 0} \frac{\|z_1(t)\|_{\mathcal{H}_\infty}}{\|F_{ext}(t)\|_{\mathcal{H}_\infty}}. \tag{4.24}$$

This gain represents the maximum gain, at any frequency, that the perturbation will affect the output of the system and should, thus, be minimized.

For a sub-optimal solution, define μ such that $\mu > \|\mathcal{H}(s)\|_\infty$. Then,

$$\mu > \frac{\|z_1(t)\|_{\mathcal{H}_\infty}}{\|F_{ext}(t)\|_{\mathcal{H}_\infty}} = \sqrt{\frac{\int_0^\infty z_1^\top(t) z_1(t)\,\mathrm{d}t}{\int_0^\infty F_{ext}^\top(t) F_{ext}(t)\,\mathrm{d}t}}. \tag{4.25}$$

By minimizing μ one is also minimizing the $\mathcal{H}_\infty$ gain from F_{ext} to z_1, given that rearranging (4.23) implies (4.25).

Consider now the complete closed-loop augmented system

$$\bar{S}_a := \begin{cases} \dot{x}_a(t) = (A_a + B_{u,a}K)x_a(t) + B_{\phi,a}F_{ext}(t) \\ z_1(t) = (C_a + D_{u,a}K)x_a + D_{\phi,a}F_{ext}. \end{cases} \tag{4.26}$$

Rearrange (4.19.b) to closed-loop form

$$\begin{aligned} &((A_a + B_{u,a}K)x_a + B_{\phi,a}F_{ext})^\top P x_a \\ &+x_a^\top P((A_a + B_{u,a}K)x_a + B_{\phi,a}F_{ext}) \\ &+((C_a + D_{u,a}K)x_a + D_{\phi,a}F_{ext})^\top((C_a + D_{u,a}K)x_a + D_\phi F_{ext}) \\ &-\mu^2 F_{ext}^\top F_{ext} < 0, \end{aligned} \tag{4.27}$$

and rewrite (4.27) into the quadratic form

$$\begin{bmatrix} x_a^\top \\ F_{ext}^\top \end{bmatrix} \begin{bmatrix} a_{11} & a_{12} \\ a_{21} & a_{22} \end{bmatrix} \begin{bmatrix} x_a & F_{ext} \end{bmatrix} < 0. \tag{4.28}$$

This allows for a more concise approach of determining the necessary inequalities for the optimization problem, given that (4.28) is in the quadratic form. The only condition thus needed to satisfy (4.19.b) is

$$\begin{bmatrix} a_{11} & a_{12} \\ a_{21} & a_{22} \end{bmatrix} < 0, \tag{4.29}$$

where

$$\begin{aligned} a_{11} &= (A_a + B_{u,a}K)^\top P + P(A_a + B_{u,a}K) \\ &+(C_a + D_{u,a}K)^\top(C_a + D_{u,a}K) \\ a_{12} &= PB_{\phi,a} + (C_a + D_{u,a}K)^\top D_{\phi,a} \\ a_{21} &= B_{\phi,a}^\top P + D_{\phi,a}^\top(C_a + D_{u,a}K) \\ a_{22} &= D_{\phi,a}^\top D_{\phi,a} - \mu^2 I. \end{aligned} \tag{4.30}$$

Since the only condition needed is (4.29), rewrite it as a sum of two matrices

$$\begin{bmatrix} (A_a + B_{u,a}K)^\top P + P(A_a + B_{u,a}K) & PB_{\phi,a} \\ B_{\phi,a}^\top P & -\mu^2 I \end{bmatrix} + \begin{bmatrix} (C_a + D_{u,a}K)^\top (C_a + D_{u,a}K) & (C_a + D_{u,a}K)^\top D_{\phi,a} \\ D_{\phi,a}^\top (C_a + D_{u,a}K) & D_{\phi,a}^\top D_{\phi,a} \end{bmatrix} < 0, \tag{4.31}$$

and apply a congruence transformation to obtain

$$\begin{bmatrix} (A_a + B_{u,a}K)^\top P + P(A_a + B_{u,a}K) & PB_{\phi,a} \\ B_{\phi,a}^\top P & -\mu^2 I \end{bmatrix} - \begin{bmatrix} (C_a + D_{u,a}K)^\top \\ D_{\phi,a}^\top \end{bmatrix} (-I^{-1}) \begin{bmatrix} (C_a + D_{u,a}K) & D_{\phi,a} \end{bmatrix} < 0. \tag{4.32}$$

Now that the matrices are in a proper formulation for this, apply the Schur complement on (4.32) to result in

$$\begin{bmatrix} (A_a + B_{u,a}K)^\top P + P(A_a + B_{u,a}K) & PB_{\phi,a} & (C_a + D_{u,a}K)^\top \\ B_{\phi,a}^\top P & -\mu^2 I & D_{\phi,a}^\top \\ (C_a + D_{u,a}K) & D_{\phi,a} & -I^{-1} \end{bmatrix} < 0. \tag{4.33}$$

Since in the original augmented system the inputs do not directly influence the outputs, i.e. $D_{u,a} = D_{\phi,a} = \mathbf{0} \in \mathbb{R}^{21\times 3}$, define those matrices as zero and multiply both sides of (4.33) by

$$\begin{bmatrix} P^{-1} & 0 & 0 \\ 0 & 1 & 0 \\ 0 & 0 & 1 \end{bmatrix}, \tag{4.34}$$

to obtain the second inequality from (4.12), after performing the substitution of the state-feedback control gain as $K = YQ^{-1}$ and defining $P = P^\top = Q^{-1} > 0$. Therefore, by minimizing μ and solving for Q and Y, a static control law $u_F = Kx_a$ can be implemented on the dynamic augmented model S_a, so as to solve Problem 4.1 subject the performance criteria **PC1** and **PC2**. □

4.2 Rotation Control

This section is dedicated to the development of the state-feedback controller that acts on the rotation submodel of the platform.

The rotation submodel is clearly nonlinear, so the set of control techniques used on system S_1 does not apply directly. To that extent, the proposed control includes nonlinear control methods, namely a nonlinear $\mathcal{H}_\infty$ control law that achieves full $\mathcal{L}_2$ gain performance via the Hamilton-Jacobi inequality.

This proposed control law comprehends full realization of $\mathcal{L}_2$ gain performance by defining a Lyapunov candidate function that also meets the Hamilton-Jacobi partial differential inequality. Furthermore, the closed-loop system obtained is then linearized and augmented to reject external sinusoidal perturbations via a dynamic resonant controller. This composition is further subjected to the static-gain control law of a $\mathcal{D}$-stability controller tuned by an optimization problem constrained by LMIs.

4.2.1 Nonlinear $\mathcal{H}_\infty$ Controller

Recall the rotation submodel $\bar{S}_2$ which represents the dynamics around the equilibrium point ($\eta = \pm 1, \varepsilon = \mathbf{0}, \omega = \mathbf{0}$) regarding the attitude q and angular velocities w of the platform. This system can be rewritten in a more general form, i.e.

$$S_2 := \begin{cases} \dot{x}_2 = f(x_2) + g_1(x_2)\tau_{ext} + g_2(x_2)u_\tau, \\ z_2 = \begin{bmatrix} h(x_2) \\ \rho u_\tau \end{bmatrix}, \end{cases} \tag{4.35}$$

where

$$f(x_2) = \begin{bmatrix} \frac{1}{2}\begin{bmatrix} -\varepsilon^\top \\ \eta I + S(\varepsilon) \end{bmatrix}\omega \\ -{I_m}^{-1}S(\omega)I_m\omega \end{bmatrix}, g_1(x_2) = g_2(x_2) = \begin{bmatrix} 0 \\ 0 \\ I_m^{-1} \end{bmatrix}, \tag{4.36}$$

$x_2 = \begin{bmatrix} q^\top & \omega^\top \end{bmatrix}^\top \in \mathbb{R}^7$ is the state vector, $q = \begin{bmatrix} \eta & \varepsilon^\top \end{bmatrix}^\top \in \mathbb{R}^4$ is the body orientation error quaternion (with scalar and vector parts $\eta \in \mathbb{R}$, $\varepsilon \in \mathbb{R}^3$, respectively), ρ is a positive scalar, $u_\tau \in \mathbb{R}^3$ is the input, $\tau_{ext} \in \mathbb{R}^3$ is the perturbation that affects the system and $h(x_2) \in \mathbb{R}^6$ is the output function

$$h(x_2) = \begin{bmatrix} \sqrt{\rho_1}\varepsilon \\ \sqrt{\rho_2}\omega \end{bmatrix}, \tag{4.37}$$

given positive scalars ρ_1 and ρ_2.

While function z_2 is the virtual output considered in the design, it is better described as an objective function. The scalar ρ serves as a control signal weighting variable, so as to better account for the control energy, and $h(x_2)$ can be used to better tune the attitude control performance.

The main goal of this section is to present a nonlinear control law for the rotation submodel S_2 of the Stewart platform that stabilizes the system and guarantees $\mathcal{L}_2$ gain performance with tunable attitude performance control. In this sense, consider the stabilization task as defined in Problem 4.2, together with additional performance criteria.

Problem 4.2. *Design a nonlinear state-feedback law $\zeta(x_2)$ such that*

$$\dot{x}_2 = f(x_2) + g_1(x_2)\tau_{ext} + g_2(x_2)\zeta(x_2) \tag{4.38}$$

is finite-gain $\mathcal{L}_2$ stable and satisfy the following performance criteria:

PC3. *Achieve $\mathcal{L}_2$ gain performance so that the $\mathcal{L}_2$ gain from τ_{ext} to z_2 is less than or equal a positive scalar ν.*

PC4. *Allow the control law to be tunable by scalars ρ, ρ_1 and ρ_2 to account for control energy and attitude control performance.*

This is similar to what was done on (4.25), but instead of minimizing the effect external disturbia have on the system, this controller guarantees that it is bounded by a scalar ν, which may be arbitrarily small.

The solution of Problem 4.2 subject to the performance criteria **PC3** and **PC4** is presented in the next Theorem (SHOW et al., 2003).

Theorem 4.2. *Consider the nonlinear rotation system S_2. If there are positive scalars ρ, ρ_1, ρ_2, a, b_1 and b_2 subject to*

$$\begin{cases} aI - (b_1 + 2b_2)^2 I_m > 0, & (a) \\ \dfrac{1}{2}\rho_1 + 2(b_1 - 2b_2)^2\left(\dfrac{1}{\nu^2} - \dfrac{1}{\rho^2}\right) < 0, & (b) \\ (b_1 + 2b_2)\|I_m\| + \dfrac{1}{2}\rho_2 + 2a^2\left(\dfrac{1}{\nu^2} - \dfrac{1}{\rho^2}\right) < 0, & (c) \end{cases} \tag{4.39}$$

then the control law

$$\zeta(x_2) = -\frac{2}{\rho^2}(a\omega + b_1\varepsilon + b_2\eta\varepsilon) \tag{4.40}$$

*solves Problem 4.2 and satisfies **PC3**, **PC4**.* ■

Proof. Define the Lyapunov candidate function

$$V(x_2) = a\omega^\top I_m \omega + 2(b_1 + 2b_2\eta)\varepsilon^\top I_m \omega + 2(1-\eta)(c_1 + c_2\eta). \tag{4.41}$$

By using characteristics of the orientation unit quaternion, i.e., $2(1-\eta) = \varepsilon^\top\varepsilon + (1-\eta)^2$, the candidate function becomes

$$V(x_2) = a\omega^\top I_m \omega + 2(b_1 + 2b_2\eta)\varepsilon^\top I_m \omega + (\varepsilon^\top\varepsilon + (1-\eta)^2)(c_1 + c_2\eta). \tag{4.42}$$

To that extent, rewrite (4.42) into the quadratic form

$$\begin{aligned} V(x_2) = &\begin{bmatrix} \eta - 1 & \varepsilon^\top & \omega^\top \end{bmatrix} \\ &\begin{bmatrix} (c_1 + c_2\eta) & \mathbf{0} & \mathbf{0} \\ 0 & (c_1 + c_2\eta)I & (b_1 + 2b_2\eta)I_m \\ 0 & (b_1 + 2b_2\eta)I_m & aI_m \end{bmatrix} \begin{bmatrix} \eta - 1 \\ \varepsilon \\ \omega \end{bmatrix}. \end{aligned} \tag{4.43}$$

This allows for a more concise approach of determining the definiteness of $V(x_2)$, given that from (4.43) the quadratic terms

$$\begin{bmatrix} \eta - 1 & \varepsilon^\top & \omega^\top \end{bmatrix} \begin{bmatrix} \eta - 1 \\ \varepsilon \\ \omega \end{bmatrix} > 0. \tag{4.44}$$

Therefore, the only condition needed to satisfy $V(x_2) > 0$, i.e. for the candidate function to be positive definite, is

$$\begin{bmatrix} (c_1 + c_2\eta) & \mathbf{0} & \mathbf{0} \\ 0 & (c_1 + c_2\eta)I & (b_1 + 2b_2\eta)I_m \\ 0 & (b_1 + 2b_2\eta)I_m & aI_m \end{bmatrix} > 0. \tag{4.45}$$

By Sylvester's criterion (Chapter 2.3.2), $V(x_2)$ is positive definite if

$$\begin{aligned} D_1 &= (c_1 + c_2\eta) > 0, \\ D_2 &= (c_1 + c_2\eta)^2 I > 0, \\ D_3 &= aI - (b_1 + 2b_2\eta)^2 I_m > 0, \end{aligned} \tag{4.46}$$

that is, $\forall\ \eta \in [-1, 1]$

$$\begin{cases} (c_1 + c_2\eta) > 0 & \text{(a)} \\ aI - (b_1 + 2b_2\eta)^2 I_m > 0. & \text{(b)} \end{cases} \tag{4.47}$$

By considering the worst case scenario (WCS) of $\eta = -1$ for (4.47.a) and $\eta = 1$ for (4.47.b), the conditions can be rewritten as

$$\begin{cases} c_1 > c_2, & \text{(a)} \\ aI - (b_1 + 2b_2)^2 I_m > 0. & \text{(b)} \end{cases} \tag{4.48}$$

Note that (4.48.b) is the condition (4.39.a) from Theorem 4.2. For evaluating $\mathcal{L}_2$ gain performance of the system, consider Theorem 2.7.

Assume the inertia matrix I_m to be symmetric and recall (4.41) to define the corresponding gradient and its transpose

$$\begin{aligned} \left(\frac{\partial V(x_2)}{\partial x_2}\right) = [&4b_2\varepsilon^\top I_m\omega - 2c_1 + 2c_2(1-\eta) \\ &2(b_1 + 2b_2\eta)\omega^\top I_m \quad 2a\omega^\top I_m + 2(b_1 + 2b_2\eta)\varepsilon^\top I_m], \end{aligned} \tag{4.49}$$

$$\frac{\partial V^\top(x_2)}{\partial x_2} = \begin{bmatrix} 4b_2\omega^\top I_m\varepsilon - 2c_1 + 2c_2(1-2\eta) \\ 2(b_1 + 2b_2\eta)I_m\omega \\ 2aI_m\omega + 2(b_1 + 2b_2\eta)I_m\varepsilon \end{bmatrix}. \tag{4.50}$$

Now compute the term $\left(\frac{\partial V(x_2)}{\partial x_2}\right) f(x_2)$ by using the property $\omega^\top S(\omega) = \mathbf{0}$ to result in

$$\left(\frac{\partial V(x_2)}{\partial x_2}\right) f(x_2) = \omega^\top((b_1 + 2b_2\eta(\eta I + S(\varepsilon))I_m - 2b_2 I_m\varepsilon^\top\varepsilon)\omega + \varepsilon^\top(c_1 + c_2(2\eta - 1))\omega. \tag{4.51}$$

In order to account for all the terms of system S_2, consider the Hamilton-Jacobi inequality (2.39) from Theorem 2.8. Since in this particular case $g_1(x_2) = g_2(x_2) = g(x_2)$,

$$\begin{aligned} H_v = \left(\frac{\partial V(x_2)}{\partial x_2}\right) f(x_2) + \frac{1}{2}\left(\frac{1}{\nu^2} - \frac{1}{\rho^2}\right)\left(\frac{\partial V(x_2)}{\partial x_2}\right)\left(g(x_2)g(x_2)^\top\right)\left(\frac{\partial V(x_2)}{\partial x_2}\right)^\top \\ + \frac{1}{2}h(x_2)^\top h(x_2) < 0. \end{aligned} \tag{4.52}$$

Therefore, the Hamilton-Jacobi inequality can be described by

$$\begin{aligned} H_v = &\omega^\top\left((b_1 + 2b_2\eta)(\eta I + S(\varepsilon))I_m - 2b_2 I_m\varepsilon^\top\varepsilon + \left(\frac{1}{2}\rho_2 + 2a^2\left(\frac{1}{\nu^2} - \frac{1}{\rho^2}\right)\right)I\right)\omega \\ &+ \varepsilon^\top\left(c_1 + c_2(2\eta - 1) + 4a(b_1 + 2b_2\eta)\left(\frac{1}{\nu^2} - \frac{1}{\rho^2}\right)\right)\omega \\ &+ \varepsilon^\top\left(\frac{1}{2}\rho_1 I + 2(b_1 + 2b_2\eta)^2\left(\frac{1}{\nu^2} - \frac{1}{\rho^2}\right)I\right)\varepsilon < 0. \end{aligned} \tag{4.53}$$

It is clear to see that the quadratic terms $\omega^\top\omega$ and $\varepsilon^\top\varepsilon$ are always positive, and, thus, the terms that are multiplied by them must be negative for the inequality (4.53) to be true. In contrast, for this same inequality to be proven, the cross-multiplication term $\varepsilon^\top\omega$ must be null. For that to be valid,

$$c_1 + c_2(2\eta - 1) + 4a(b_1 + 2b_2\eta)\left(\frac{1}{\nu^2} - \frac{1}{\rho^2}\right) = 0, \forall\ \eta \in [-1, 1]. \tag{4.54}$$

To better grasp the conditions necessary for (4.54) to hold true, define the sub-conditions

$$\begin{cases} c_1 - c_2 + 4ab_1\left(\dfrac{1}{\nu^2} - \dfrac{1}{\rho^2}\right) = 0, & (a) \\ 2c_2\eta + 8ab_2\eta\left(\dfrac{1}{\nu^2} - \dfrac{1}{\rho^2}\right) = 0, & (b) \end{cases} \tag{4.55}$$

in order to obtain the necessary values of c_1 and c_2, that is,

$$c_1 = 4a(b_1 + b_2)\left(\frac{1}{\rho^2} - \frac{1}{\nu^2}\right), \tag{4.56}$$

and

$$c_2 = -4ab_2\left(\frac{1}{\nu^2} - \frac{1}{\rho^2}\right). \tag{4.57}$$

Recall condition (4.48.a) to result in

$$\begin{aligned} &4a(b_1 + b_2)\left(\frac{1}{\rho^2} - \frac{1}{\nu^2}\right) > 4ab_2\left(\frac{1}{\rho^2} - \frac{1}{\nu^2}\right) \\ &\therefore b_1 + b_2 > b_2 \\ &\therefore b_1 > 0, \end{aligned} \tag{4.58}$$

which is feasible from the conditions of Theorem 4.2.

Since the cross-multiplication term $\varepsilon^\top\omega$ is now null, H_v becomes

$$\begin{aligned} H_v = \omega^\top &\left((b_1 + 2b_2\eta)(\eta I + S(\varepsilon))I_m - 2b_2 I_m\varepsilon^\top\varepsilon + \left(\frac{1}{2}\rho_2 + 2a^2\left(\frac{1}{\nu^2} - \frac{1}{\rho^2}\right)\right) I\right)\omega \\ &+ \varepsilon^\top\left(\frac{1}{2}\rho_1 I + 2(b_1 + 2b_2\eta)^2\left(\frac{1}{\nu^2} - \frac{1}{\rho^2}\right) I\right)\varepsilon < 0. \end{aligned} \tag{4.59}$$

The last quadratic term $\varepsilon^\top\varepsilon$ is easily brought to negative values by choosing WCS of $\eta = -1$, resulting in

$$\frac{1}{2}\rho_1 + 2(b_1 - 2b_2)^2\left(\frac{1}{\nu^2} - \frac{1}{\rho^2}\right) < 0, \tag{4.60}$$

which is the condition (4.39.b) from Theorem 4.2. The other quadratic term $\omega^\top\omega$ must also be negative, and for that to hold true

$$(b_1 + 2b_2\eta)(\eta I + S(\varepsilon))I_m - 2b_2 I_m\varepsilon^\top\varepsilon + \left(\frac{1}{2}\rho_2 + 2a^2\left(\frac{1}{\nu^2} - \frac{1}{\rho^2}\right)\right)I < 0. \tag{4.61}$$

For the WCS analysis, consider just the following portion of (4.61)

$$(b_1 + 2b_2\eta)(\eta I + S(\varepsilon))I_m - 2b_2 I_m\varepsilon^\top\varepsilon. \tag{4.62}$$

It is obvious that the last term $-2b_2 I_m\varepsilon^\top\varepsilon \leq 0\ \forall\ \varepsilon$, and, as such, the worst case is when $-2b_2 I_m\varepsilon^\top\varepsilon = 0$. Thus,

$$\begin{aligned}&(b_1 + 2b_2\eta)(\eta I + S(\varepsilon))I_m - 2b_2 I_m\varepsilon^\top\varepsilon\\ &\leq (b_1 + 2b_2\eta)(\eta I + S(\varepsilon))I_m.\end{aligned} \tag{4.63}$$

Note that from the quaternion characteristics, $\|\eta I + S(\varepsilon)\| \leq 1$, therefore

$$\begin{aligned}&(b_1 + 2b_2\eta)(\eta I + S(\varepsilon))I_m - 2b_2 I_m\varepsilon^\top\varepsilon\\ &\leq (b_1 + 2b_2\eta)(\eta I + S(\varepsilon))I_m\\ &\leq (b_1 + 2b_2\eta)\|I_m\|,\end{aligned} \tag{4.64}$$

is the WCS for (4.62).

Recall (4.61) to define the condition

$$(b_1 + 2b_2\eta)\|I_m\| + \frac{1}{2}\rho_2 + 2a^2\left(\frac{1}{\nu^2} - \frac{1}{\rho^2}\right) < 0, \tag{4.65}$$

which is the inequality (4.39) from Theorem 4.2.

The state-feedback control law is devised using Theorem 2.8, so that the input

$$\begin{aligned}u_\tau = \zeta(x_2) &= -\frac{1}{\rho^2}g_2^\top(x_2)\left(\frac{\partial V(x_2)}{\partial x_2}\right)^\top\\ &= -\frac{2}{\rho^2}(a\omega + b_1\varepsilon + b_2\eta\varepsilon)\end{aligned} \tag{4.66}$$

solves Problem 4.2 while meeting **PC3** and **PC4**. □

Remark 4.1. The condition from (4.58) results from the chosen worst case scenario of $\eta = -1$ in (4.48). Had the other value be chosen, i.e. $\eta = 1$, the result would be as follows.

$$\begin{aligned} &4a(b_1 + b_2)\left(\frac{1}{\rho^2} - \frac{1}{\nu^2}\right) > 4ab_2\left(\frac{1}{\nu^2} - \frac{1}{\rho^2}\right) \\ &\therefore 4a(b_1 + b_2)\left(\frac{1}{\rho^2} - \frac{1}{\nu^2}\right) > -4ab_2\left(\frac{1}{\rho^2} - \frac{1}{\nu^2}\right) \\ &\therefore b_1 + b_2 > -b_2 \\ &\therefore b_1 > -2b_2, \end{aligned} \tag{4.67}$$

which is also feasible, given that, from definition of Theorem 4.2, $b_1 \geq 0$ and $b_2 \geq 0$.

Remark 4.2. The resulting control law (4.66) stems from the chosen Lyapunov candidate function (4.41). Had the function be defined without the terms c_1 and c_2, i.e.,

$$\bar{V}(x_2) = a\omega^\top I_m \omega + 2(b_1 + 2b_2\eta)\varepsilon^\top I_m \omega + 2(1 - \eta), \tag{4.68}$$

the condition (4.39.a) would be rewritten as

$$a = -\frac{1}{4b_1}\left(\frac{1}{\nu^2} - \frac{1}{\rho^2}\right)^{-1} \geq 0, \tag{4.69}$$

and the nonlinear term of the control law would be zero, given that another condition $b_2 = 0$ would arise. The omission of this nonlinear term would result in a lower performance of the controller (SHOW et al., 2003).

Remark 4.3. As can be seen from conditions (4.39), the most sensitive parameter of the controller is ρ, the control signal weighting variable. If ρ is large, the control signal will be small and the controller will not be able to guarantee the desired $\mathcal{L}_2$ gain of the system, and, thus, the conditions from (4.39) will not be met.

Remark 4.4. Likewise, variables ρ_1 and ρ_2 are attitude control parameters which govern the values of b_1 and b_2, and a, respectively, that satisfy (4.39). The parameters that successfully meet these conditions can be found either by using a numerical solver or by trial and error.

4.2.2 Resonant Rotation Controller

Given that the controller presented on Section 4.2.1 only achieves $\mathcal{L}_2$ finite-gain stability, attitude errors on the rotation submodel still present significant oscillatory values, i.e., the control law attenuates both known and unknown external disturbia, but does not asymptotically reject either. To that extent, by leveraging the IMP, a new controller can be implemented in addition to the stabilizing controller (4.40). In order to do so, the

linearization of the closed-loop system is computed and some techniques discussed in Section 4.1 applied, namely the development of an augmented model that includes resonant states and an optimization problem subject to LMI constraints.

4.2.2.1 System Linearization

Recall the rotation submodel S_2 and assume that the control law (4.40) brings the system near the equilibrium point $(\eta = 1, \varepsilon = \mathbf{0}, \omega = \mathbf{0})$. If the attitude errors to the aforementioned equilibrium point are small, a linearized model of S_2 correctly represents the system near this equilibrium and linear control techniques may be applied on it.

To validate this assumption, consider the scenario from Section 4.1.1.2, with the system subject only to the $\mathcal{L}_2$ control law. Let α, β and γ be the equivalent Euler angle errors relative to $q_{ref} = \begin{bmatrix} 1 & 0 & 0 & 0 \end{bmatrix}^\top$, that is, to a horizontal platform. The resulting orientation errors, thus, on steady-state of the upper platform would be as presented on Figure 9.

Figure 9 – Equivalent Euler angles of the attitude error of the platform, when subject to the $\mathcal{L}_2$ control law on steady-state.

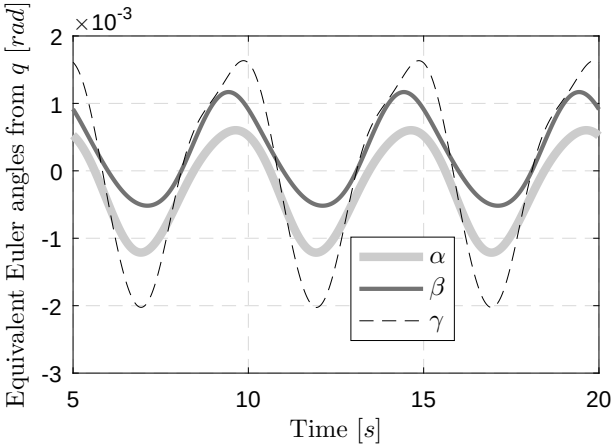

Source: the author (2016).

It is clear to see from Figure 9 that the system is very close to the chosen equilibrium point. As such, consider that the input of system S_2 is now composed of the $\mathcal{L}_2$ controller and a second control law $u_{\tau_2} \in \mathbb{R}^3$, i.e.

$$u_\tau = \zeta(x_2) + u_{\tau_2}, \tag{4.70}$$

and substitute (4.70) on (4.35) to obtain

$$\begin{bmatrix}\dot{\eta}\\ \dot{\varepsilon}\\ \dot{\omega}\end{bmatrix} = \begin{bmatrix} -\frac{1}{2}\varepsilon^{\top}\omega \\ \frac{1}{2}(\eta\omega + S(\varepsilon)\omega) \\ -I_m^{-1}\left(S(\omega)I_m\omega - \frac{2}{\rho^2}(a\omega + b_1\varepsilon + b_2\eta\varepsilon) + \tau_{ext} + u_{\tau_2}\right)\end{bmatrix}. \tag{4.71}$$

Let the linearization take form of

$$\begin{aligned}\partial\dot{x}_2(t) \approx \frac{\partial f(x_2(t),\tau_{ext}(t),u_{\tau_2}(t))}{\partial x_2(t)}\partial x_2(t) + \frac{\partial f(x_2(t),\tau_{ext}(t),u_{\tau_2}(t))}{\partial \tau_{ext}(t)}\partial\tau_{ext}(t) \\ + \frac{\partial f(x_2(t),\tau_{ext}(t),u_{\tau_2}(t))}{\partial u_{\tau_2}(t)}\partial u_{\tau_2}(t)\end{aligned} \tag{4.72}$$

when the higher order terms are not considered. Since the linearization technique is trivial, the resulting linear system for the equilibrium point $(\eta = 1, \varepsilon = \mathbf{0}, \omega = \mathbf{0})$ is

$$\bar{S}_l := \begin{cases} \begin{bmatrix}\partial\dot{\eta}\\ \partial\dot{\varepsilon}\\ \partial\dot{\omega}\end{bmatrix} \approx \begin{bmatrix} 0 & \mathbf{0} & \mathbf{0} \\ \mathbf{0} & \mathbf{0} & \frac{1}{2}I \\ \mathbf{0} & -\frac{2(b_1+b_2)I_m^{-1}}{\rho^2} & -\frac{2aI_m^{-1}}{\rho^2}\end{bmatrix}\begin{bmatrix}\partial\eta\\ \partial\varepsilon\\ \partial\omega\end{bmatrix} + \begin{bmatrix}\mathbf{0}\\ \mathbf{0}\\ I_m^{-1}\end{bmatrix}(\partial\tau_{ext}(t) + \partial u_{\tau_2}(t)), \\ \partial\bar{z}_2(t) = \begin{bmatrix}\partial\eta\\ \partial\varepsilon\\ \partial\omega\end{bmatrix}. \end{cases} \tag{4.73}$$

Note that this system has one non-controllable state, namely $\partial\eta$. Given that the goal of this control design is to develop an optimization problem subject to LMI constraints, this non-controllable state must be removed, else the solver will not converge on a solution. In order to do so, the quaternion unitary length is explored, so that $\varepsilon = 0 \implies \eta = 1$. In other words, by enforcing $\varepsilon = 0$, one is effectively solving the control problem for the whole linearized system in (4.73). Define, then, system S_l, which removes $\partial\eta$ from system $\bar{S}_l$ as follows.

$$S_l := \begin{cases} \dot{x}_l(t) = A_l x_l(t) + B_{u,l}\partial u_{\tau_2}(t) + B_{\tau_{ext},l}\partial\tau_{ext}(t), \\ \partial z_2(t) \approx \mathbf{I}\, x_l(t), \end{cases} \tag{4.74}$$

where $x_l(t) = \begin{bmatrix} \partial\varepsilon^\top & \partial\omega^\top \end{bmatrix}^\top \in \mathbb{R}^6$ and

$$A_l = \begin{bmatrix} \mathbf{0} & \frac{1}{2}I \\ -\dfrac{2(b_1+b_2)I_m^{-1}}{\rho^2} & -\dfrac{2aI_m^{-1}}{\rho^2} \end{bmatrix} \in \mathbb{R}^{6\times6}, B_{u,l} = B_{\tau_{ext},l} = \begin{bmatrix} \mathbf{0} \\ I_m^{-1} \end{bmatrix} \in \mathbb{R}^{6\times3}. \tag{4.75}$$

Once again, if the periodic perturbation applied to the system is a sinusoidal signal of fundamental frequency σ_r, the control loop must include additional resonant states $x_r \in \mathbb{R}^2$ in the form of (4.4).

4.2.2.2 FFT Analysis

In a similar way to what was done on Section 4.1.1.2, an FFT analysis was carried out on the nonlinear closed-loop rotation system S_2 with perturbations as previously described (Section 4.2.2.1). Take Figure 9 as reference and see that the sinusoidal disturbia applied on the bottom platform have visually perceptible DC-gain, e.g. on the α and β angles, and skewed sinusoidal characteristics. For a more objective evaluation of the frequency characteristics of the nonlinear closed-loop system S_2, refer to the resulting 2SPS of a Discrete Fast Fourier Transform with sampling frequency $f_s = 100$Hz presented on Figure 10. This represents the FFT of the attitude error on the top platform, considering the error quaternion as described in Section 2.1.4.

Figure 10 – FFT analysis of the attitude error shown on Figure 9.

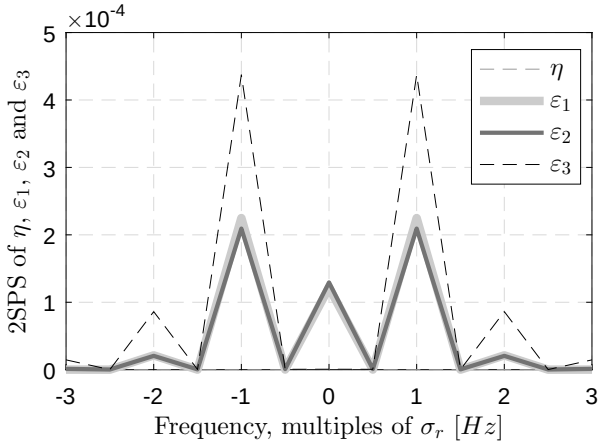

Source: the author (2016).

It is clear to see that even though the $\mathcal{L}_2$ controller contributes to attenuate the effect perturbations have on the system, both the fundamental frequency and the second harmonic of the attitude error still possess a considerable amplitude and can be better attenuated. Higher harmonics are found to not significantly impact the performance of the system so as to require adding additional states to the resonant controller, given that

such higher-order harmonics were already attenuated by the $\mathcal{L}_2$ control law. In addition, the state η of the error quaternion does not have oscillatory characteristics.

For the purposes of this work, based on the result of Figure 10, both the fundamental frequency and the second harmonic the attitude error will be further attenuated. Define, thus, matrices A_r and A_h with $h = 1$ and $h = 2$ respectively

$$A_r = \begin{bmatrix} 0 & 1 \\ -(\sigma_r)^2 & 0 \end{bmatrix}, A_h = \begin{bmatrix} 0 & 1 \\ -(2\sigma_r)^2 & 0 \end{bmatrix}, \tag{4.76}$$

which represent the fundamental frequency and its second harmonic to be attenuated. Since the error quaternion imaginary component ε has three states and the resonant controller has two states for each frequency to be rejected, i.e. σ_r and $2\sigma_r$, for each state, twelve states have to be introduced in the control loop, or rather, in the augmented model of the system.

4.2.2.3 Complete Augmented Model

Similarly to what was the case in Section 4.1.1.3, in order to deal with unknown load conditions, e.g. loads placed outside the center of mass, model uncertainties and to remove DC components of the attitude error as seen on Figure 10, three extra states are introduced in the controller. Namely, integrator states in the form $\dot{x}_I(t) = e(t)$, $y_I(t) = x_I(t)$, one for each state of ε.

To better define the proposed control loop, consider an augmented system $S_{l,a}$ in the form of (4.74), where the matrices and vectors denoted with subscript l, a are the equivalent augmented counterparts of (4.75) given by

$$A_{l,a} = \begin{bmatrix} A_l & \mathbf{0} & \mathbf{0} & \mathbf{0} & \mathbf{0} & \mathbf{0} & \mathbf{0} & \mathbf{0} \\ -B_r C_{\varepsilon_1} & A_r & \mathbf{0} & \mathbf{0} & \mathbf{0} & \mathbf{0} & \mathbf{0} & \mathbf{0} \\ -B_r C_{\varepsilon_1} & \mathbf{0} & A_h & \mathbf{0} & \mathbf{0} & \mathbf{0} & \mathbf{0} & \mathbf{0} \\ -B_r C_{\varepsilon_2} & \mathbf{0} & \mathbf{0} & A_r & \mathbf{0} & \mathbf{0} & \mathbf{0} & \mathbf{0} \\ -B_r C_{\varepsilon_2} & \mathbf{0} & \mathbf{0} & \mathbf{0} & A_h & \mathbf{0} & \mathbf{0} & \mathbf{0} \\ -B_r C_{\varepsilon_3} & \mathbf{0} & \mathbf{0} & \mathbf{0} & \mathbf{0} & A_r & \mathbf{0} & \mathbf{0} \\ -B_r C_{\varepsilon_3} & \mathbf{0} & \mathbf{0} & \mathbf{0} & \mathbf{0} & \mathbf{0} & A_h & \mathbf{0} \\ -C_{\varepsilon_1} & \mathbf{0} & \mathbf{0} & \mathbf{0} & \mathbf{0} & \mathbf{0} & \mathbf{0} & \mathbf{0} \\ -C_{\varepsilon_2} & \mathbf{0} & \mathbf{0} & \mathbf{0} & \mathbf{0} & \mathbf{0} & \mathbf{0} & \mathbf{0} \\ -C_{\varepsilon_3} & \mathbf{0} & \mathbf{0} & \mathbf{0} & \mathbf{0} & \mathbf{0} & \mathbf{0} & \mathbf{0} \end{bmatrix}, \tag{4.77}$$

$$B_{u,l,a} = \begin{bmatrix} B_{u,l} \\ \mathbf{0} \end{bmatrix}, B_{\tau_{ext},l,a} = \begin{bmatrix} B_{\tau_{ext},l} \\ \mathbf{0} \end{bmatrix}, \begin{aligned} C_{\varepsilon_1} &= \begin{bmatrix} 1 & 0 & 0 & 0 & 0 & 0 \end{bmatrix}, \\ C_{\varepsilon_2} &= \begin{bmatrix} 0 & 1 & 0 & 0 & 0 & 0 \end{bmatrix}, \\ C_{\varepsilon_3} &= \begin{bmatrix} 0 & 0 & 1 & 0 & 0 & 0 \end{bmatrix}, \end{aligned}$$

such that $x_{l,a}(t) \in \mathbb{R}^{21}$ encompasses the plant and controller states, $A_{l,a} \in \mathbb{R}^{21\times 21}$, $B_{u,l,a}$ and $B_{\tau_{ext},l,a} \in \mathbb{R}^{21\times 3}$. That is,

$$S_{l,a} := \begin{cases} \dot{x}_{l,a}(t) & = A_{l,a}x_{l,a}(t) + B_{u,l,a}\partial u_{\tau_2}(t) + B_{\tau_{ext},l,a}\partial\tau_{ext}(t), \\ \partial z_{l,a}(t) & \approx C_{l,a}x_{l,a}(t), \end{cases} \tag{4.78}$$

with $C_{l,a} = \mathbf{I} \in \mathbb{R}^{21\times 21}$.

4.2.3 Optimization Subject to LMI Constraints

Consider a state feedback in the form of $u_{\tau_2} = K_{rt}x_{l,a}$ is applied on system $S_{l,a}$ in order to guarantee closed-loop stability, while also meeting additional performance criterion, namely region-based eigenvalue placement.

The main goal of this section is to present an optimization problem subject to constraints in the form of LMIs to systematically design the proposed controller for the linearized closed-loop rotation augmented submodel of the Stewart platform presented on (4.78). In this sense, consider the stabilization task as defined in Problem 4.3, together with additional performance criterion.

Problem 4.3. *Design a feedback gain K_{rt} such that*

$$\dot{x}_{l,a} = \mathbb{A}_{l,a}x_{l,a}, \tag{4.79}$$

for $\mathbb{A}_{l,a} = (A_{l,a} + B_{u,l,a}K_{rt})$, is asymptotically stable and satisfy the following performance criterion:

PC5. *Place the closed loop eigenvalues $\lambda_{l,a}$ of $\mathbb{A}_{l,a}$ inside a stable subregion of the complex plane*

$$\mathcal{D}_{rt} = \mathcal{D}_{c_{rt}} \cap \mathcal{D}_{p_{rt}} \tag{4.80}$$

composed by the intersection of a circular region $\mathcal{D}_{c_{rt}}$ centered at $-c_{rt} < 0$ with radius r_{rt} and the plane $\mathcal{D}_{p_{rt}} := \{\lambda_{l,a} \in \mathbb{C} \mid \Re(\lambda_{l,a}) < -\xi_{rt} < 0\}$.

The solution of Problem 4.3 subject to the performance criteria **PC5** is presented in the next theorem.

Theorem 4.3. *Consider the linearized augmented system $S_{l,a}$ and given constant matrices L and M. If there are matrices $P = P^\top = Q^{-1} > 0$ and Y with appropriate dimensions subject to the following constraint*

$$L \otimes Q + M \otimes \Gamma(Q,Y) + M^\top \otimes \Gamma(Q,Y)^\top < 0, \tag{4.81}$$

*with $\Gamma(Q,Y) = (A_{l,a}Q + B_{u,l,a}Y)$, then the control law $u_{\tau_2} = K_{rt}x_{l,a}$, with $K_{rt} = YQ^{-1}$, solves Problem 4.3 and satisfies **PC5**.* ■

Proof to Theorem 4.3 is similar to the proof to Theorem 4.1 and will, thus, be omitted.

With these developments in mind, system S_2 is subject to the control law

$$u_\tau = \zeta(x_2) + u_{\tau_2}(x_{l,a}), \tag{4.82}$$

where $\zeta(x_2)$ provides $\mathcal{L}_2$ finite-gain performance and u_{τ_2} accounts for known sinusoidal perturbations and unknown load conditions, as well as model uncertainties and DC components of the attitude error.

4.3 Control Signal Coupling

Notice that the dynamic control of the translation and the rotation control of the platform output two different and decoupled vectors, u_F and u_τ, respectively. To unify both controllers, consider the Jacobian $J^{-\top}$, which relates the forces and torques applied on the platform to the linear forces of the actuators, such as

$$f_l = J^{-\top} \begin{bmatrix} F_T \\ \tau_T \\ F_B \\ \tau_B \end{bmatrix}, \tag{4.83}$$

which, in turn, calculates the actual control signal to be applied on the linear actuators. This proposed control method of the Stewart platform allows for the use of two independent controllers, facilitating the design of the control system, given that the attitudes of the platform are not singular (Section 3.2.1)[3].

Finally, since $J^\top \in \mathbb{R}^{12\times 6}$, a pseudo inverse algorithm must be used to obtain $J^{-\top}$, such as the Moore-Penrose pseudoinverse computed via singular value decomposition (BARATA; HUSSEIN, 2012).

4.4 Inverse Dynamics Controller

For comparison purposes of the numerical results presented in this work on Chapter 5, an inverse dynamics controller (IDC) will also be designed to evaluate the performance of the proposed control method. The IDC (ASADA; SLOTINE, 1986), also known as computed-torque controller, is a control method that aims to cancel the undesired dynamics and to impose the desired behavior on the controlled system. Given sufficiently

[3] In effect, since the presented controller relies on the Jacobian matrix for signal coupling, no stability guarantees can be made because the system may be in a singular stance. This can be mitigated by avoiding such configurations and attitudes of the platform, so that the stability proofs presented still hold.

accurate modeling of the manipulator, this controller exhibits good control performance. For the IDC, recall the Newton-Euler equations from (3.18) and rewrite them as

$$\begin{bmatrix} mI & \mathbf{0} \\ \mathbf{0} & I_m \end{bmatrix} \begin{bmatrix} \dot{v} \\ \dot{\omega} \end{bmatrix} = \begin{bmatrix} mg \\ -S(\omega) I_m \omega \end{bmatrix} + \begin{bmatrix} u_F \\ u_\tau \end{bmatrix}. \tag{4.84}$$

Considering the Euler angle representation of the manipulator, the states of the system are $X = \begin{bmatrix} p^\top & \theta^\top \end{bmatrix}^\top \in \mathbb{R}^6$, where $p \in \mathbb{R}^3$ is the translational position and $\theta \in \mathbb{R}^3$ is the angular position, in Euler angles, of the end effector, and $\dot{X} = \begin{bmatrix} v^\top & \omega^\top \end{bmatrix}^\top \in \mathbb{R}^6$. Equation (4.84) can be further described by

$$M(X)\ddot{X} + h(X, \dot{X}) = \begin{bmatrix} u_F \\ u_\tau \end{bmatrix}, \tag{4.85}$$

where matrices M and h may be inferred from (4.84). The control law that describes the IDC is as follows (LEE et al., 2003):

$$u = \begin{bmatrix} u_F \\ u_\tau \end{bmatrix} = u_c + u_h, \tag{4.86}$$

where

$$\begin{aligned} u_c &= M \left(\ddot{X}_{ref} + K_p(X_{ref} - X) + K_d(\dot{X}_{ref} - \dot{X}) + K_i \int (X_{ref} - X)\, \mathrm{d}t \right) \\ u_h &= h(X, \dot{X}), \end{aligned} \tag{4.87}$$

and the subscript ref denotes the reference values for $X, \dot{X}$ and $\ddot{X}$. The constant gains K_p, K_d and K_i are designed to achieve the desired behavior of the closed-loop system. Essentially, u_c is the control effort to drive the errors $X - X_{ref}, \dot{X} - \dot{X}_{ref}$ to zero and u_h is the term that cancels nonlinearities and undesired characteristics of the platform. Therefore, in closed-loop the system becomes

$$\begin{bmatrix} \dot{v} \\ \dot{\omega} \end{bmatrix} = \ddot{X}_{ref} + K_p(X_{ref} - X) + K_d(\dot{X}_{ref} - \dot{X}) + K_i \int (X_{ref} - X)\, \mathrm{d}t, \tag{4.88}$$

given that the matrix $M^{-1}(X)$ from u_c cancels the matrix $M(x)$ from the dynamics of the system, as well as the matrix $h(X, \dot{X})$ from u_h cancels the nonlinearities from the model. In this case, the dynamics of the system are imposed by the gains K_p, K_d and K_i, given an accurate mathematical description of the manipulator. On the other hand, if the model is not accurate, the dynamics and nonlinearities will not be canceled and the performance of this controller will not generally be acceptable.

5 Numerical Results

In this chapter, the numerical results of this work will be presented along with the procedures, values and considerations used throughout the simulations. First, the simulation method itself will be described, followed by the necessary parameters of the environment, the constructive constants considered for the Stewart platform and the designed control parameters for the proposed controller. Next, three scenarios will be presented for validating this work, and, finally, a comparison to another control method, namely the inverse dynamics controller (IDC), will be demonstrated.

5.1 Simulation Procedure

For the results of this work, a numeric simulation was performed in a MATLAB environment, while the optimization problems with LMI constraints were solved using the YALMIP (LÖFBERG, 2004) and SDPT3 (TOH; TODD; TÜTÜNCÜ, 1999) software packages. The simulation is performed as follows.

From the platform and control parameters, calculate the static state-feedback gains for the linear translational and linearized rotational augmented systems K and K_{rt}, respectively. Then, perform a simulation loop with given sampling period and total simulation time:

Step 1 Simulate the resonant and integrator states and compute the augmented model for the translational submodel (4.8);

Step 2 Simulate the resonant and integrator states and compute the augmented linearized model for the rotational submodel (4.78);

Step 3 Compute the control signal to the translational system from control law (4.13);

Step 4 Compute the control signal to the rotational system from control law (4.82);

Step 5 Compute the Jacobian matrix J from (3.4);

Step 6 Compute the linear forces of the actuators via the Jacobian matrix J such as (4.83);

Step 7 Simulate the dynamics of the top platform using the model from (3.20), while applying the control signals to the actuators;

Step 8 Apply the desired perturbations on the bottom (e.g. sinusoidal translations and rotations) and top platforms (e.g. load conditions, instrumentation noise);

Step 9 Naturally propagate the perturbations of the bottom platform to the end effector by use of rotation matrices and displacement vectors[1], i.e., for the top platform,

$$G_T = \begin{bmatrix} R_T & p_T \\ \mathbf{0} & 1 \end{bmatrix} \in \mathbb{R}^{4\times4}, \tag{5.1}$$

where G_T is the transformation matrix, R_T is the rotation matrix and p_T is the position vector for the top platform, such as those presented on Chapter 3.

Given that, the simulation must have some parameters defined in order to correctly represent a given scenario, such as simulation and control parameters and also geometric and constructive parameters of the platform. These will be presented on the next section.

5.2 Simulation, Platform and Control Parameters

While the systematic representation of the simulation procedure from the last section covers the necessary steps to perform a dynamic representation of the Stewart platform, some important constants need to be defined beforehand. First, define the main simulation parameters as shown on Table 1, which will govern how the environment will compute the simulation scenario.

Table 1 – Considered simulation parameters.

Parameter	Symbol	Value
Sampling period $[s]$	T	0.001
Total simulation time $[s]$	t_{total}	20
ODE23 solver relative tolerance	R_{tol}	1×10^{-5}
Gravity acceleration $[m/s^2]$	g	9.85

Source: the author (2016).

Going further, the geometric and constructive parameters were chosen similarly to (HAJIMIRZAALIAN; MOOSAVI; MASSAH, 2010), the only difference being that the joints of the upper platform were placed in such way to present a gap between them, i.e. with $\varphi_T \neq 0$. Therefore, the platform parameters were as follows on Table 2[2]. With the given constructive and geometric parameters, the resulting platform is shown on Figure 11.

As for the control parameters, the constants needed for the $\mathcal{D}$-stability, resonant and $\mathcal{L}_2$ controllers are as presented on Table 3. The chosen fundamental frequency to

[1] This propagation is needed for simulation purposes because (3.20) is built with different reference frames than the simulation environment, which uses the global inertial frame as basis.

[2] The inertia matrix I_m has non-zero terms only on its diagonal because it is distributed along the axis of its reference frame.

Table 2 – Chosen platform parameters.

Parameter	Symbol	Value
Top platform mass $[kg]$	m	1.36
Top platform tensor of inertia $[kgm^2]$	I_m	$diag\left(\begin{bmatrix}1.705\times10^{-4}\\1.705\times10^{-4}\\3.408\times10^{-4}\end{bmatrix}\right)$
Platform radius, top $[mm]$	r_T	125
Platform radius, bottom $[mm]$	r_B	200
Gap between actuator pair, top $[rad]$	φ_T	$\pi/2$
Gap between actuator pair, bottom $[rad]$	φ_B	$\pi/4$
Initial position, top platform $[mm]$	$p_T(0)$	$\begin{bmatrix}0 & 0 & 180\end{bmatrix}^\top$
Initial orientation, top platform	$q_T(0)$	$\begin{bmatrix}1 & 0 & 0 & 0\end{bmatrix}^\top$
Initial position, bottom platform $[mm]$	$p_B(0)$	$\begin{bmatrix}0 & 0 & 0\end{bmatrix}^\top$
Initial orientation, bottom platform	$q_B(0)$	$\begin{bmatrix}1 & 0 & 0 & 0\end{bmatrix}^\top$

Source: the author (2016).

Figure 11 – The Stewart platform with constructive parameters from Table 2.

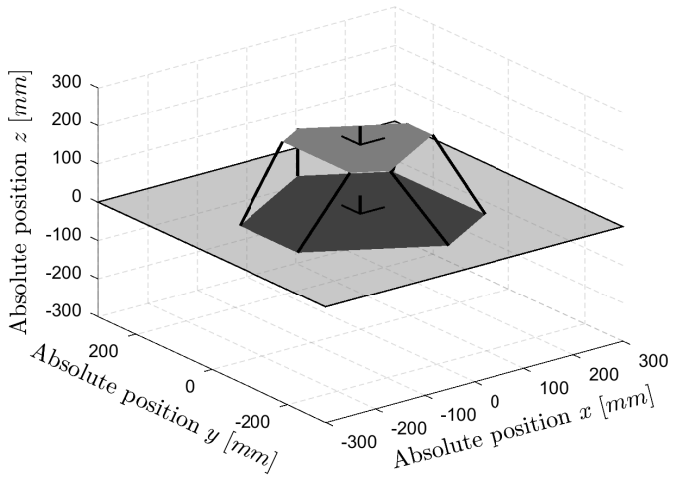

Source: the author (2016).

be rejected on the resonant controllers was 0.2Hz, which is the highest frequency value used on (MELLO, 2011), considering the perturbations affecting a large vessel floating atop ocean waves. More specifically, with the considered $\mathcal{L}_2$ constants, the $\mathcal{L}_2$ gain of the rotational system is less than or equal $\nu = 35$.

Given these considerations, the resulting control gains for the translational and

Table 3 – Designed controller parameters.

Parameter	Symbol	Value
Translational $\mathcal{D}_c$ radius	r	7
Translational $\mathcal{D}_c$ center	c	7
Translational $\mathcal{D}_p$ placement	ξ	1.4
Rotational $\mathcal{D}_{c_{rt}}$ radius	r_{rt}	10
Rotational $\mathcal{D}_{c_{rt}}$ center	c_{rt}	10
Rotational $\mathcal{D}_{p_{rt}}$ placement	ξ_{rt}	1.2
Fundamental resonant frequency to reject	σ_r	0.4π
Harmonic resonant frequency to reject	σ_h	0.8π
First $\mathcal{L}_2$ constant	ρ	20
Second $\mathcal{L}_2$ constant	a	13
Third $\mathcal{L}_2$ constant	b_1	11
Fourth $\mathcal{L}_2$ constant	b_2	12
$\mathcal{L}_2$ gain goal	ν	35

Source: the author (2016).

rotational state-feedback control laws K and K_{rt}, respectively, are as follows:

$$K = \begin{bmatrix} -331.3 & 0 & 0 \\ 0 & -293.7 & 0 \\ 0 & 0 & -293.7 \\ -34.1 & 0 & 0 \\ 0 & -31.6 & 0 \\ 0 & 0 & -31.6 \\ 1,765.1 & 0 & 0 \\ 1,150.9 & 0 & 0 \\ 2,381.5 & 0 & 0 \\ -484.4 & 0 & 0 \\ 0 & 1,260.3 & 0 \\ 0 & 941.1 & 0 \\ 0 & 1,998.5 & 0 \\ 0 & -279.5 & 0 \\ 0 & 0 & 1,260.3 \\ 0 & 0 & 941.1 \\ 0 & 0 & 1,998.5 \\ 0 & 0 & -279.5 \\ 993.5 & 0 & 0 \\ 0 & 745.4 & 0 \\ 0 & 0 & 745.4 \end{bmatrix}^\top \in \mathbb{R}^{3\times 21}, K_{rt} = \begin{bmatrix} -0.01 & 0 & 0 \\ 0 & 0.0695 & 0 \\ 0 & 0 & 0.0241 \\ 0.0596 & 0 & 0 \\ 0 & 0.0618 & 0 \\ 0 & 0 & 0.0587 \\ 0.6509 & 0 & 0 \\ 0.4183 & 0 & 0 \\ 0.8994 & 0 & 0 \\ -0.1596 & 0 & 0 \\ 0 & 0.0659 & 0 \\ 0 & 0.0963 & 0 \\ 0 & 0.1981 & 0 \\ 0 & 0.0173 & 0 \\ 0 & 0 & 0.1316 \\ 0 & 0 & 0.1924 \\ 0 & 0 & 0.3959 \\ 0 & 0 & 0.0346 \\ 0.3733 & 0 & 0 \\ 0 & 0.0549 & 0 \\ 0 & 0 & 0.1097 \end{bmatrix}^\top \in \mathbb{R}^{3\times 21}. \tag{5.2}$$

It is important to draw attention to the values which compose these static state-feedback gains just described. While the translational gain vector K is comprised of high gains, the reader should recall the augmented system from (4.8) and notice that the highest values are those that influence the resonant and integral controller states, not those of the position and velocities of the manipulator. This follows the disturbance rejection characteristics of the design while also allowing robust treatment of model uncertainties and measurement noise. On another note, the rotational gain vector K_{rt} is populated with small gains, since the $\mathcal{L}_2$ gain goal is relatively relaxed and the control signal weighting variable ρ successfully tames the control effort dispensed by the controller.

After applying the control laws and the aforementioned gain vectors, the closed-loop eigenvalues of the translational (λ_a) and linearized rotational ($\lambda_{l,a}$) augmented systems are as follows:

$$\lambda_a = \begin{bmatrix} -10.5292 \\ -8.2926 \\ -8.2926 \\ -2.2122 + 3.0971i \\ -2.2122 - 3.0971i \\ -4.2031 \\ -1.9362 \\ -2.0054 + 1.3597i \\ -2.0054 - 1.3597i \\ -4.1355 \\ -4.1355 \\ -2.1787 + 2.7242i \\ -2.1787 - 2.7242i \\ -2.1787 + 2.7242i \\ -2.1787 - 2.7242i \\ -2.1318 \\ -2.1318 \\ -2.1500 + 1.2342i \\ -2.1500 - 1.2342i \\ -2.1500 + 1.2342i \\ -2.1500 - 1.2342i \end{bmatrix} \in \mathbb{C}^{21}, \lambda_{l,a} = \begin{bmatrix} -11.8830 + 4.1239i \\ -11.8830 - 4.1239i \\ -8.2696 \\ -8.2613 \\ -1.5685 + 2.9023i \\ -1.5685 - 2.9023i \\ -1.7459 + 2.9344i \\ -1.7459 - 2.9344i \\ -1.7462 + 2.9342i \\ -1.7462 - 2.9342i \\ -1.5110 + 1.3836i \\ -1.5110 - 1.3836i \\ -1.5109 \\ -1.7333 + 1.5476i \\ -1.7333 - 1.5476i \\ -1.7328 + 1.5478i \\ -1.7328 - 1.5478i \\ -1.6942 + 0.4648i \\ -1.6942 - 0.4648i \\ -1.6936 + 0.4649i \\ -1.6936 - 0.4649i \end{bmatrix} \in \mathbb{C}^{21}. \tag{5.3}$$

In the next section, the simulation results of this work will be presented to the reader.

5.3 Simulation Results

For the purpose of presenting the performance of the proposed controller, three scenarios were devised. In the first scenario, the simulated environment applies a linear and angular perturbation at the center of mass of the bottom reference frame, similar to those of ocean waves, whose disturbances are then naturally propagated to the top platform. In a second scenario, a load condition is additionally imposed on the manipulator, in order to assess the compensation capabilities of the designed controller. Finally, instrumentation noise is added to the system, to evaluate robustness of the controller. In this final scenario, the suggested control method is then compared to an inverse dynamics controller (IDC), similar to what was proposed by (LEE et al., 2003).

5.3.1 Sinusoidal Perturbations

The first simulated environment applies a linear and angular perturbation p_d and r_d, respectively, at the center of mass of the bottom reference frame, as defined by

$$p_d(t) = \begin{bmatrix} 6\sin(0.2\pi t + \frac{\pi}{1.1}) \\ 3\sin(0.02\pi t + \frac{\pi}{3}) \\ 15\sin(0.2\pi t - \frac{\pi}{4}) \end{bmatrix}, r_d(t) = \begin{bmatrix} \frac{2\pi}{45}\sin(0.24\pi t - \frac{\pi}{8}) \\ \frac{3\pi}{45}\sin(0.4\pi t - \frac{\pi}{5}) \\ \frac{\pi}{180}\sin(0.12\pi t) \end{bmatrix}, \tag{5.4}$$

where r_d is the Euler angle equivalent to q_d, the angular perturbation in quaternion terms. These disturbances were chosen similarly to (GARCÍA, 2015), which are compatible frequencies from large vessels floating atop ocean waves, but applying a scaling factor of 6.6 on the amplitudes of the linear displacements, given that the length of the actuators on this particular platform are proportionally smaller.

For comparison purposes, Figs. 12 – 13 show the attitude errors and their frequency behavior of the system without control, considering that the actuators apply just the necessary reaction to gravity. In those and further figures, e_1, e_2 and e_3 are the position errors relative to $p = \begin{bmatrix} p_x & p_y & p_z \end{bmatrix}^\top$ and α, β and γ are the equivalent Euler angles related to the rotation of the top platform (see Section 2.1.3). The reference stance of the end effector is that of its initial attitude of Table 2, and the Discrete Fast Fourier Transform was performed with sampling frequency $f_s = 1000$Hz, with presented frequencies normalized by the fundamental frequency considered on the controller $\sigma_r = 0.2$Hz and the system on steady-state (SS), from $t = 10\text{s} \rightarrow 20\text{s}$.

As was explained on Section 4.1.1.2, the platform behaves in a coupled non-linear fashion as is clear to see in the displacement error pictured on Figure 12. The resulting two-sided power spectrum (2SPS) shown on Figure 13 enables one to draw the conclusion that the chosen fundamental frequency of $\sigma_r = 0.2$Hz of the resonant controllers tackles the highest frequency perturbation and that the DC gain of the translational model is small, relative to the magnitudes of the other frequencies.

Figure 12 – Displacement (left) and angular (right, in Euler angles) errors to the reference stance of the top platform, uncontrolled.

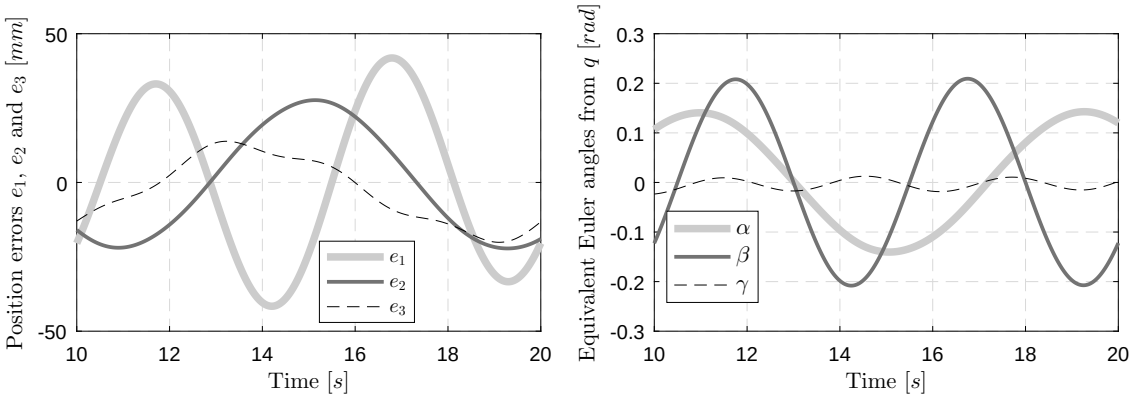

Source: the author (2016).

Figure 13 – 2SPS of the displacement (left) and angular (right, in quaternion form) errors to the reference stance of the top platform, uncontrolled, on steady-state.

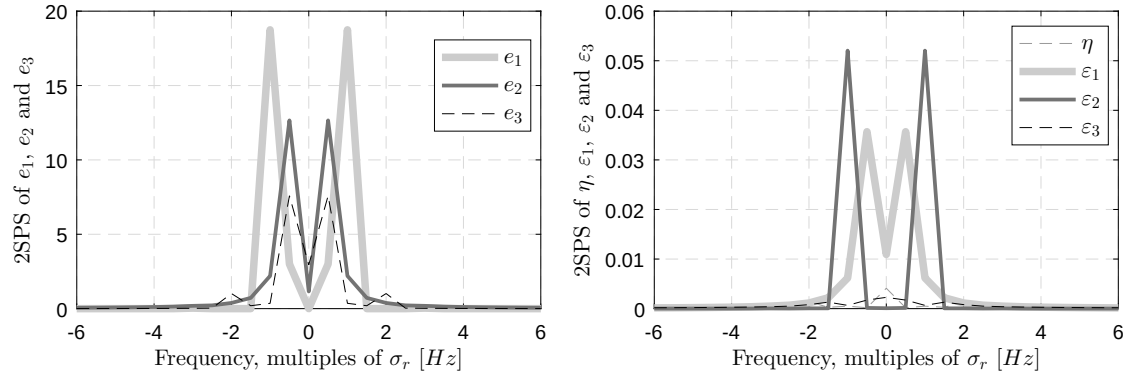

Source: the author (2016).

5.3.1.1 Proposed Controller

Now that the default behavior of the perturbed platform is known and available for comparison, the proposed controller is added to the system. The resulting attitude errors and their frequency behavior are shown in Figs. 14 – 16, with the same FFT parameters as before.

The controlled system exhibits good transient response, without significant overshoot and oscillations, while also demonstrating a fast settling time (around 2s). On steady-state, the dynamics of the controlled manipulator is also commendable, with small position and attitude errors. Referencing the FFT shown on Figure 16, it is clear to see that the magnitudes present on the output of the system have been significantly dampened, specially those regarding the perturbations. While the resonant controllers were tuned for frequencies $\sigma_r = 0.2$Hz and $\sigma_h = 0.4$Hz, the $\mathcal{H}_\infty$ and $\mathcal{L}_2$ control laws attenuate the remaining disturbia on other frequencies.

Figure 14 – Transient displacement (left) and angular (right) errors to the reference stance of the top platform, with the proposed controller.

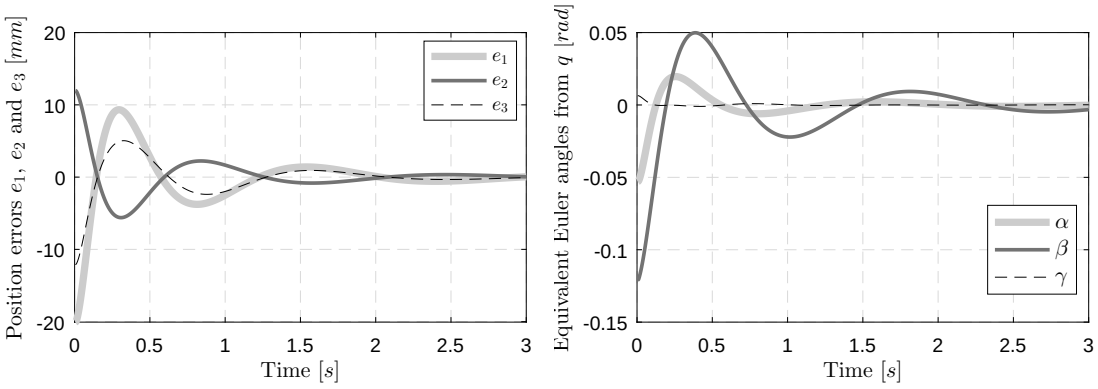

Source: the author (2016).

Figure 15 – Steady-state (SS) displacement (left) and angular (right) errors to the reference stance of the top platform, with the proposed controller.

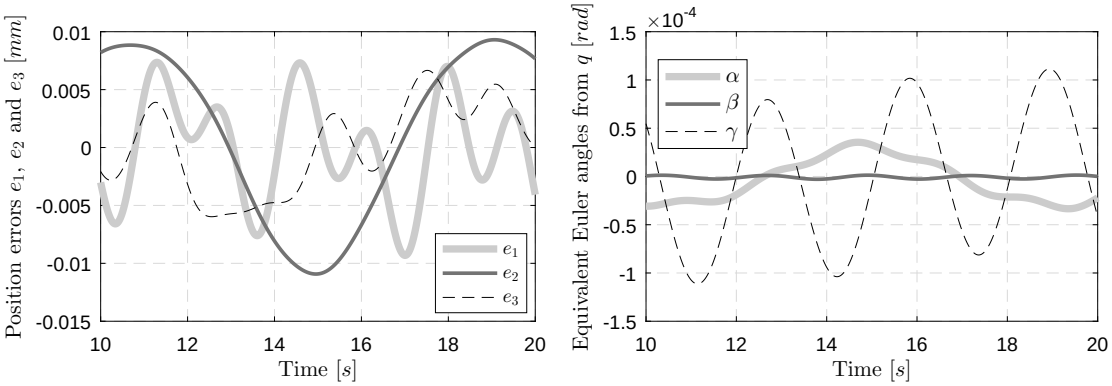

Source: the author (2016).

Figure 16 – 2SPS of the displacement (left) and angular (right) errors to the reference stance of the top platform, with the proposed controller on SS.

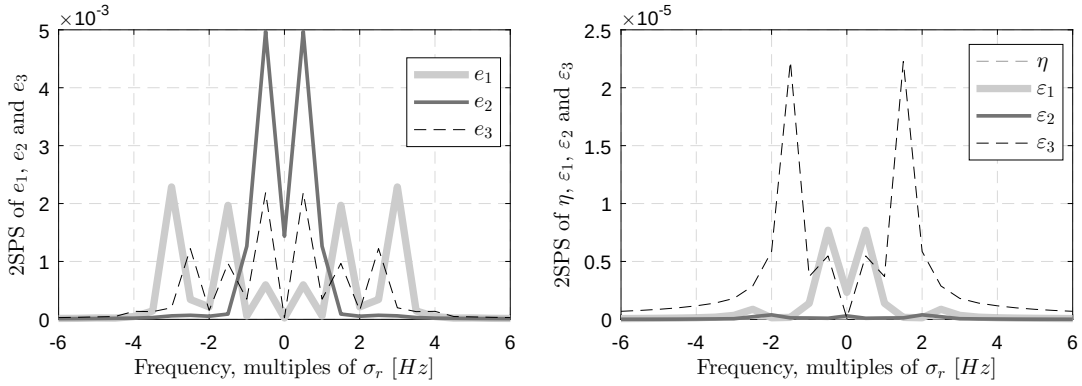

Source: the author (2016).

With the system now being controlled, the linear forces required on steady-state from the actuators are presented on Figure 17.

Figure 17 – Actuator forces 1 – 3 (left) and 4 – 6 (right) as controlled by the proposed control laws.

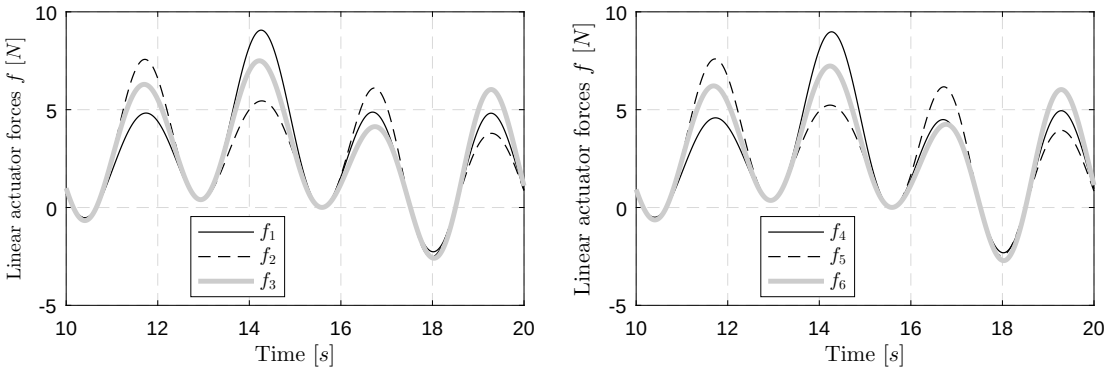

Source: the author (2016).

From Figure 17, one can see that the suggested controller is able to smoothly drive the actuators of the Stewart platform without causing chattering on the control signal, contrary to what would be typical of control methods that rely on high gains.

5.3.2 Sinusoidal Perturbations and Load Condition

Going further in testing the capabilities of the designed controller, in addition to the perturbations of Section 5.3.1, a load with mass

$$m_l = 1.56\text{kg}$$

is added on top of the end effector, i.e. the mass of the system is increased by almost 115%. Furthermore, its center of mass does not coincide with the center of mass of the manipulator. This may cause a shift of the inertia matrix to a different value than is considered by the controller. Assume that in this case the norm of the inertia matrix is increased by more than 70%, to

$$I_{m_2} = \begin{bmatrix} 3.44 \times 10^{-4} & 0 & 0 \\ 0 & 2.40 \times 10^{-4} & 0 \\ 0 & 0 & 5.88 \times 10^{-4} \end{bmatrix}.$$

This setup was devised in order to evaluate the robustness of the suggested controller, since the load condition of the manipulator is unknown at design time. It is expected that the proposed controller retain similar performance as presented on the last section, albeit with higher position and attitude errors, as well as higher actuation force to manipulate the added mass on the end effector.

5.3.2.1 Proposed Controller

Without altering the control parameters, i.e. not modifying the gains of the controller to compensate for model uncertainties, the resulting attitude errors and frequency behavior are shown in Figs. 18 – 20, with the same sampling frequency as before.

Figure 18 – Transient displacement (left) and angular (right) errors to the reference stance of the controlled manipulator, with an out-of-center load.

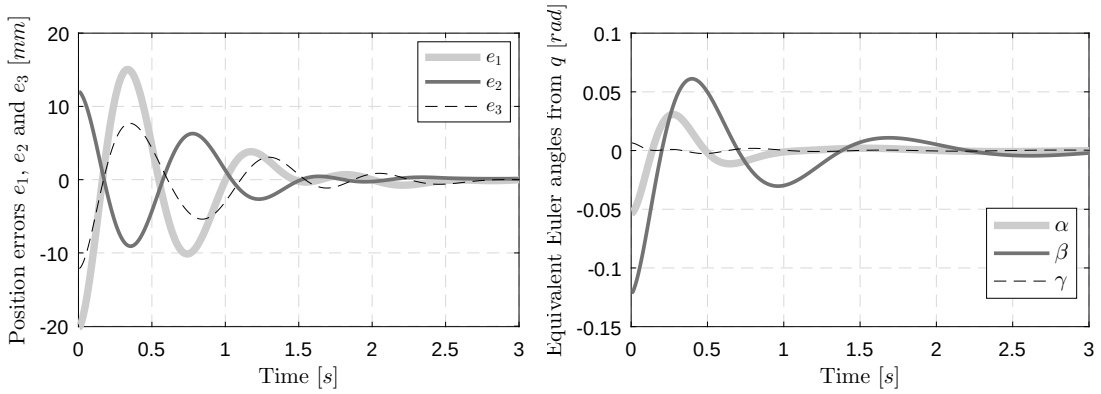

Source: the author (2016).

Figure 19 – Steady-state displacement (left) and angular (right) errors to the reference stance of the controlled manipulator, with an out-of-center load.

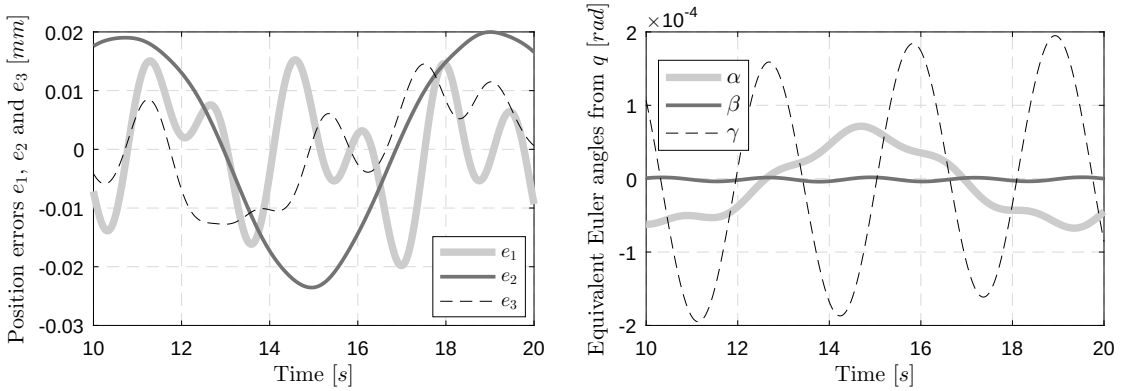

Source: the author (2016).

Figure 20 – 2SPS of the displacement (left) and angular (right) errors to the reference stance of the controlled manipulator, with an out-of-center load.

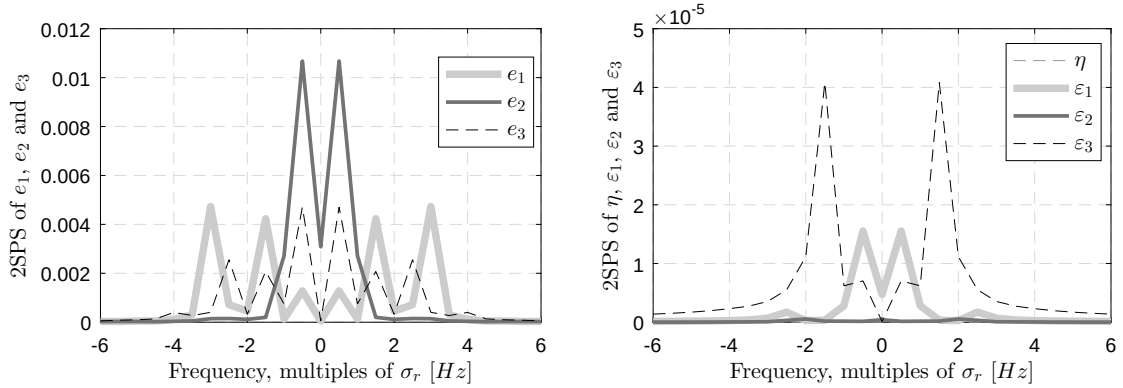

Source: the author (2016).

The controlled system considering an out-of-center load condition retains good transient response, albeit with higher overshoot and some oscillations, with settling time of 2.5s, just 0.5s slower than previously. On steady-state, the dynamics of the controlled manipulator still present good performance, even though with bigger errors than was obtained on the first scenario. Considering that the added load exceeds 115% of the platform mass considered on the controller, its response is robust enough to maintain similar performance to the first simulated setup.

Referencing the FFT shown on Figure 20, it is clear to see that the magnitudes present on the output of the system have still been significantly dampened from the original uncontrolled state, specially those regarding the perturbations, but the remaining frequencies have now higher magnitudes than previously. Still, the $\mathcal{H}_\infty$ and $\mathcal{L}_2$ methods attenuate the remaining disturbia on frequencies not pertaining to the resonant controller.

Even with this unknown at design time load condition, the actuators still present the same steady-state dynamics albeit with higher amplitudes (which are necessary to handle the added load), and without any kind of chattering, as Figure 21 shows.

Figure 21 – Actuator forces 1 – 3 (left) and 4 – 6 (right) as controlled by the proposed control laws in an out-of-center load condition.

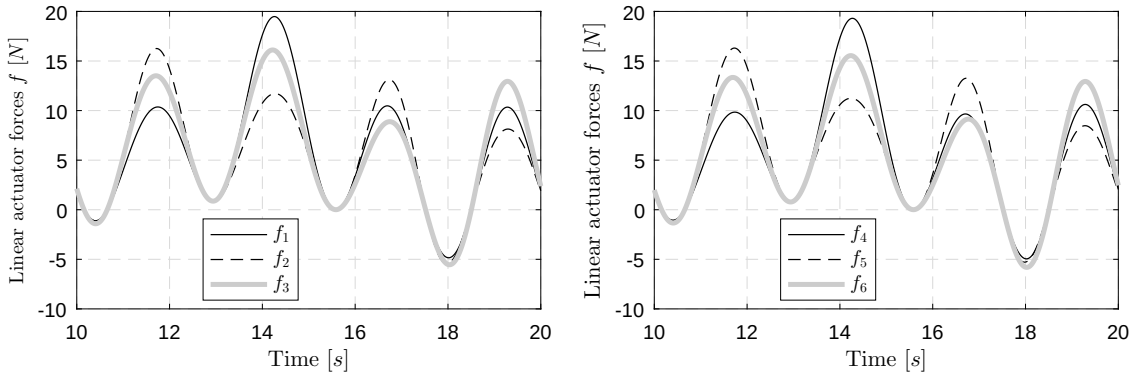

Source: the author (2016).

5.3.3 Sinusoidal Perturbations, Load Condition and Instrumentation Noise

In this last scenario, instrumentation noise is additionally included in the states p, v, q and ω that are used by the controller, namely an white Gaussian noise with signal-to-noise ratio (SNR) of 60dB. This inclusion will aid in the assessment of the robustness of the designed control laws, given that stochastic exogenous signals are directly injected in the measured states of the controller. Furthermore, the behavior of an IDC considering two proposals will be presented: one designed to match the control signals of the proposed controller and another designed to match the response of the controlled system by the control methods suggested in this work.

5.3.3.1 Proposed Controller

Without altering the control parameters, consider Figs. 22 – 24.

Figure 22 – Transient displacement (left) and angular (right) errors to the reference stance of the controlled, loaded manipulator, with added white noise.

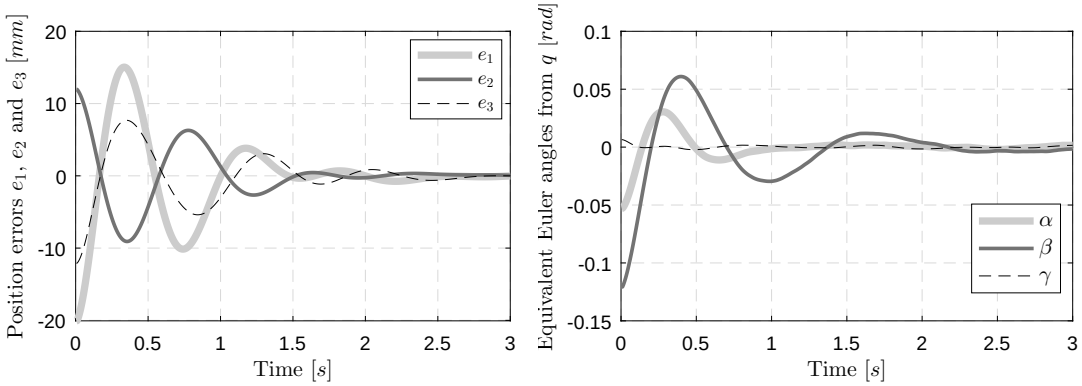

Source: the author (2016).

Figure 23 – Steady-state displacement (left) and angular (right) errors to the reference stance of the controlled, loaded manipulator, with added white noise.

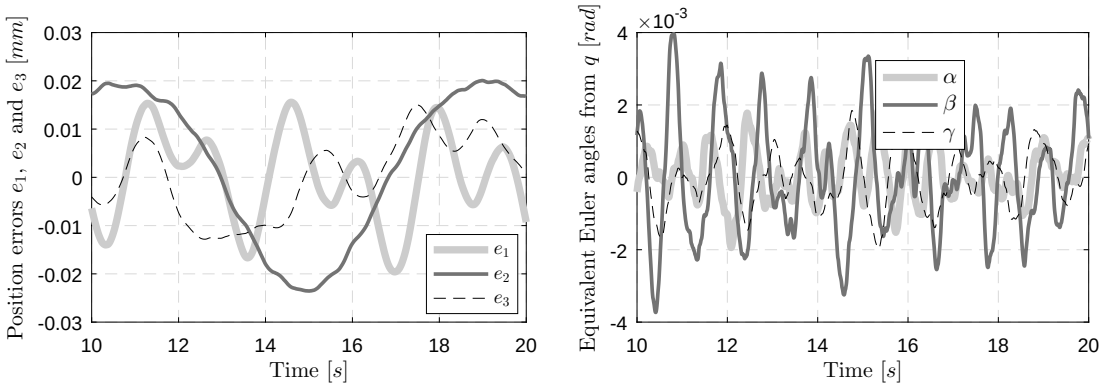

Source: the author (2016).

Figure 24 – 2SPS of the displacement (left) and angular (right) errors to the reference stance of the controlled, loaded manipulator, with added white noise.

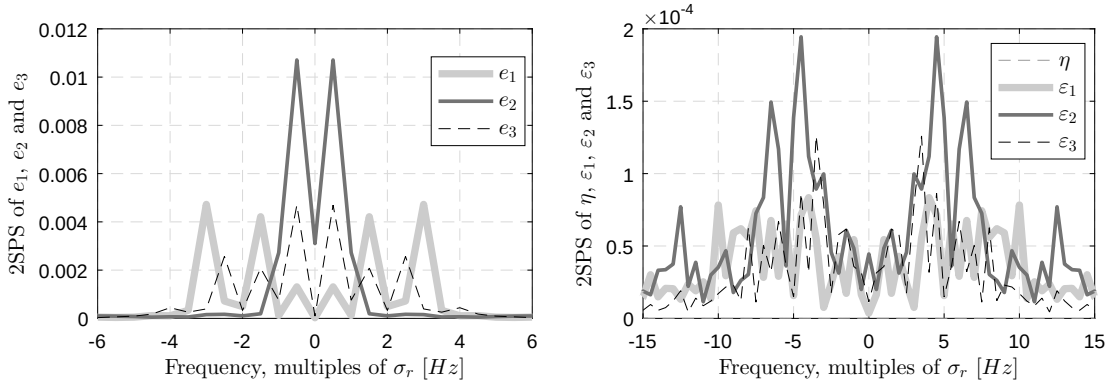

Source: the author (2016).

As is clear to see, some distortion is perceptible on the output of the controlled system on steady-state and on the frequency response of the attitude errors, but the system still converges on the reference. Even with instrumentation noise added, the actuators once again present similar steady-state dynamics without any kind of perceptible chattering, as Figure 25 shows.

Figure 25 – Actuator forces 1 – 3 (left) and 4 – 6 (right) as controlled by the proposed control laws in an out-of-center load condition with white Gaussian noise.

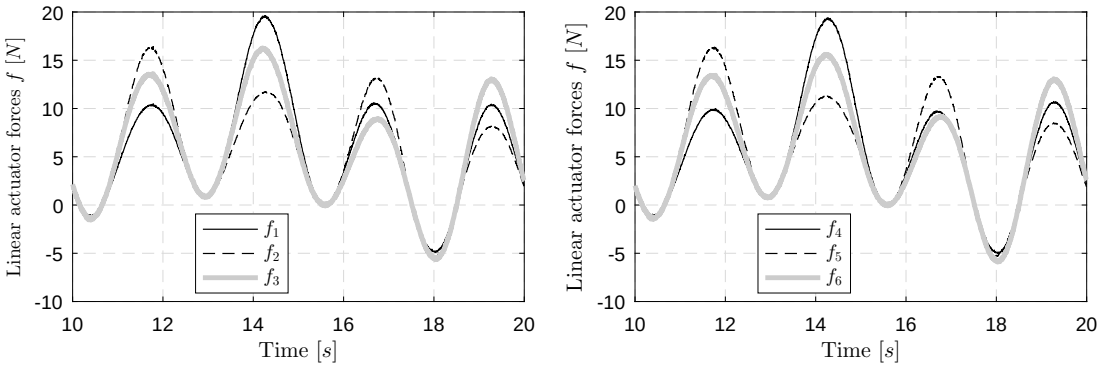

Source: the author (2016).

In the next sections (5.3.3.2 and 5.3.3.3), two inverse dynamic controllers with different design criteria will be developed, namely to possess a similar control signal and a similar system response to what was achieved in this section. Two IDC must be devised because the parameters that are used in one do not satisfy the goals of the other, and vice-versa.

5.3.3.2 Inverse Dynamics Controller with Similar Control Signal

For comparison purposes, an IDC (Section 4.4) was designed to match the control signal of the results presented on Section 5.3.3.1, as this will allow the evaluation of the effort dispensed by this controller and whether it is more effective than that of the suggested control method of this work. For this design criterion, the parameters used were as follows on Table 4, whose magnitudes are similar to those obtained on the static state-feedback gain vector (5.2) of the translational control, resonant and integral states notwithstanding.

Table 4 – Designed IDC parameters to match the control signal of Section 5.3.3.1.

Parameter	Symbol	Value
Proportional constant	K_p	250
Derivative constant	K_d	50
Integral constant	K_i	10

Source: the author (2016).

With these parameters, which are in a similar range to the gains of the controller proposed in this work, the resulting behavior of the system is shown on Figs. 26 – 28.

Figure 26 – Transient displacement (left) and angular (right) errors to the reference stance, with the IDC tuned for similar control signal.

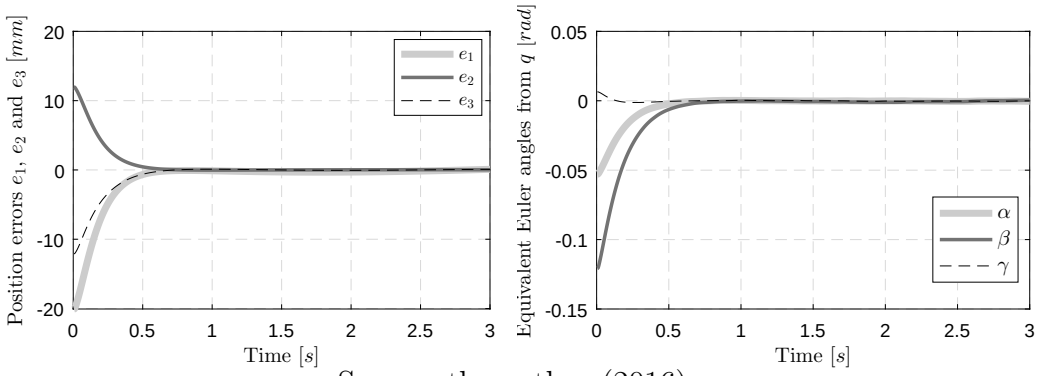

Source: the author (2016).

Figure 27 – Steady-state displacement (left) and angular (right) errors to the reference stance, with the IDC tuned for similar control signal.

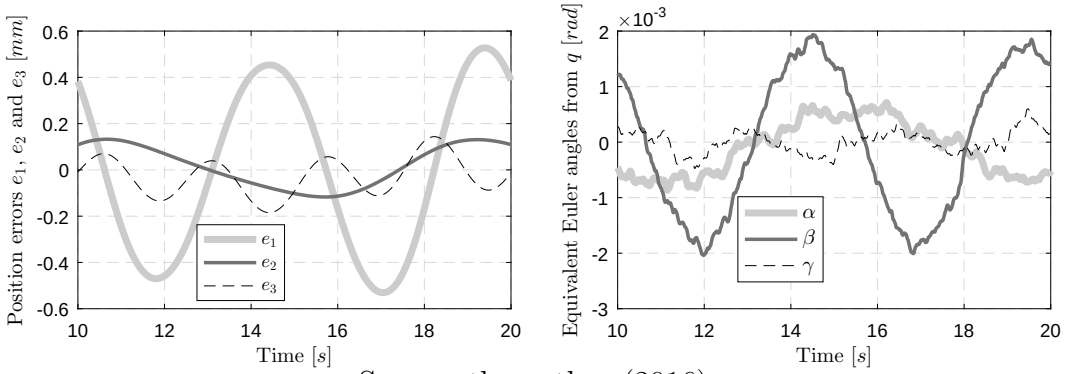

Source: the author (2016).

Figure 28 – 2SPS of the displacement (left) and angular (right) errors to the reference stance, with the IDC tuned for similar control signal.

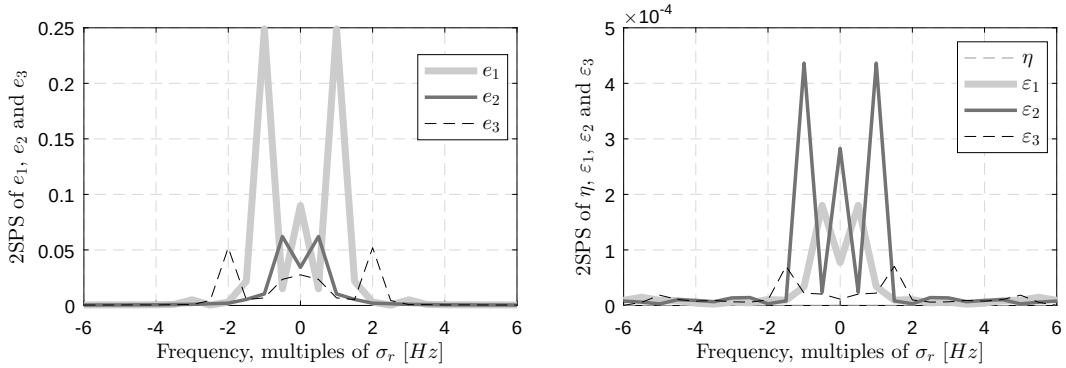

Source: the author (2016).

It is visible that the transient response of the system controlled by the IDC tuned for similar control signal is faster, with a settling time of less than one second and no visible oscillation, but the steady-state behavior is significantly worse when compared to what

was presented on Section 5.3.3.1, regarding the position error (more than 20-fold increase in the displacement error amplitude). From Figure 28 it is possible to understand the reason for this behavior: the proportional gain characteristic of this controller attenuates all frequencies in a similar fashion, without focusing on a given band of frequencies. The frequencies of the perturbations (0.2Hz and lower), whose magnitudes are higher than the others, are dampened, but still higher than that of the suggested controller in this work, seen on Figure 24.

On further note, the design goal was achieved, given that the actuators controlled by the IDC behave similarly to the suggested control method of this work on steady-state without any kind of perceptible chattering, as Figure 29 shows. As such, given similar effort, i.e. similar control signals, the steady-state response of the IDC is worse than that presented using the proposed controller of this work.

Figure 29 – Actuator forces 1 – 3 (left) and 4 – 6 (right) as controlled by the IDC tuned for similar control signal to the controller proposed in this work.

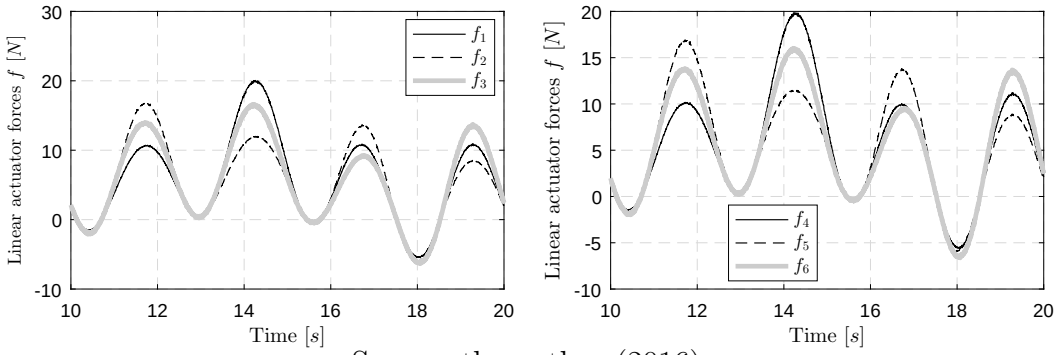

Source: the author (2016).

5.3.3.3 Inverse Dynamics Controller with Similar System Response

Going further, another IDC was now designed to match the steady-state (SS) system response of the results presented on Section 5.3.3.1 as this will allow the evaluation of how much effort should be dispensed by this controller to match the results provided by the suggested control method, specially for the displacement behavior. As such, the parameters used were as follows on Table 5.

Table 5 – Designed IDC parameters to match the system response of Section 5.3.3.1.

Parameter	Symbol	Value
Proportional constant	K_p	5500
Derivative constant	K_d	75
Integral constant	K_i	30

Source: the author (2016).

With these unsuitably high control gains, the resulting behavior of the system is shown on Figs. 30 – 32.

Figure 30 – Transient displacement (left) and angular (right) errors to the reference stance, with the IDC tuned for similar SS system response.

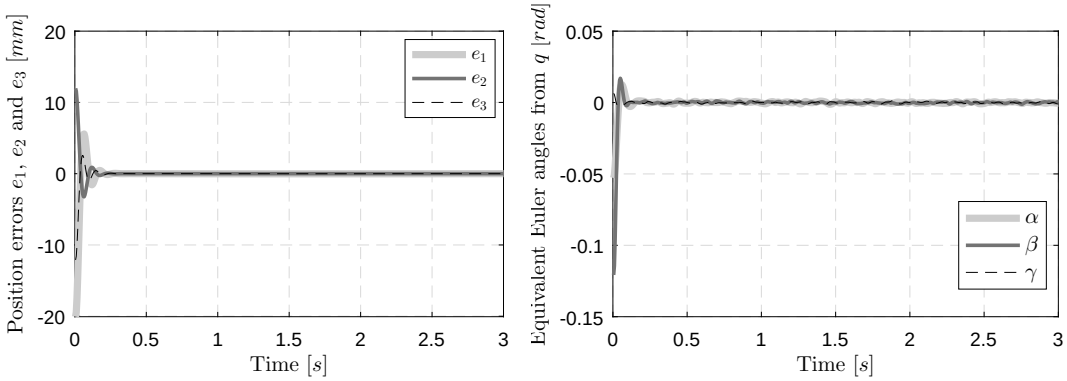

Source: the author (2016).

Figure 31 – Steady-state displacement (left) and angular (right) errors to the reference stance, with the IDC tuned for similar SS system response

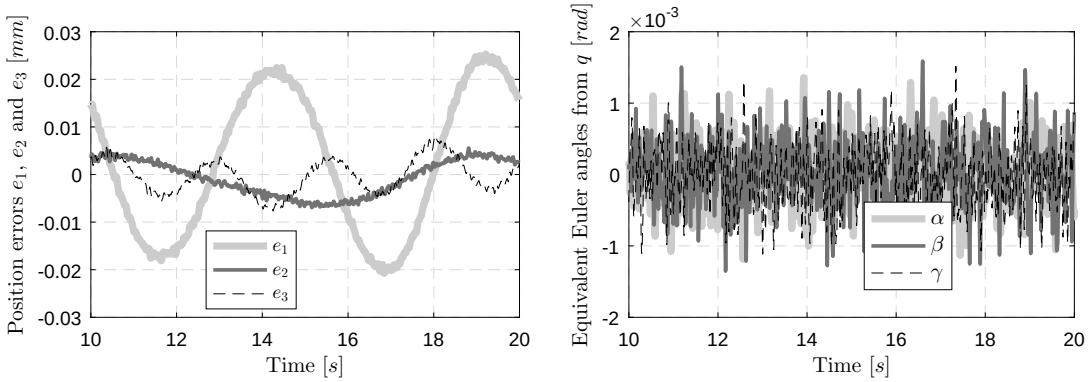

Source: the author (2016).

Figure 32 – 2SPS of the displacement (left) and angular (right) errors to the reference stance, with the IDC tuned for similar SS system response

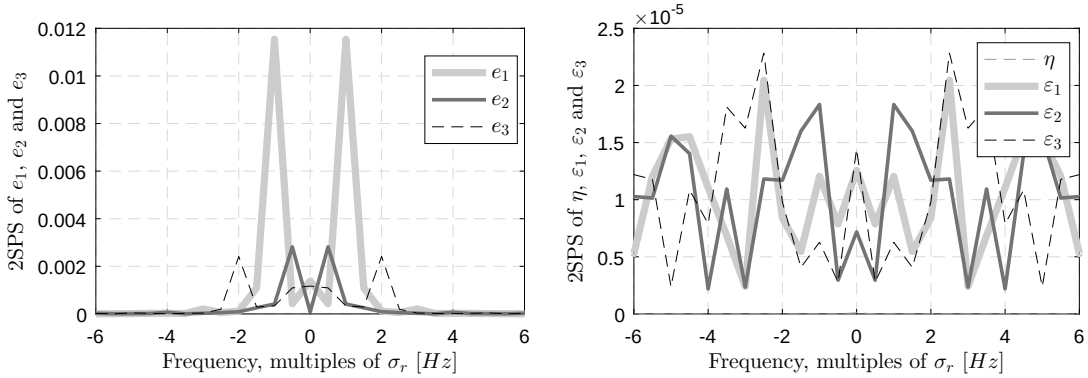

Source: the author (2016).

It is clear that the IDC needs much higher gains in order to produce comparable system response to what was achieved with the proposed controller. This is particularly so because the IDC relies on canceling the unwanted dynamics of the system. Therefore, its performance depends on an accurate modeling of the manipulator, and is severely negatively impacted by the fact that it is dealing with instrumentation noise and load conditions.

This time, the steady-state system response is similar to what was produced on Section 5.3.3.1, for the displacement behavior. However, the actuators show visible chattering, as Figure 33 shows.

Figure 33 – Actuator forces 1 – 3 (left) and 4 – 6 (right) as controlled by the IDC tuned for similar SS system response to the controller proposed in this work.

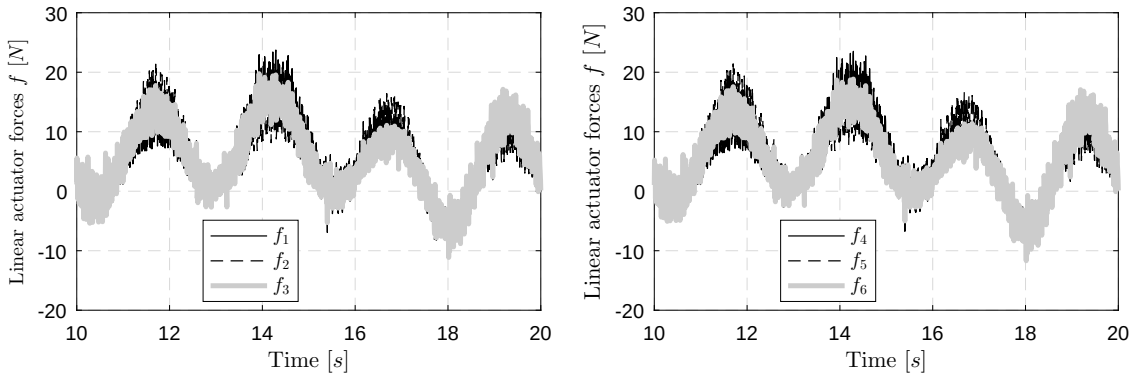

Source: the author (2016).

For a more objective approach, the signal swing of the control signal was computed in order to evaluate the chattering produced by the controllers. The resulting swing over 25 samples[3], with $f_s = 1000Hz$, is presented on Table 6.

Table 6 – Comparison of control signal swing of the controllers.

Controller	Control signal swing [N/(0.025s)]
Suggested controller	$\begin{bmatrix}0.6588 & 0.6843 & 0.6653 & 0.6584 & 0.6786 & 0.6712\end{bmatrix}^\top$
IDC, similar control signal	$\begin{bmatrix}0.7385 & 0.6809 & 0.7158 & 0.7180 & 0.6802 & 0.7200\end{bmatrix}^\top$
IDC, similar system response	$\begin{bmatrix}8.8455 & 8.8296 & 8.6450 & 8.5948 & 8.8067 & 8.6967\end{bmatrix}^\top$

Source: the author (2016).

[3] The control signal swing was computed by

$$f_{sw} = max(f_l) - min(f_l), l = (1, \ldots, 6),$$

where max and min return the maximum and minimum values of the signal over a 25 sample period. The resulting swing presented is the maximum control signal swing f_{sw} over 10s on steady-state.

From Table 6, it is clear that the proposed controller has the smallest chattering on the control signal. Going further, consider the results of Table 7, where the $\mathcal{L}_2$ norm of the position and attitude errors, as well as the control effort and control swing on steady-state ($t = 10\text{s} \rightarrow 20\text{s}$) were computed.

Table 7 – Comparison of the controllers by $\mathcal{L}_2$ norm.

Controller	Pos. error	Att. error	Control effort	Control swing
Suggested controller	0.7320	0.0556	852.4643	1.6054
IDC, similar control signal	16.3439	0.0612	871.9080	1.7372
IDC, similar system response	0.7360	0.0241	873.0287	21.4010

Source: the author (2016).

In terms of direct comparison, consider Table 8 which presents the relative differences between the suggested controller and the IDC, with positive values representing improvements and negative values performance degradation.

Table 8 – Direct comparison of the controllers, relative to the suggested controller.

Controller	Pos. error	Att. error	Control effort	Control swing
Suggested controller	—	—	—	—
IDC, similar control signal	$-2,132\%$	-10.07%	-2.28%	-8.20%
IDC, similar system response	-0.54%	$+56.65\%$	-2.41%	$-1,233\%$

Source: the author (2016).

As is evidently obvious from the previous figures and results, the suggested controller is very effective in meeting the objectives of this work, as proposed on Section 1.1.

Remark 5.1. For the sake of completeness, consider that the system is perturbed with frequencies that match those of the resonant controllers, i. e.,

$$\bar{p}_d(t) = \begin{bmatrix} 6\sin(0.4\pi t) \\ 3\sin(0.4\pi t) \\ 15\sin(0.4\pi t) \end{bmatrix}, \bar{r}_d(t) = \begin{bmatrix} \frac{2\pi}{45}\sin(0.4\pi t) \\ \frac{3\pi}{45}\sin(0.4\pi t) \\ \frac{\pi}{180}\sin(0.4\pi t) \end{bmatrix}. \tag{5.5}$$

Since the resonant controller is exactly tuned for the perturbation frequencies, it is expected that the first and second harmonics are asymptotically rejected. Consider, thus, the Figures 34 and 35, which show the position and angular errors to the reference stance, and the 2SPS for the position and angular errors, respectively. It is clear to see that, indeed, the frequencies tuned on the resonant controllers were successfully rejected on both the translational and rotational controllers. In fact, the harmonics that once

(Figures 8 and 10) were small enough to be neglected, now present comparatively the highest magnitudes (albeit small in absolute values).

Figure 34 – Transient displacement (left) and angular (right) errors to the reference stance, using the proposed controller, with the perturbations following (5.5).

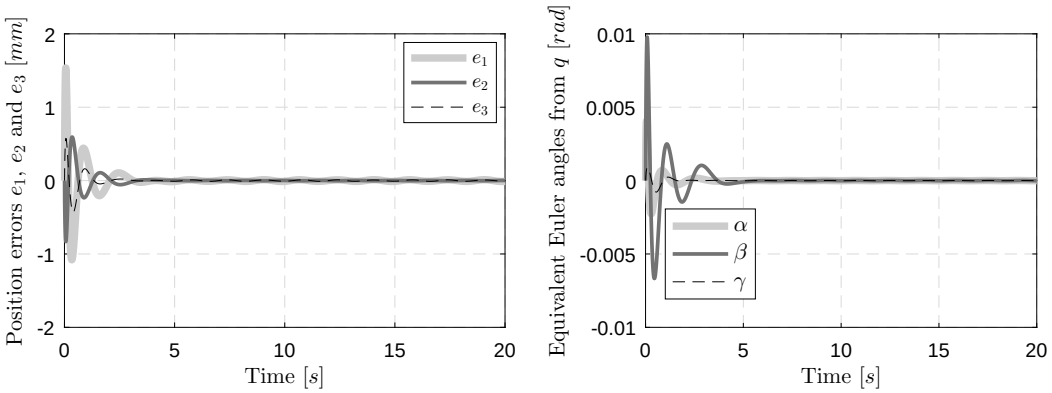

Source: the author (2016).

Figure 35 – 2SPS of the displacement (left) and angular (right) errors to the reference stance, using the proposed controller, with the perturbations following (5.5).

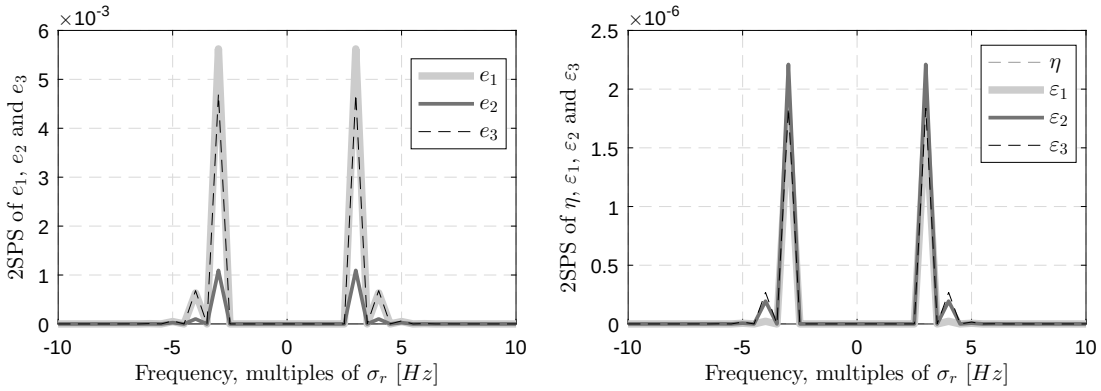

Source: the author (2016).

6 Conclusions

This work proposed a dynamic control method for the Stewart platform that aims at rejecting periodic perturbations which may adversely affect the system. The presented control strategies are based on the inverse kinematics and the Jacobian of the end effector and, more importantly, on the quaternion-based Newton-Euler representation from Chapter 3. In this chapter, the platform was geometrically described and its most significant constructive parameters were defined. In addition, the Jacobian singularities were presented and the suggested dynamic model validated against the more classical Euler-angle-based Lagrange model. The presented model may, thus, be used for describing the Stewart platform.

With the mathematical description of the system validated, the decoupled nature of the model was leveraged on Chapter 4 to propose two different control strategies. First, a state-feedback law was designed to control the augmented translational submodel via an optimization problem subject to LMIs and given performance criteria ($\mathcal{H}_\infty$ gain minimization and $\mathcal{D}$-stability-based eigenvalue placement). In this case, the augmented states from the resonant and integral controllers provide the dynamic aspect of this control method. In this context, the resonant controller provides periodic disturbance rejection characteristics for the designed frequencies while the static state-feedback gain minimizes the $\mathcal{H}_\infty$ gain of the external perturbations. In fact, the closed-loop translational system is asymptotically stable when unperturbed and $\mathcal{H}_\infty$ finite-gain stable when subject to perturbations.

Chapter 4 also addressed the nonlinear state-feedback control law of the rotational submodel of the manipulator. This control strategy was particularly designed to achieve $\mathcal{L}_2$ gain performance by making use of the Hamilton-Jacobi inequality and a Lyapunov candidate function. The resulting closed-loop system was then linearized and augmented with resonant and integral states to allow a state-feedback control law to also provide periodic disturbance rejection characteristics to the rotational submodel. In fact, the closed-loop rotational system is asymptotically stable when unperturbed and $\mathcal{L}_2$ finite-gain stable when subject to perturbations.

Going further, the coupling of the two suggested controllers was addressed via the Jacobian matrix, and, finally, an inverse dynamics controller was presented to provide a solid comparison between the control method described in this work and the strategies proposed in other endeavors.

The proposed controller is robust in the sense that it minimizes the perturbation to output $\mathcal{L}_2$ gain (rotational subsystem), the $\mathcal{H}_\infty$ gain of the external perturbations

(translational subsystem) and that any perturbation with a given spectrum is attenuated (resonant states for the rotational and translational submodels), provided its frequency spectrum is known a priori and dominated by resonant peaks. The proposed control technique relies in the fact that the system is not in a singular stance, which can be guaranteed by avoiding such configurations on the trajectory of the platform.

Next, Chapter 5 presents the main results of this work. The first simulated environment replicates the effect ocean waves have on a floating Stewart platform. Going further, an out-of-center load condition was devised in order to evaluate the robustness on the suggested control methods. In the third and last scenario, instrumentation noise was injected in the measured states of the controller to assess its behavior given stochastic exogenous signals. In this same context, an inverse dynamics controller was implemented with two design criteria for a head-on comparison, namely to possess a similar control signal and a similar system response to that of the proposed control method. While the IDC with similar control signal did not present control signal chattering, its steady-state performance fell short of that of the proposed controller. On the other hand, the IDC with similar system response was negatively affected by the use of high gains, showing visible chattering on the actuator forces.

Contrary to the IDC, the proposed controllers need some parameter tuning, such as the constants of the $\mathcal{L}_2$ controller for example, but cope much better to model uncertainties and load conditions. In addition, the approach used may be further extended and improved with the techniques presented on Section 6.1, which by itself should provide another set of interesting results and research topics.

In conclusion, the control method suggested in this work had both a smooth control signal and a significant attenuation of external perturbations. These results validate, thus, the effectiveness of the suggested control strategy for periodic disturbance rejection on the Stewart platform.

6.1 Future Works

This work addresses some important topics concerning the rejection of periodic disturbances on the Stewart platform. Nevertheless, the control strategies presented here may be further improved by the use of some additional techniques. It is suggested for future research that the stability of the complete platform be taken into account by using the passivity concept, which relates nicely to $\mathcal{L}_2$ stability (KHALIL; GRIZZLE, 1996) and may allow the Jacobian to be considered in the stability proof formulation. Another useful contribution would be the consideration of actuator saturation in such proof, as well as on the developed control law. Furthermore, instead of relying on FFT to define the harmonics to attenuate, one could also perform trigonometric relations to compute

the resulting harmonics to reject.

Given that LMI constraints were widely applied in this work, it is suggested also that a polytopic approach be used to guarantee further robustness of the closed-loop system. In addition, a repetitive controller may be used in a unified approach with the resonant controller to reduce the residual steady-state error presented (SALTON et al., 2013) and the system linearization performed on Section 4.2.2.1 may be avoided by using the nonlinear internal model principle formulation (ISIDORI; MARCONI; SERRANI, 2012).

Bibliography

ASADA, H.; SLOTINE, J.-J. *Robot analysis and control*. [S.l.]: John Wiley & Sons, 1986. 69

AYAS, M.; SAHIN, E.; ALTAS, I. Trajectory tracking control of a stewart platform. *Power Electronics and Motion Control Conference and Exposition (PEMC)*, v. 16, p. 720–724, 2014. 18

BARATA, J. C. A.; HUSSEIN, M. S. The moore–penrose pseudoinverse: A tutorial review of the theory. *Brazilian Journal of Physics*, Springer, v. 42, n. 1-2, p. 146–165, 2012. 40, 69

BOYD, S. P. et al. *Linear matrix inequalities in system and control theory*. [S.l.]: SIAM, 1994. v. 15. 27, 28

CASTRO, R. d. S. *Controladores Ressonante e Repetitivo Modificados para o Tratamento de Sinais com Período Variante no Tempo*. Dissertação (Mestrado) — Pontifícia Universidade do Rio Grande do Sul, 2015. 26

CHARTERS, T.; ENGUIÇA, R.; FREITAS, P. Detecting singularities of stewart platforms. *Mathematics-in-Industry Case Studies Journal*, v. 1, n. 1, p. 66–80, 2009. 41

CHILALI, M.; GAHINET, P.; APKARIAN, P. Robust pole placement in lmi regions. *Automatic Control, IEEE Transactions on*, v. 44, n. 12, p. 2257–2270, Dec 1999. 29

DIEBEL, J. Representing attitude: Euler angles, unit quaternions, and rotation vectors. *Matrix*, v. 58, n. 15-16, p. 1–35, 2006. 23

FICHTER, E. A stewart platform-based manipulator: general theory and practical construction. *The International Journal of Robotics Research*, v. 5, n. 2, p. 157–182, 1986. 18

FRANCIS, B. A.; WONHAM, W. M. The internal model principle for linear multivariable regulators. *Applied mathematics and optimization*, Springer, v. 2, n. 2, p. 170–194, 1975. 25

GARCÍA, R. M. L. *Controle de um Manipulador Plataforma de Stewart com Atuadores Hidráulicos como Simulador de Movimentos de Navios*. Dissertação (Mestrado) — Universidade Federal do Rio Grande do Sul, 2015. 41, 76

GILBERT, G. T. Positive definite matrices and sylvester's criterion. *The American Mathematical Monthly*, Mathematical Association of America, v. 98, n. 1, p. 44–46, 1991. ISSN 00029890, 19300972. 31

GONZALEZ, H.; DUTRA, M. S.; LENGERKE, O. Direct and inverse kinematics of stewart platform applied to offshore cargo transfer simulation. *13th World Congress in Mechanism and Machine Science*, 2011. 18

GOSSELIN, C.; ANGELES, J. Singularity analysis of closed-loop kinematic chains. *IEEE transactions on robotics and automation*, IEEE, v. 6, n. 3, p. 281–290, 1990. 40

HAJIMIRZAALIAN, H.; MOOSAVI, H.; MASSAH, M. Dynamics analysis and simulation of parallel robot stewart platform. v. 5, p. 472–477, 2010. 72

HAMILTON, W. R. On quaternions, or on a new system of imaginaries in algebra. v. 25, n. 3, p. 489–495, 1844. 21

HIGHAM, N. J. Qr factorization with complete pivoting and accurate computation of the svd. *Linear Algebra and its Applications*, Elsevier, v. 309, n. 1, p. 153–174, 2000. 40

HUNT, K. H. *Kinematic geometry of mechanisms*. [S.l.]: Oxford University Press, 1978. 18

ISIDORI, A.; MARCONI, L.; SERRANI, A. *Robust autonomous guidance: an internal model approach*. [S.l.]: Springer Science & Business Media, 2012. 25, 92

KHALIL, H. K.; GRIZZLE, J. *Nonlinear systems*. [S.l.]: Prentice hall New Jersey, 1996. v. 3. 30, 31, 91

KIM, D. H.; KANG, J.-Y.; LEE, K.-I. Robust tracking control design for a 6 dof parallel manipulator. *Journal of Robotic Systems*, Wiley Online Library, v. 17, n. 10, p. 527–547, 2000. 43

KUIPERS, J. B. et al. *Quaternions and rotation sequences*. [S.l.]: Princeton university press Princeton, 1999. v. 66. 21

KUMAR, P.; CHALANGA, A.; BANDYOPADHYAY, B. Position control of stewart platform using continuous higher order sliding mode control. *Asian Control Conference (ASCC)*, v. 10, p. 1–6, May 2015. 18

LEE, S.-H. et al. Position control of a stewart platform using inverse dynamics control with approximate dynamics. *Mechatronics*, Elsevier, v. 13, n. 6, p. 605–619, 2003. 41, 70, 76

LIU, K.; LEBRET, G.; LEWIS, F. L. Dynamic analysis and control of a stewart platform manipulator. *Journal of Robotic Systems*, v. 10, n. 5, p. 629–655, 1993. 18

LÖFBERG, J. Yalmip: A toolbox for modeling and optimization in matlab. p. 284–289, 2004. 71

MACKAY, A. L. Quaternion transformation of molecular orientation. *Acta Crystallographica Section A: Foundations of Crystallography*, International Union of Crystallography, v. 40, n. 2, p. 165–166, 1984. 21

MAGED, S.; ABOUELSOUD, A.; BAB, A. F. E. A comparative study of unscented and extended kalman filter for position and velocity estimation of stewart platform manipulator. *Cyber Technology in Automation, Control, and Intelligent Systems (CYBER), 2015 IEEE International Conference on*, p. 1216–1222, June 2015. 18

MELLO, C. B. *Controle de Trajetória de uma Plataforma Stewart para Simulação de Transferência de Carga Fora de Porto*. Dissertação (Mestrado) — Universidade Federal do Rio de Janeiro, 2011. 18, 36, 41, 47, 73

NGUYEN, C. C. et al. Analysis and implementation of a 6 dof stewart platform-based robotic wrist. *Computers Elect. Engng.*, v. 17, n. 3, p. 191–203, 1991. 18

SALTON, A. T. et al. A resonant-repetitive control scheme applied to uninterruptible power supplies (ups). *Journal of Control, Automation and Electrical Systems*, v. 24, n. 3, p. 253–262, 2013. 92

SCHAFT, A. J. Van der. L2-gain analysis of nonlinear systems and nonlinear state-feedback hinf control. *IEEE transactions on automatic control*, IEEE, v. 37, n. 6, p. 770–784, 1992. 33

SHOW, L.-L. et al. Quaternion feedback attitude control design: a nonlinear hinf approach. *Asian Journal of Control*, Wiley Online Library, v. 5, n. 3, p. 406–411, 2003. 58, 63

STEWART, D. A platform with six degrees of freedom. *Proc. Inst. Mech. Engr.*, v. 180, n. 1, p. 371–386, 1965. 18

TOH, K.-C.; TODD, M. J.; TÜTÜNCÜ, R. H. Sdpt3—a matlab software package for semidefinite programming, version 1.3. *Optimization methods and software*, Taylor & Francis, v. 11, n. 1-4, p. 545–581, 1999. 71

WASER, A. Quaternions in electrodynamics. 2000. 21

XU, D.; MANDIC, D. P. The theory of quaternion matrix derivatives. *IEEE Transactions on Signal Processing*, v. 63, n. 6, p. 1543–1556, 2014. 42